# Effects of daily meteorology on the interpretation of space-based remote sensing of $NO_2$

## Response to Anonymous Referee #1

Joshua L. Laughner, Azimeh Zare, and Ronald C. Cohen

October 20, 2016

We thank the reviewer for their positive response and very careful reading of both the main article and the supplement. Below we respond to the individual comments. The reviewer's comments will be shown in red, our response in blue, and changes made to the paper are shown in black block quotes. Unless otherwise indicated, page and line numbers correspond to the original paper. Figures, tables, or equations referenced as "R$n$" are numbered within this response; if these are used in the changes to the paper, they will be replaced with the proper number in the final paper. Figures, tables, and equations numbered normally refer to the numbers in the original discussion paper.

Figure 1 is a very nice example of how the AMF is influenced by monthly and daily a prioris. From the manuscript, the authors suggest that this is based on the prior vertical information of NO2 from the model and the scattering weighting function. However, in the introduction there was no reference to why the AMFs are smaller/larger in the scenarios in Figure 1. I think adding a short explanation of what causes the AMFs to be different would be useful. Also, as far as I can tell, the manuscript doesnt quantify which of the two processes in Eqn 2 & 3 influencing the AMFs are most important. Which is it?

The paragraph on P4, L7–18 discusses each of the scenarios in Fig. 1. We have added a sentence near the beginning of this paragraph to remind the reader of the physical cause for the dependence on the $NO_2$ profile illustrated in each panel, so the paragraph now begins as:

> "In this paper we explore how day-to-day changes in the a priori $NO_2$ profiles affect satellite retrievals of urban $NO_2$. Several scenarios are illustrated in Fig. 1. In each case the change in the AMF results because, over low albedo surfaces, a UV/visible satellite spectrometer is less sensitive to near surface trace gases, necessitating a smaller AMF to account for the reduced sensitivity. In Fig. 1a..."

Regarding which process is more important, and taking this to mean the calculation of scattering weights vs. the a priori profile, there is no one answer, as this varies with the amount of $NO_2$ present. We have expanded the part at P.1 L.25–27 to explain this and noted that previous work has found a priori profiles to be very significant near urban areas:

"...the AMF must account for the varying sensitivity of the satellite to $NO_2$ at different altitudes, and therefore a priori knowledge of that sensitivity and the vertical profile of $NO_2$ is required. Over low-reflectivity surfaces, light scattered in the atmosphere is the primary source of radiance at the detector. The probability of back-scattered light penetrating to a given altitude is greater for higher altitudes; thus there is greater interaction with, and therefore greater sensitivity to, $NO_2$ at higher altitudes (Richter and Wagner, 2011; Hudson et al., 1995). Because of this, the correct AMF is smaller in locations influenced by surface $NO_x$ sources. The relative contribution of errors in the calculated sensitivity and in the a priori profiles of $NO_2$ to error in the final VCD varies between polluted and clean pixels (Boersma et al., 2004). Previous work (e.g. Russell et al. 2011) has sought to reduce errors in both, and highlighted the importance of accurate a priori profiles in urban areas."

In section 2.5 the EMG is discussed in detail (and in the supplementary information), but often with reference to how Matlab functions are used to calculate the required equations. For someone who has not used Matlab before, this might be difficult to follow (e.g. fmincon, nansum etc). Could the authors just discuss the mathematical and statistical methods used and leave discussion of Matlab functions in the supplementary material? I also think that there should be discussion on what a, x0, $\mu$x, $\sigma$x and B are in the text of section 2.5, instead of just referring to Table 1.

This comment is well taken. Similar comments were made by other reviewers. We have moved the technical elements (P.8 L.9–29) to the supplement and included a description of the fitting parameters here instead, after Eq. (9):

"Eq. (9) is minimized using an interior-point algorithm, finding the values of $a$, $x_0$, $\mu_x$, $\sigma_x$, and $B$ that best fit the line densities. The values of $a$, $x_0$, $\mu_x$, $\sigma_x$, and $B$ have physical significance and so their optimum values yield information about the $NO_x$ emission and chemistry occurring within the plume (Beirle et al., 2011; de Foy et al., 2014; Lu et al., 2015). Specifically:

- $a$ describes the total amount of $NO_2$ in the plume (referred to as the burden)
- $x_0$ is the distance the plume travels in one lifetime, $\tau$. It relates to $\tau$ by $x_0 = \tau \times w$, where $w$ is wind speed.
- $u_x$ describes the effective center of the emission source. In the supplement to Beirle et al. (2011), it is represented by $X$ which is the point at which exponential decay of the $NO_2$ plume begins.
- $\sigma_x$ is the standard deviation of the Gaussian component of the EMG function. Lu et al. (2015) terms this a "smoothing length scale," which describes smoothing of the data due to the spatial resolution and overlap of OMI pixels (Boersma et al., 2011). It can also be thought of as capturing effects of both the spatial extent of emissions and the turbulent wind field.
- $B$ is the background line density.

”

In section 2.3, there is discussion on weighting schemes (i.e. Eqn 5). Unfortunately, I do not understand how and why this is used. If you are trying to calculate the model monthly mean relative to the OMI sampling, could you not just subsample the model to the individual satellite overpass times (e.g. within 1 hour of 14.00LT)? This text (Page 6, Lines 5-10) needs to be improved to make the motivation for Eqn 5 clearer.

We have added a paragraph after Eq. (5) explaining our reasoning for these weights:

> “The weighting scheme in Eq. (5) was chosen over simply using the model output for 1400 local standard time for each longitude to create smooth transitions between adjoining time zones. This attempts to account for the day-to-day variability in OMI overpass tracks as well as the fact that pixels on the edge of a swath can be observed in two consecutive overpasses at different local times. More detail is given in the supplement.”

And in the supplement:

> “When computing the monthly average profiles, it is necessary to use profiles that represent OMI’s overpass time, typically quoted as 13:30 to 13:45 local standard time (e.g. McLinden et al. 2014; Levelt et al. 2006). To average the profiles output from WRF-Chem, weights were calculated that fulfilled two requirements:
>
> 1. The weights should be 1 at OMI overpass time and 0 when more than 1 hour away from overpass time.
> 2. The transition between profiles from different hours should be smooth.
>
> For #1, we assume that the average overpass time is 1330 local standard time. We compute local standard time as:
>
> $$t_{\text{apriori, local}} = \frac{l}{15} + t_{\text{apriori, utc}} \tag{R1}$$
>
> where $t_{\text{local}}$ is the local standard time in hours past midnight, $t_{\text{utc}}$ the UTC time in hours past midnight, and $l$ the longitude (west is negative). To meet the second requirement, this is a continuous function, rather than a step function (where each 15° longitudinal segment/time zone has a single local time). Areas further west in a time zone are more likely to be observed on the east edge of a later OMI swath, and vice versa for areas further east. This weighting includes some influence from later profiles to account for this.
>
> The weights from Eq. (5) are derived from:
>
> $$w = 1 - |t_{\text{overpass}} - t_{\text{apriori, local}}| = 1 - \left|13.5 - \frac{l}{15} - h\right| \tag{R2}$$

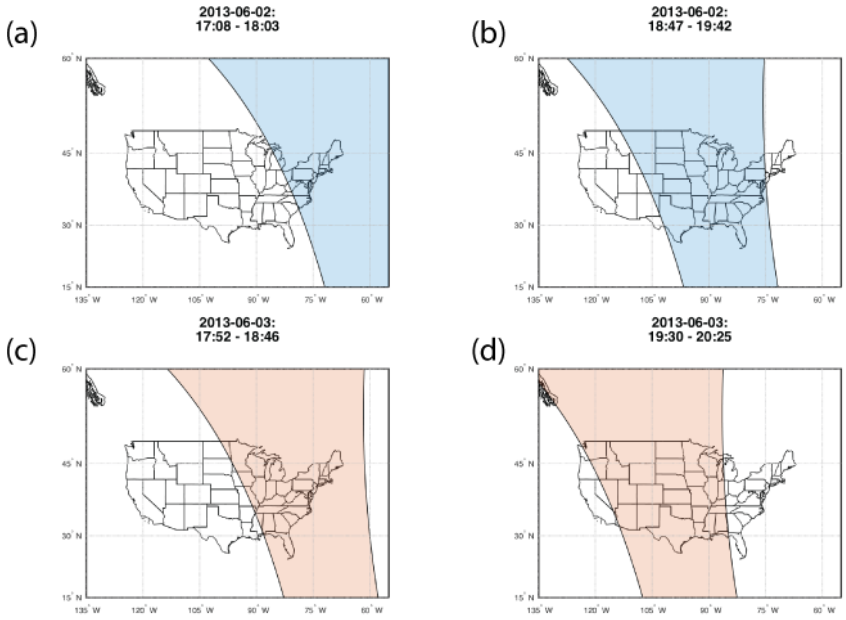


Figure R1: Swaths covering the east coast of the US for 2 June 2013 (a,b) and 3 June 2013 (c,d). The times given are the start and end times of the daytime half of the orbit in UTC. As shown, on different days, the time of the OMI swath that covers Atlanta can vary by up to an hour.

where $t_{\text{overpass}}$ is the assumed overpass time for OMI and $h \equiv t_{\text{apriori, utc}}$. If $w < 0$, $w$ is set to 0. This gives us the desired form where the weights smoothly vary in time.

”

In the abstract and introduction any reference to “Atlanta, GA should be “Atlanta, GA, USA as not everyone will know Atlanta is in the USA.

We have added “USA” to any instance where the city is given as “Atlanta, GA,” and did the same for “Birmingham, AL” and “Montgomery, AL.” Cases of the city name alone were left as such (i.e. just “Atlanta” not “Atlanta, GA”).

On Page 2, Lines 26-27, “Because the satellite is less sensitive to NO2 near the surface, the AMF should be smaller in locations influenced by surface NOx sources this is discussed in detail throughout the manuscript, but it would be good to add a short sentence here explaining why this is the case.

We have added two sentences before Eq. 1 explaining the physical basis for the lower near-surface sensitivity:

“Over low-reflectivity surfaces, light scattered in the atmosphere is the primary source of radiance at the detector. The probability of back-scattered light penetrating to a given altitude is greater for higher altitudes; thus there is greater

interaction with, and therefore greater sensitivity to, $NO_2$ at higher altitudes (Richter and Wagner, 2011; Hudson et al., 1995). Because of this, the correct AMF is smaller in locations influenced by surface $NO_x$ sources."

Page 3, Line 11: BEHR needs to be defined here, not later in the section.
Definition of BEHR added.

"The current generation Berkeley High Resolution (BEHR) (Russell et al., 2011, 2012) and OMI-EC (McLinden et al., 2014) retrievals simulate monthly average $NO_2$ profiles at 12 and 15 km, respectively."

Page 3, Lines 13-14: "2° x 3° and 0.5° x 0.667°. Im assuming this is lons then lats? These are actually lat x lons. We have reversed the order and clearly defined it:

"Conversely, the DOMINOv2 (Boersma et al., 2011), POMINO (Lin et al., 2015), and DOMINO2_GC (Vinken et al., 2014) retrievals simulate daily profiles at 3° lon × 2° lat (DOMINO) and 0.667° lon × 0.5° lat (POMINO and DOMINO2_GC), respectively..."

For the statement "Valin et al. (2013) showed that the concentration of NO2 downwind of a city increases significantly with wind speed. on Page 3 Lines 24-25, can a range be provided to which this statement is true.
We have added specific numbers based on Fig. 4 in Valin et al. 2013:

"Valin et al. (2013) showed that the concentration of $NO_2$ downwind of a city increases significantly with wind speed, observing that $NO_2$ 100–200 km downwind from Riyadh, Saudi Arabia was approximately 130–250% greater for wind speeds between 6.4–8.3 m $s^{-1}$ than wind speeds $< 1.9$ m $s^{-1}$."

Page 3, Lines 27-29: The authors should explain why OMI is less sensitive at lower altitudes or provide a reference which explains this.
In response to the fifth comment, we added this before Eq. 1. We have included a phrase directing the reader to that explanation here:

"As discussed before Eq. (1), UV/visible satellite observations of $NO_2$ are less sensitive to $NO_2$ at low altitudes..."

In the Introduction, we are informed that this study focuses on Atlanta. The reasoning for this is explained later on in the manuscript, but needs to be mentioned here as well to make it clear why this region is the focus of the study.
We have added a sentence to page 4, around lines 21–22 that explains this reasoning:

"...to demonstrate the impact of day-to-day variations in the modeled $NO_2$ profiles on the calculated AMFs surrounding a major urban area such as Atlanta, GA, USA. Atlanta provides an example of a strong $NO_x$ area source relatively isolated from other sources, with straightforward response of the day-to-day a priori profiles to meteorological variables."

Please reword Lines 30 (P4) 2 (P5) to make the text clearer. i.e. These have been classified as the row anomaly and as of 5 July 2011 affect one-third of the pixels http://projects.knmi.nl/omi/research/product/rowanomaly-background.php), reducing coverage from global daily to global every two days.

We have reworded this to:

"It has a continuous data record since 1 Oct 2004, with global daily coverage for the first $\sim$ 3 years of operation. Since 25 June 2007, anomalous radiances have been observed in several of the pixel rows. These have been classified as the "row anomaly"..."

In the title of section 2.2 please expand out what BEHR represents. Also, P5, L5, BEHR doesnt need to be expanded again as it is done so in the Introduction.

These changes have been made.

In Eqn 2,3 please specifically state what p represents. Also, how is ptp defined (e.g. dynamical, chemical tropopause)?

We have added this to lines 16–21 on p. 5 ($p$ is the vertical coordinate pressure, the tropopause is defined as a static value of 200 hPa). This paragraph has been expanded to address other reviewers' comments as well:

"...$p$ represents the vertical coordinate as pressure. $w(p)$ represents scattering weights derived from the NASA SP v2 look up table. $g(p)$ represents the mixing ratio $NO_2$ a priori profile taken from WRF-Chem, simulated at 12 km resolution in the published BEHR product. $p_0$ represents the surface pressure (clear sky AMF) or cloud pressure (cloudy AMF) of the satellite pixel, and $p_{tp}$ the tropopause pressure. The cloud pressure is that provided in the NASA SP v2 product, and is retrieved using the OMI $O_2$-$O_2$ cloud algorithm (Acarreta et al., 2004; Sneep et al., 2008; Bucsela et al., 2013). A static tropopause pressure of 200 hPa is used. $p_{surf}$ in Eq. (3) is the terrain surface pressure. The integration is carried out using the scheme described in Ziemke et al. (2001) which allows integration of mixing ratio over pressure."

Please provide a reference or explanation why "an assumed cloud albedo of 0.8" is used, on P5 , L 21.

Citations for Stammes et al. (2008) and Bucsela et al. (2013) have been added, this paragraph has been expanded for other comments as well:

"The scattering weights, $w(p)$, depend on the viewing geometry, surface albedo, and terrain pressure altitude. The BEHR algorithm uses the $0.05° \times 0.05°$ combined MODIS MCD43C3 black-sky albedo product and a surface pressure derived from the Global Land One-km Base Elevation project database (`http://www.ngdc.noaa.gov/mgg/topo/globe.html`; Hastings and Dunbar 1999) with a 7.4 km scale height as inputs to the clear sky scattering weights. Cloudy scattering weights treat the cloud pressure as the surface pressure and use an assumed cloud albedo of 0.8 (Stammes et al., 2008; Bucsela et al., 2013). The final AMF is computed as the cloud radiance fraction ($f_{\text{rad}}$) weighted average of the clear and cloudy AMFs (Eq. 4). The cloud radiance fraction is taken from the SP v2 data product (Bucsela et al., 2013)."

P5 Line 29: What does NE1 11 stand for/represent?
This stands for National Emissions Inventory 2011; the abbreviation has been expanded.

The manuscript should not reference papers in prep such as Zare, (in prep) on P6 Line 4.
We have removed this citation; this now reads:

"...the RACM2 scheme is customized to reflect recent advancements in understanding of alkyl nitrate chemistry using Browne et al. (2014) and Schwantes et al. (2015) as a basis."

P5 L5: Please provide justification for using a spin up period of just 5 days.
This is similar to Browne et al. (2014). Qualitatively, after about 24 hours, the initial conditions of $NO_2$ appear to have little effect on the modeled concentrations significantly due to the short lifetime of $NO_2$. The initial concentrations are removed chemically, and the modeled concentrations are driven by the emissions and meteorology. Other species affecting $NO_x$ chemistry, such as ozone and peroxy acetylnitrates (PANs) appear to require about 3 days before the initial concentration no longer has a large impact on the modeled concentrations. We have added a reference to Browne et al. (2014).

"The model is run from 27 May to 30 August, 2013. Similar to Browne et al. (2014), the five day period 27–31 May is treated as a spin up period, thus we use 1 June to 30 August as our study time period."

P6, L20: Please rephrase " 'pseudo-retrieval' that is much simplified compared to a full operational NO2 retrieval" and outline how it is much simpler. Also on L21, please state some examples of co-founding variables.
Both the simplification and confounding variables are addressed in the numbered points below this paragraph (P7, L15–24). We have removed the sentence mentioned in this comment, as we see how it can be confusing, and believe that by doing so, we direct the reader to these points further on in the paragraph where they are addressed in more detail. The paragraph beginning on P.6, L.20 now begins with:

"Two retrievals are used to study the effects of incorporating daily a priori profiles in the BEHR algorithm. The first is what we term a "pseudo-retrieval." To create this retrieval, an 11 × 19 (across × along track) subset of pixels..."

Section 2.5: Firstly, I cannot find an example of where EMG is expanded (i.e. what does it stand for)? Secondly it should be expanded in the introduction where EMG is first mentioned. It should also be written in full for the title of this section.

We have expanded it in both the section title and introduction.

P7 L20: An explanation on why the WRF winds are transformed to earth-relative from grid-relative would be much appreciated.

We have added a concise explanation to P.7, L.16–20:

"The surface wind direction and speed are calculated as the average of the first five layers ($\sim$ 500 m) of the 9 WRF 12 km grid cells closest to Atlanta at 1400 local standard time for each day. WRF wind fields are given relative to the model grid; however, the $x$ and $y$ coordinates of the grid do not correspond directly to longitude and latitude. Therefore, the wind fields must be transformed from grid-relative to earth-relative..."

Eqn 8: Please define specifically what F(x. . ...) represents. Also stating what "erfc" stands for would be useful as well. Im assuming it is "error function"?

We have expanded the paragraph between Eq. 8 and 9 to address both of these concerns, as well as better connect these two equations for the reader:

"where erfc is the error function complement, i.e. $\mathrm{erfc}(x) = 1 - \mathrm{erf}(x)$. $F(x|a, x_0, \mu_x, \sigma_x, B)$ serves as an analytical function that can be fitted to the observed line densities. We find the values of $a$, $x_0$, $\mu_x$, $\sigma_x$, and $B$ that minimize the sum of squared residuals between $F(x|a, x_0, \mu_x, \sigma_x, B)$ and the line densities, $\mathrm{NO_2}(x)$:"

P9, L8-9: As stated above, the reasoning for choosing Atlanta needs to be outlined earlier on in the manuscript.

This was addressed at the previous comment.

In Figure 2b, it would be useful to add a scale for the wind speed or add some text to the caption stating what the min, mean and max winds in the domain are for that period.

We have added these statistics to the caption, which now reads:

"Average conditions for June 2013. (a) The red box indicates the part of the SE US being considered. (b) Surface wind directions from the WRF model; average wind speed is 5.0 m $\mathrm{s^{-1}}$ (min 1.7 m $\mathrm{s^{-1}}$, max 12.7 m $\mathrm{s^{-1}}$). (c) WRF-Chem tropospheric $\mathrm{NO_2}$ columns. (d) AMFs for the pseudo-retrieval calculated using the average monthly $\mathrm{NO_2}$ a priori. The direction of the colorbar is reversed in (d), as small AMFs correspond to high modeled VCDs. In all panels, the star (★) indicates the position of Atlanta. Longitude and latitude are marked on the $x$- and $y$- axes, respectively."

P9-10, L30-1: Please expand on "All pixels show a positive change." Is this correct. Should there not be negative changes somewhere in the domain?

We were also surprised initially that all pixels showed a positive change. The remainder of that paragraph (P10, L1–5 in the original paper) explains the cause of this positive everywhere change. We have added a connective clause that makes it clearer that the rest of the paragraph addresses this point:

> "All pixels show a positive change. This occurs because 77% of the daily profiles have less $NO_2$ than the corresponding monthly average profile..."

Please expand VCDs in the section 3.2 title

We have expanded the definition of VCDs in the section 3.2 title.

P11, L9-11, the authors state that the uncertainty value of 1015 molecules per cm2 can be reduced by a factor of the SQRT(n). However, this assumes that all errors in this uncertainty value are random. Surely, some of the error will be systematic or smoothing errors? Therefore, the authors show take this into account or explain why it can be done like this.

Another reviewer also made this point. Boersma et al. (2004) notes that an explicit separation of the random and systematic components is very difficult, so the errors are usually treated as entirely random. Nevertheless, while we retain the $1 \times 10^{15}$ molec. $cm^{-2}$ criteria for the discussion because of its simplicity, we also added a second criterion that separates error due to spectral fitting, stratospheric separation, and AMF calculation. We assume that the spectral fitting and stratospheric subtraction errors are random, and half of the AMF error. The expanded paragraph is:

> "Implementing the daily profiles also changes the average VCDs, in addition to the day-to-day changes in VCDs discussed above. Figure 4b shows the changes in VCDs averaged over the period studied. The largest decrease around Atlanta is to the northeast, along the direction that the monthly average model results placed the $NO_2$ plume, but clear decreases can also be seen to the northwest and southwest. In these directions, a systematic decrease of up to 8% ($4 \times 10^{14}$ molec. $cm^{-2}$) is observed. Although this change is small, it is expected to be systematic. Statistically, a pixel's a priori profile is more likely to have less surface $NO_2$ when different wind directions are no longer averaged in, thus decreases in the VCD when using a daily a priori profile are more common.
>
> Greater relative changes are observed around the smaller cities of Birmingham (down to $-12.5\%$, $5 \times 10^{-14}$ molec. $cm^{-2}$) and Montgomery (down to $-13\%$, $4 \times 10^{-14}$ molec. $cm^{-2}$). This appears to be due primarily because the areas of emissions are smaller which makes shifts in wind direction have a greater average relative effect on the plume shape.
>
> We also compare this average change to the measurement uncertainty. The uncertainty due to random errors in the retrieval should reduce as the square root of the number of observations, but delineating random and systematic errors

in the retrieval is challenging (Boersma et al., 2004). The most optimistic approach assumes that the global average uncertainty of $1 \times 10^{15}$ molec. cm$^{-2}$ (Bucsela et al., 2013) can be treated entirely as random error, and can be reduced by $\sqrt{40}$ for the number of observations (not impacted by clouds or the row anomaly), to a lower bound of $\sim 1.6 \times 10^{14}$ molec. cm$^{-2}$. Most of the changes near the three cities exceed this lower limit. More realistically, the spectral fitting and stratospheric uncertainty may be considered largely random, but only part of the error in the AMF calculation is random, due to spatial or temporal autocorrelation in the models or ancillary products (Boersma et al., 2004). For simplicity, we assume that the spectral fitting and stratospheric subtraction errors are entirely random, while only half of the error in the AMF is random. This reduces the error from $\sqrt{(0.7 \times 10^{15})^2 + (0.2 \times 10^{15})^2 + (20\%)^2}$ to $\sqrt{(0.11 \times 10^{15})^2 + (0.03 \times 10^{15})^2 + (11.6\%)^2}$. Only the largest changes near Birmingham and Montgomery exceed this threshold. This more conservative estimate suggests that the changes in averages are primarily important for smaller or very geographically concentrated cities, where wind direction can have a large effect. Nevertheless, larger cities may exhibit important changes as well."

The two sentences on P11, L7-9 "The main decrease around Atlanta is to the northeast, along the direction that the monthly average model results placed the NO2 plume. A systematic decrease of 5-10% to the northeast of Atlanta is observed; this is the plume direction in the monthly average profiles." need to be reworded as discussing "northeast" twice is repetitive.

This has been done; we've also better indicated that decreases are seen in other directions as well (see first paragraph of revision for previous comment).

Just double checking on P11, L17, this should definitely "southeast"?

Yes, the wind blows to the southeast most frequently. The average wind direction for June 2013 is to the northeast, but this is because the wind direction usually falls within a 180° arc centered on the northeast.

P12, L12. Should be "a x0" and not "an x0".

According to the Chicago Manual of Style, "an" before the "ex" sound is acceptable, and we prefer that. (http://www.chicagomanualofstyle.org/qanda/data/faq/topics/Usage/faq0068.html)

On P13, L14-19, the t-test is discussed to determine if "differences in emissions and lifetimes are significantly different among the results derived from using the three different a priori profiles...." The t-test assumes that data within the sample population are independent. However, I imagine there will be lots of temporal autocorrelations in the samples. Do the authors account for this and if not, why?

We agree with the reviewer that it is likely that there would be some degree of autocorrelation in the temporal evolution of VCDs over the study period, and so in the day-by-day line densities as well. However, the emissions and lifetime are derived from fitting parameters that fit the dependence of the temporal average line densities as a function of space. Of

course, there will naturally be spatial autocorrelations as well, given the physical processes governing the evolution of the $NO_2$ plume. The EMG function used to fit these line densities should account for these physical processes (Beirle et al., 2011), and according to Chatterjee and Hadi (2012), autocorrelation often appears when the fitting model does not include dependence on a key variable. Since a Durbin-Watson test indicates that there is still unaccounted for spatial autocorrelation, we now acknowledge in the paper that the $t$-tests may underestimate the uncertainty and focus on the fact that these changes will be systematic:

> "We also use 2-sample $t$-tests at the 95% confidence level (Harris, 2010) to determine if differences in emissions and lifetimes given in Table 3 are significantly different among the results derived from using the three different a priori profile sets for a given city and wind speed bin (i.e. we compare the three values of emissions derived using different a priori profiles for Atlanta and wind speeds $\geq 3$ m $s^{-1}$). This found that, for emissions, the choice of a priori leads to statistically different emissions for all five cases. For the derived lifetimes, in all cases the monthly 108 km and daily 12 km a priori are statistically indistinguishable, but the monthly 12 km a priori is statistically different. We note that a Durbin-Watson test indicates some spatial autocorrelation remains, and so the uncertainty may be underestimated and the $t$-tests may be incorrectly identifying the differences as significant in this case (Chatterjee and Hadi, 2012). Even if this is true, with a longer averaging period such as those in Beirle et al. (2011), Valin et al. (2013), and Lu et al. (2015), we would expect the random uncertainties to reduce while the systematic difference from the choice of a priori profile remains. Therefore, the choice of a priori profiles does have an important effect on derived emissions and lifetimes."

On P14, Lines 3-15, comparisons to the NEI 11 emissions are discussed. From the text, the NE1 11 emissions are overestimated by 50%. If the NEI 11 emissions took this into account, which results (e.g. monthly or daily apriori ) which have best agreement with them. Also, on L7, the authors state that the "daily 12 km a priori are within 5- 24%". Are they lower or higher than the NEI 11 emissions or both? The authors have stated that the "coarse monthly a priori" are lower by 43-62%.

We have reorganized this paragraph to accommodate this comment; the sentence indicating which emissions agree with the current and 50% reduced NEI emissions has been brought closer to the statement about the uncertainty in the NEI inventory. That emissions derived from daily 12 km profiles are both greater and less than the NEI inventory has been explicitly stated:

> "We also compare the derived emissions rates to the emissions in a 12 km WRF-Chem model driven by the NEI 11 emission inventory with $NO_x$ emissions scaled to 88.9% of the 2011 values to account for the decrease between 2011 and 2013 (EPA, 2016). WRF-Chem emissions are calculated as the sum of all grid cells within a 50 km radius of the city. 50 km was chosen as the line densities were integrated for $\sim$ 50 km to either side perpendicular to the wind direction. The coarse monthly a priori are 43–61% lower than the NEI-driven emissions, while

emissions derived using daily 12 km a priori are within 5–24% (both greater and less than the NEI emissions). Recent work (e.g. Travis et al. 2016 and references within) suggests that the NEI inventory is overestimated by $\sim$ 50% using both satellite and in situ observations. Emissions derived using daily 12 km show the best agreement to the current NEI inventory, and emissions derived using monthly 108 km a priori profile agree with the NEI inventory reduced by 50%. Therefore, we cannot say which a priori profiles provide the best measurement of emissions by comparing to NEI...."

**Supplement**

P1, L16: Why would we expect the mean and median differences to be 0?

Since the upper troposphere is generally removed from $NO_x$ sources, we expect $NO_2$ concentrations there to be fairly stable. Deviations from the average should mostly be due to larger scale motions of air masses, also separated from direct influence from $NO_x$ sources, so the deviations should be essentially random and normal. Only at the surface with direct influence of $NO_x$ sources do we expect a non-normal distribution of $NO_2$ concentrations, and so a non-zero mean difference in the average of AMF calculated from the monthly average profile vs. the daily profiles.

P1, L20-22: "This, combined with the greater scattering weights at these altitudes, explains why the effect on the AMF is as large as it is, although day-to-day changes in the boundary layer still dominate the effect using daily profiles has on the AMFs,". The "," at the end of the sentence should be a full stop. Secondly, can the impact of the scattering weights at this altitude be quantified, say in comparison to the impact of the apriori on the AMFs?

Thank you again for careful proofreading. As far as quantifying the effect of the scattering weights, the response of the upper tropospheric scattering weights to perturbations in the inputs to the radiative transfer model that computes them could be calculated, but is not particularly relevant to this part of the work. More important here is that scattering weights in the UT are 2–8x higher than near the surface, so small perturbations in the $NO_2$ profile have larger effects on the AMF than the same perturbations would have near the surface. We have included this factor of 2–8x:

"Day-to-day changes in the free tropospheric a priori profile are smaller in magnitude than those in the boundary layer, but usually occur over a much greater vertical extent. Further, the scattering weights are greater at these altitudes ($\sim$2–8 times those near the surface), amplifying the effect of small changes in the profile shape at these altitudes. This explains why the effect on the AMF is as large as it is, although day-to-day changes in the boundary layer still dominate the effect using daily profiles has on the AMFs."

P1, L30: Is this period of 91 days long enough for the averaging to have no net impact?

Yes, as evidenced by the fact that the average difference between the hybrid and full profiles is 0 (Fig. S3).

P2, L 9: Should be "Atlanta, nevertheless" or "Atlanta. Nevertheless".
Corrected, thank you.

P4, L4-5: Should be these "]" brackets and not ")"?
No, in a range, infinity should be accompanied by a round parenthesis since no finite range can truly include infinity.

P5, L20: "as the errors contributing to it should be random in nature". Why is this the case? No systematic errors?
This is similar to a previous comment on the uncertainty in VCDs; while there is definitely some systematic component, the errors are usually treated as random in practice (Boersma et al., 2004). Removing the factor of $\sqrt{n}$ does not alter our conclusions however, because we calculated $n$ conservatively, so we will use the flat 25% from Lu et al. (2015). Table 4 and this section have both been updated accordingly (P.5 L.19–24 of supplement removed).
Updated Table 4:

| | | Atlanta | | | Birmingham | | |
|---|---|---|---|---|---|---|---|
| | Wind speed bin | Monthly 108 km | Monthly 12 km | Daily 12 km | Monthly 108 km | Monthly 12 km | Daily 12 km |
| E (Mg $NO_x$ $h^{-1}$) | WRF-Chem NEI | | **13.74** | | | **10.49** | |
| | $\geq 3.0$ | $6. \pm 4$ | $16. \pm 9$ | $11. \pm 7$ | $4. \pm 2$ | $10. \pm 6$ | $8. \pm 5$ |
| | $\geq 4.0$ | $6. \pm 3$ | $17 \pm 11$ | $11. \pm 6$ | $4. \pm 2$ | $13. \pm 7$ | $9. \pm 5$ |
| | $\geq 5.0$ | - | - | - | $6. \pm 3$ | $15. \pm 9$ | $11. \pm 6$ |
| $\tau$ (h) | $\geq 3.0$ | $1.6 \pm 0.7$ | $1.3 \pm 0.5$ | $1.7 \pm 0.7$ | $2.5 \pm 1.0$ | $1.8 \pm 0.7$ | $2.6 \pm 1.0$ |
| | $\geq 4.0$ | $1.8 \pm 0.7$ | $1.2 \pm 0.5$ | $1.8 \pm 0.7$ | $2.1 \pm 0.9$ | $1.5 \pm 0.6$ | $2.2 \pm 0.9$ |
| | $\geq 5.0$ | - | - | - | $1.8 \pm 0.7$ | $1.3 \pm 0.5$ | $1.8 \pm 0.7$ |

Table R1: Values of the emission rates ($E$) and effective lifetime ($\tau$) obtained when the separation between slow and fast winds is set at 3, 4, and 5 m $s^{-1}$. For comparison, the total $NO_x$ emission for all 12 km WRF-Chem grid cells within 50 km of each city is given. These emissions are derived from NEI 11 and scaled to 88.9% to account for 2011–2013 reductions. Uncertainties calculated as described in the supplement.

P6, L15: "). nfit"?
The period should go inside the parenthesis (as it is) when the full sentence in parenthetical.

## References


Acarreta, J. R., De Haan, J. F., and Stammes, P.: Cloud pressure retrieval using the O2-O2 absorption band at 477 nm, J. Geophys. Res. Atmos., 109, doi:10.1029/2003JD003915, URL `http://dx.doi.org/10.1029/2003JD003915`, d05204, 2004.

Beirle, S., Boersma, K., Platt, U., Lawrence, M., and Wagner, T.: "Megacity Emissions and Lifetimes of Nitrogen Oxides Probed from Space", Science, 333, 1737–1739, 2011.

Boersma, K., Eskes, H., and Brinksma, E.: "Error analysis for tropospheric $NO_2$ retrieval from space, J. Geophys. Res. Atmos., 106, D04 311, doi:10.1029/2003JD003962, 2004.

Boersma, K., Eskes, H., Dirksen, R., van der A, R., Veefkind, J., Stammes, P., Huijnen, V., Kleipool, Q., Sneep, M., Claas, J., Leitão, J., Richter, A., Zhou, Y., and Brunner, D.: "An improved tropospheric $NO_2$ column retrieval algorithm for the Ozone Monitoring Instrument, Atmos. Meas. Tech., 4, 1905–1928, doi:10.5194/amt-4-1905-2011, 2011.

Browne, E. C., Wooldridge, P. J., Min, K.-E., and Cohen, R. C.: On the role of monoterpene chemistry in the remote continental boundary layer, Atmos. Chem. Phys., 14, 1225–1238, doi:10.5194/acp-14-1225-2014, 2014.

Bucsela, E., Krotkov, N., Celarier, E., Lamsal, L., Swartz, W., Bhartia, P., Boersma, K., Veefkind, J., Gleason, J., and Pickering, K.: "A new tropospheric and stratospheric $NO_2$ retrieval algorithm for nadir-viewing satellite instruments: applications to OMI, Atmos. Meas. Tech., 6, 2607–2626, doi:10.5194/amt-6-2607-2013, 2013.

Chatterjee, S. and Hadi, A.: Regression Analysis by Example, Ch 8: The Problem of Correlated Errors, John Wiley & Sons Inc., 2012.

de Foy, B., Wilkins, J., Lu, Z., Streets, D., and Duncan, B.: Model evaluation of methods for estimating surface emissions and chemical lifetimes from satellite data, Atmos. Environ., 98, 66–77, doi:10.1016/j.atmosenv.2014.08.051, 2014.

EPA: Air Pollutant Emissions Trends Data, URL `https://www.epa.gov/air-emissions-inventories/air-pollutant-emissions-trends-data`, 2016.

Harris, D.: Comparison of Means with Student's $t$, chap. 4-3, pp. 76–78, W.H. Freeman, 8th edn., 2010.

Hastings, D. and Dunbar, P.: Global Land One-kilometer Base Elevation (GLOBE) Digital Elevation Model, Documentation, Volume 1.0. National Oceanic and Atmospheric Administration, National Geophysical Data Center, 325 Broadway, Boulder, Colorado 80303, U.S.A., 1999.

Hudson, R., Kim, J.-H., and Anne M., T.: On the derivation of tropospheric column ozone from radiances measured by the total ozone mapping spectrometer, J. Geophys. Res. Atmos., 100, 11,134–11,145, 1995.

Levelt, P., van der Oord, G., Dobber, M., Mälkki, A., Visser, H., de Vries, J., Stammes, P., Lundell, J., and Saari, H.: The Ozone Monitoring Instrument, IEEE Trans. Geosci. Remote Sense., 44, 1093–1101, doi:10.1109/TGRS.2006.872333, 2006.

Lin, J.-T., Liu, M.-Y., Xin, J.-Y., Boersma, K. F., Spurr, R., Martin, R., and Zhang, Q.: Influence of aerosols and surface reflectance on satellite $NO_2$ retrieval: seasonal and spatial characteristics and implications for $NO_x$ emission constraints, Atmos. Chem. Phys., 15, 11 217–11 241, doi:10.5194/acp-15-11217-2015, 2015.

Lu, Z., Streets, D., de Foy, B., Lamsal, L., Duncan, B., and Xing, J.: "Emissions of nitrogen oxides from US urban areas: estimation from Ozone Monitoring Instrument retrievals for 2005–2014", Atmos. Chem. Phys., 15, 10 367–10 383, doi:10.5194/acp-15-10367-2015, 2015.

McLinden, C. A., Fioletov, V., Boersma, K. F., Kharol, S. K., Krotkov, N., Lamsal, L., Makar, P. A., Martin, R. V., Veefkind, J. P., and Yang, K.: Improved satellite retrievals of $NO_2$ and $SO_2$ over the Canadian oil sands and comparisons with surface measurements, Atmos. Chem. Phys., 14, 3637–3656, doi:10.5194/acp-14-3637-2014, 2014.

Richter, A. and Wagner, T.: The Use of UV, Visible and Near IR Solar Back Scattered Radiation to Determine Trace Gases, in: The Remote Sensing of Tropospheric Composition from Space, edited by Burrows, J., Platt, U., and Borrell, P., Springer, New York, 2011.

Russell, A., Perring, A., Valin, L., Bucsela, E., Browne, E., Min, K., Wooldridge, P., and Cohen, R.: "A high spatial resolution retrieval of $NO_2$ column densities from OMI: method and evalutation", Atmos. Chem. Phys., 11, 8543–8554, doi:10.5194/acp-11-8543-2011, 2011.

Russell, A. R., Valin, L. C., and Cohen, R. C.: Trends in OMI $NO_2$ observations over the United States: effects of emission control technology and the economic recession, Atmos. Chem. Phys., 12, 12 197–12 209, doi:10.5194/acp-12-12197-2012, 2012.

Schwantes, R. H., Teng, A. P., Nguyen, T. B., Coggon, M. M., Crounse, J. D., St. Clair, J. M., Zhang, X., Schilling, K. A., Seinfeld, J. H., and Wennberg, P. O.: Isoprene $NO_3$ Oxidation Products from the $RO_2$ + $HO_2$ Pathway, J. Phys. Chem. A, 119, 10 158–10 171, doi:10.1021/acs.jpca.5b06355, 2015.

Sneep, M., de Haan, J. F., Stammes, P., Wang, P., Vanbauce, C., Joiner, J., Vasilkov, A. P., and Levelt, P. F.: Three-way comparison between OMI and PARASOL cloud pressure products, J. Geophys. Res. Atmos., 113, doi:10.1029/2007JD008694, d15S23, 2008.

Stammes, P., Sneep, M., de Haan, J. F., Veefkind, J. P., Wang, P., and Levelt, P. F.: Effective cloud fractions from the Ozone Monitoring Instrument: Theoretical framework and validation, J. Geophys. Res. Atmos., 113, n/a–n/a, doi:10.1029/2007JD008820, URL 10.1029/2007JD008820, d16S38, 2008.

Travis, K. R., Jacob, D. J., Fisher, J. A., Kim, P. S., Marais, E. A., Zhu, L., Yu, K., Miller, C. C., Yantosca, R. M., Sulprizio, M. P., Thompson, A. M., Wennberg, P. O., Crounse, J. D., St. Clair, J. M., Cohen, R. C., Laugher, J. L., Dibb, J. E., Hall, S. R., Ullmann, K., Wolfe, G. M., Pollack, I. B., Peischl, J., Neuman, J. A., and Zhou, X.: NOx emissions, isoprene oxidation pathways, vertical mixing, and implications for surface ozone in the Southeast United States, Atmos. Chem. Phys. Discuss., 2016, 1–32, doi: 10.5194/acp-2016-110, 2016.

Valin, L., Russell, A., and Cohen, R.: "Variations of OH radical in an urban plume inferred from $NO_2$ column measurements", Geophys. Res. Lett., 40, 1856–1860, doi:10.1002/grl.50267, 2013.

Vinken, G. C. M., Boersma, K. F., van Donkelaar, A., and Zhang, L.: Constraints on ship $NO_x$ emissions in Europe using GEOS-Chem and OMI satellite $NO_2$ observations, Atmos. Chem. Phys., 14, 1353–1369, doi:10.5194/acp-14-1353-2014, URL `http://www.atmos-chem-phys.net/14/1353/2014/`, 2014.

Ziemke, J., Chandra, S., and Bhartia, P.: "Cloud slicing: A new technique to derive upper tropospheric ozone from satellite measurements", J. Geophys. Res. Atmos., 106, 9853–9867, 2001.

# Effects of daily meteorology on the interpretation of space-based remote sensing of $NO_2$

## Response to Anonymous Referee #2

Joshua L. Laughner, Azimeh Zare, and Ronald C. Cohen

October 20, 2016

We thank the reviewer for their positive response and very careful reading of the manuscript. The reviewer's comments will be shown in red, our response in blue, and changes made to the paper are shown in black block quotes. Unless otherwise indicated, page and line numbers correspond to the original paper. Figures, tables, or equations referenced as "R$n$" are numbered within this response; if these are used in the changes to the paper, they will be replaced with the proper number in the final paper. Figures, tables, and equations numbered normally refer to the numbers in the original discussion paper.

While I see the nice qualitative discussion of the effects as a strong point of this manuscript, the quantitative results are much less convincing in my opinion. The reason for my skepticism is the large change in emissions and lifetimes the authors find when changing their a priori spatial or temporal resolution in combination with the large uncertainties given in the tables. Most of the results are in agreement within uncertainties when changing from monthly to daily a priori in spite of the large changes seen. To me this indicates that the time period used for averaging is too short to really separate the effect of a priori changes from noise in the data, and as the authors acknowledge, all previous studies used much longer averaging times. Please comment on the magnitude of uncertainties and the significance of differences seen.

We do understand the reviewer's skepticism, given the magnitude of the uncertainties. In the original paper, we had already included statistical tests of the significance of these differences using $t$-tests (P14, L18–23) which showed that, in most cases, the differences due to the choice of a priori profiles are statistically significant at the 95% confidence level, except for lifetimes derived using the monthly 108 km and daily 12 km profiles. Reviewer #1 raised the possibility of autocorrelations in the data, which would indicate that the uncertainties were underestimated. While we do not believe that temporal autocorrelations are significant in this method, some spatial autocorrelation seems to be unaccounted for by the EMG fit. In response to Reviewer #1, we have acknowledged this possibility in the revised paper, but note that the differences are systematic, and therefore are not expected to be reduced by additional averaging, while the uncertainties will be. Added at P.13, L.19:

> "We note that a Durbin-Watson test indicates some spatial autocorrelation remains, and so the uncertainty may be underestimated and the $t$-tests may be

incorrectly identifying the differences as significant in this case (Chatterjee and Hadi, 2012). Even if this is true, with a longer averaging period such as those in Beirle et al. (2011), Valin et al. (2013), and Lu et al. (2015), we would expect the random uncertainties to reduce while the systematic difference from the choice of a priori profile remains. Therefore, the choice of a priori profiles does have an important effect on derived emissions and lifetimes."

In the discussion of the results both in the text and in the abstract, I'm confused by statements such as "Comparing an optimized retrieval to a more standard one, we find that NOx emissions estimated from space-based remote sensing can increase by 100% when daily variations in plume location and shape are accounted for in the retrieval." If I'm not misinterpreting Table 4, the change in emissions when moving from monthly to daily a priori is closer to 45% and actually is a decrease, not an increase of estimated emissions. This also makes more sense considering the qualitative discussion given in the first part of the paper. The factor of 2 increase is relative to a low spatial resolution a priori which is also interesting but not the focus of the study and also not what is suggested by the formulations in the text. I think these statements need to be rephrased.

Thank you for clearly explaining what you found confusing about this statement; we agree now that its present form is unclear. We have reworded it in both the abstract and conclusions to clearly indicate that there are different effects of spatial and temporal resolution on the emissions. While the effect of temporal resolution is indeed the main focus of this paper, it is important to separate the effects of spatial and temporal resolution since no application of the EMG fitting method has yet used a retrieval with high spatial resolution profiles (Beirle et al., 2011; Valin et al., 2013; Lu et al., 2015; Liu et al., 2016).

In the abstract, P.2 L.8–9 changed to:

> "Additionally, we show that $NO_x$ emissions estimated from space-based remote sensing using daily, high spatial resolution a priori profiles are $\sim$ 100% greater compared to a retrieval using spatially coarse a priori profiles, and 20–45% less compared to a retrieval using monthly averaged high spatial resolution profiles."

And in the conclusion, P.15 L.3–5 changed to:

> "When the methods of Lu et al. (2015) are applied to these prototype retrievals, significant changes in derived $NO_x$ emissions are found, increasing by as much as 100% for Atlanta compared to emissions derived from a retrieval using coarse a priori profiles."

The discussion of standard mathematical methods for fitting a function to the decay curve is a bit out of place in such an article, in particular as the method used for emission estimation is not the topic of the paper. I would suggest to shorten this part and to remove the discussion of Matlab internals which are of little interest to the reader.

Both other reviewers also requested that references to Matlab functions be made more general, which we have done. The technical considerations have also been moved to the supplement (P.8, L.9–29).

The approach taken to averaging the model data in time (Equation 5) appears overly complex and not transparent. The obvious way to treat this problem is simple interpolation in time to the OMI overpass.

Effectively this approach is an interpolation, as an interpolation can be recast as a weighed average. If we are interpolating to a point $(x_q, y_q)$ between $(x_1, y_1)$ and $(x_2, y_2)$:

$$\begin{aligned} y_q &= y_1 + m(x_q - x_1) \\ &= y_1 + \left(\frac{y_2 - y_1}{x_2 - x_1}\right)(x_q - x_1) \\ &= \frac{x_q - x_1}{x_2 - x_1} y_2 + \left(1 - \frac{x_q - x_1}{x_2 - x_1}\right) y_1 \\ &\equiv w y_2 + (1 - w) y_1 \text{ where } w = \frac{x_q - x_1}{x_2 - x_1} \end{aligned}$$

This approach assumes that the average OMI overpass time varies linearly with longitude. We have added a paragraph after Eq. (5) and a section to the supplement explaining this reasoning; essentially, as shown in Fig. R1, there is the possibility that an area (such as Atlanta) may be covered by the west edge of an earlier swath or the east edge of a later swath, so these weights are an *ad hoc* attempt to choose profiles that approximate the average overpass time.

After Eq. (5):

> "The weighting scheme in Eq. (5) was chosen over simply using the model output for 1400 local standard time for each latitude to create smooth transitions between adjoining time zones. This attempts to account for the day-to-day variability in OMI overpass tracks as well as the fact that pixels on the edge of a swath can be observed in two consecutive overpasses at different local times. More detail is given in the supplement."

And in the supplement:

> "When computing the monthly average profiles, it is necessary to use profiles that represent OMI's overpass time, typically quoted as 13:30 to 13:45 local standard time (e.g. McLinden et al. 2014; Levelt et al. 2006). To average the profiles output from WRF-Chem, weights were calculated that fulfilled two requirements:
>
> 1. The weights should be 1 at OMI overpass time and 0 when more than 1 hour away from overpass time.
> 2. The transition between profiles from different hours should be smooth.
>
> For #1, we assume that the average overpass time is 1330 local standard time. We compute local standard time as:

$$t_{\text{apriori, local}} = \frac{l}{15} + t_{\text{apriori, utc}} \tag{R1}$$

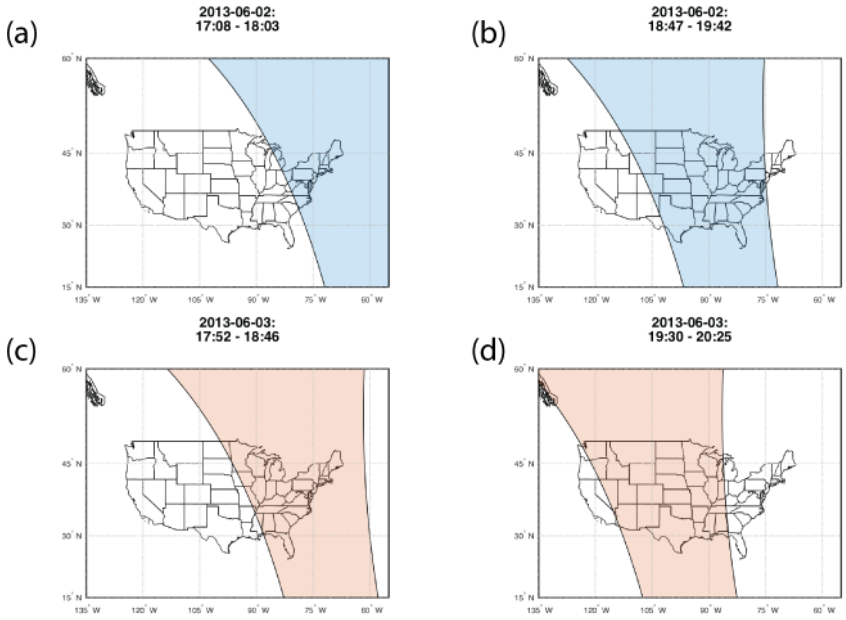


Figure R1: Swaths covering the east coast of the US for 2 June 2013 (a,b) and 3 June 2013 (c,d). The times given are the start and end times of the daytime half of the orbit in UTC. As shown, on different days, the time of the OMI swath that covers Atlanta can vary by up to an hour.

where $t_{\text{apriori, local}}$ is the local standard time in hours past midnight, $t_{\text{apriori, utc}}$ the UTC time in hours past midnight, and $l$ the longitude (west is negative). To meet the second requirement, this is a continuous function, rather than a step function (where each 15° longitudinal segment/time zone has a single local time). Areas further west in a time zone are more likely to be observed on the east edge of a later OMI swath, and vice versa for areas further east. This weighting includes some influence from later profiles to account for this.

The weights from Eq. (5) are derived from:

$$w = 1 - |t_{\text{overpass}} - t_{\text{apriori, local}}| = 1 - \left|13.5 - \frac{l}{15} - h\right| \tag{R2}$$

where $t_{\text{overpass}}$ is the assumed overpass time for OMI and $h \equiv t_{\text{apriori, utc}}$. If $w < 0$, $w$ is set to 0. This gives us the desired form where the weights smoothly vary in time.

”

In the course of revisiting this weighting method, we redid the key runs using an assumed OMI overpass time of 1330 LST (which is more consistent with previous papers, e.g. McLinden et al. 2014, compared to 1400 LST used originally). The difference is very small and does not affect the conclusions of the paper, but we have updated the appropriate figures and parts of the text.

On a more general note I think that the paper would benefit from a short discussion of the impact model errors could have on the results. It is obvious that in theory, using daily a priori data is better than using monthly averages as the process of NO2 retrieval is not linear. However, in real data this might not necessarily be true. At the high spatial resolution of the model used here, even a small uncertainty in wind direction, emission height or emission source location can move the NO2 plume into different model grid cells, potentially leading to poor matching of plume position in measurement and model and thus wrong air mass factors and NO2 columns. I find this an interesting topic in particular in view of future instruments having improved spatial resolution.

Agreed, model uncertainty is an important (and deep) topic highly relevant to this paper, so we have added a section to the discussion with our thoughts on this topic. There has been some interesting work comparing WRF-Chem simulations to measurements both directly (Tie et al., 2007; Zhang et al., 2009) and in terms of spatial variability (Follette-Cook et al., 2015) which suggest WRF does capture daily wind fields and $NO_2$ distribution reasonably accurately. We would also expect the overall uncertainty to change source, but not necessarily magnitude between monthly and daily profiles, as monthly profiles effectively have the true day-to-day variability as a source of uncertainty that daily profiles do not; but in exchange, the random error in the monthly profiles is reduced through averaging. We have added a new section at the beginning of the discussion that covers this point:

> "WRF-Chem has generally been found to reproduce wind fields, especially above 2 m $s^{-1}$ (Tie et al., 2007; Zhang et al., 2009), and spatial variability of trace gases (Follette-Cook et al., 2015) well. Nevertheless, a natural concern when modeling daily $NO_2$ profiles for satellite retrievals is the accuracy of the plume location. We, however, note that the transition from monthly average to daily profiles does not necessarily result in increased model uncertainty, but rather a change in the type of uncertainty.
>
> When using monthly average profiles, the uncertainty in the modeled $NO_2$ concentrations compared to the true mean will be reduced (assuming at least some component of the error is random in nature), but the true day-to-day variability not captured by the monthly average effectively becomes a new error term. In contrast, when using daily profiles, the random model error is not reduced, but the day-to-day variability is also not averaged out. Ideally, the error in a set of daily profiles will manifest as deviation from the true set of profiles for that day, rather than the monthly profiles' smaller deviation from a mean set of profiles that itself may not represent any single day.
>
> An important step in managing the uncertainty in the daily profiles is to constrain the modeled meteorology with observations or reanalysis datasets. By default, meteorology in WRF is constrained via initial and boundary conditions only. With larger domains and longer runs, further constraints using four-dimensional data assimilation (FDDA, Liu et al. 2006) and/or objective analysis (Follette-Cook et al., 2015; Wang et al., 2014; Yegorova et al., 2011), possibly combined with periodic model reinitialization (Otte, 2008) are strongly recommended."

Page 7, line 5: Cloudy AMF is smaller, not lager [larger] for boundary layer NO2 profiles

Thank you for bringing this up; we double checked this statement by comparing clear sky and cloudy AMFs from both the NASA standard product and our own, and found that in both products, the regression slope of cloudy vs. clear sky AMFs is $> 1$, but that there is sufficient scatter that it is hard to say definitively that one is larger or smaller. Thus, we've reworded this point to simply identify that clear and cloudy AMFs can be significantly *different*, but not that one is necessarily greater than the other. P.7, L.5 changed to:

> "Day-to-day variations in cloud fraction also lead to large changes in AMF because the presence of clouds changes both the scattering weights (due to high assumed reflectivity of clouds and smaller effective surface pressure compared to ground) while also obscuring the $NO_2$ profile below the cloud."

Page [15] line 6: I do not understand the sentence Further work is needed to understand the impact of this change on top down constraints of NOx emissions, given the recent work showing that bottom up estimates are high by 50%. I think the relevance is obvious if you believe your own results all previous estimates based on this technique and using monthly high resolution a priori profiles give too high emission estimates. Whether or not the emission inventory is off is another topic (which could of course also impact on your AMF values and thus emission estimates) and should not be mixed here.

Indeed, any previous work using monthly high resolution profiles would be biased high, which would fit in nicely with Travis et al. (2016) indicating that the bottom up inventory is too high. However, the previous application of the EMG method to US emissions used a retrieval with coarse a priori profiles (Lu et al. 2015); our results indicate that emissions found using a retrieval with spatially coarse set of a priori profiles will be lower than when using daily, fine spatial resolution profiles. Hence the need for more work–Travis et al. (2016) found that the bottom up inventory should be reduced by $\sim 50\%$ using GEOS-Chem as a transfer standard between aircraft and satellite measurements, while we find that, with better a priori, the bottom up inventory is about 25% high.

We have edited this sentence to make this clearer, it now reads:

> "Emissions derived using the fine daily a priori are within 25% of the bottom up number from the NEI inventory, a smaller reduction than that suggested by Travis et al. (2016). Future work will aim to resolve this difference."

Finally, each of the following technical issues has been addressed

Equation 2: $w_s(p)$ is later written as $w(p)$

Equation 4: Please add how cloud radiance fraction was computed
Added just before Eq.(4):

> "The cloud radiance fraction is taken from the SP v2 data product (Bucsela et al., 2013)."

Page 6: Add reference for MOZART model
Added Emmons et al. (2010).

Page 14, line 17: something missing here?
The "and" after "*a*" was unnecessary.

Conclusions, line 28: Please add again that you count days even if only a single pixel shows a change larger than the noise (which I personally find a strange way of counting)

> "Up to 59% of days with valid observations exhibit changes in VCDs $> 1 \times 10^{15}$ molec. cm$^{-2}$ in at least one pixel."

## References


Beirle, S., Boersma, K., Platt, U., Lawrence, M., and Wagner, T.: "Megacity Emissions and Lifetimes of Nitrogen Oxides Probed from Space", Science, 333, 1737–1739, 2011.

Bucsela, E., Krotkov, N., Celarier, E., Lamsal, L., Swartz, W., Bhartia, P., Boersma, K., Veefkind, J., Gleason, J., and Pickering, K.: "A new tropospheric and stratospheric $NO_2$ retrieval algorithm for nadir-viewing satellite instruments: applications to OMI, Atmos. Meas. Tech., 6, 2607–2626, doi:10.5194/amt-6-2607-2013, 2013.

Chatterjee, S. and Hadi, A.: Regression Analysis by Example, Ch 8: The Problem of Correlated Errors, John Wiley & Sons Inc., 2012.

Emmons, L. K., Walters, S., Hess, P. G., Lamarque, J.-F., Pfister, G. G., Fillmore, D., Granier, C., Guenther, A., Kinnison, D., Laepple, T., Orlando, J., Tie, X., Tyndall, G., Wiedinmyer, C., Baughcum, S. L., and Kloster, S.: Description and evaluation of the Model for Ozone and Related chemical Tracers, version 4 (MOZART-4), Geosci. Model Dev., 3, 43–67, doi:10.5194/gmd-3-43-2010, URL `http://www.geosci-model-dev.net/3/43/2010/`, 2010.

Follette-Cook, M., Pickering, K., Crawford, J., Duncan, B., Loughner, C., Diskin, G., Fried, A., and Weinheimer, A.: Spatial and temporal variability of trace gas columns derived from WRF/Chem regional model output: Planning for geostationary observations of atmospheric composition, Atmos. Environ., 118, 28–44, doi:10.1016/j.atmosenv.2015.07.024, 2015.

Levelt, P., van der Oord, G., Dobber, M., Mälkki, A., Visser, H., de Vries, J., Stammes, P., Lundell, J., and Saari, H.: The Ozone Monitoring Instrument, IEEE Trans. Geosci. Remote Sense., 44, 1093–1101, doi:10.1109/TGRS.2006.872333, 2006.

Liu, F., Beirle, S., Zhang, Q., Dörner, S., He, K., and Wagner, T.: NOx lifetimes and emissions of cities and power plants in polluted background estimated by satellite observations, Atmos. Chem. Phys., 16, 5283–5298, doi:10.5194/acp-16-5283-2016, 2016.

Liu, Y., Bourgeois, A., Warner, T., Swerdlin, S., and Hacker, J.: Implementation of the observation-nudging based on FDDA into WRF for supporting AFEC test operations. 6th WRF Conference, NCAR, Boulder, CO, USA, 2006.

Lu, Z., Streets, D., de Foy, B., Lamsal, L., Duncan, B., and Xing, J.: "Emissions of nitrogen oxides from US urban areas: estimation from Ozone Monitoring Instrument retrievals for 2005–2014", Atmos. Chem. Phys., 15, 10 367–10 383, doi:10.5194/acp-15-10367-2015, 2015.

McLinden, C. A., Fioletov, V., Boersma, K. F., Kharol, S. K., Krotkov, N., Lamsal, L., Makar, P. A., Martin, R. V., Veefkind, J. P., and Yang, K.: Improved satellite retrievals of $NO_2$ and $SO_2$ over the Canadian oil sands and comparisons with surface measurements, Atmos. Chem. Phys., 14, 3637–3656, doi:10.5194/acp-14-3637-2014, 2014.

Otte, T.: The Impact of Nudging in the Meteorological Model for Retrospective Air Quality Simulations. Part I: Evaluation against National Observation Networks., J. Appl. Meteorol. Clim., 47, 1853–1867, doi:10.1175/2007JAMC1790.1, 2008.

Tie, X., Madronich, S., Li, G., Ying, Z., Zhang, R., Garcia, A., Lee-Taylor, J., and Liu, Y.: Characterizations of chemical oxidants in Mexico City: A regional chemical dynamical model (WRF-Chem) study, Atmos. Environ., 41, 1989 – 2008, doi:10.1016/j.atmosenv.2006.10.053, 2007.

Travis, K. R., Jacob, D. J., Fisher, J. A., Kim, P. S., Marais, E. A., Zhu, L., Yu, K., Miller, C. C., Yantosca, R. M., Sulprizio, M. P., Thompson, A. M., Wennberg, P. O., Crounse, J. D., St. Clair, J. M., Cohen, R. C., Laugher, J. L., Dibb, J. E., Hall, S. R., Ullmann, K., Wolfe, G. M., Pollack, I. B., Peischl, J., Neuman, J. A., and Zhou, X.: NOx emissions, isoprene oxidation pathways, vertical mixing, and implications for surface ozone in the Southeast United States, Atmos. Chem. Phys. Discuss., 2016, 1–32, doi:10.5194/acp-2016-110, 2016.

Valin, L., Russell, A., and Cohen, R.: "Variations of OH radical in an urban plume inferred from $NO_2$ column measurements", Geophys. Res. Lett., 40, 1856–1860, doi:10.1002/grl.50267, 2013.

Wang, W., Bruyère, C., Duda, M., Dudhia, J., Gill, D., Kavulich, M., Keene, K., Lin, H.-C., Michalakes, J., Rizvi, S., and Zhang, X.: WRF-ARW Version 3.5 User's Guide: Chapter 7: Objective Analysis (OBSGRID), 2014.

Yegorova, E. A., Allen, D. J., Loughner, C. P., Pickering, K. E., and Dickerson, R. R.: Characterization of an eastern U.S. severe air pollution episode using WRF/Chem, J. Geophys. Res. Atmos., 116, doi:10.1029/2010JD015054, d17306, 2011.

Zhang, Y., Dubey, M. K., Olsen, S. C., Zheng, J., and Zhang, R.: Comparisons of WRF/Chem simulations in Mexico City with ground-based RAMA measurements during the 2006-MILAGRO, Atmos. Chem. Phys., 9, 3777–3798, doi:10.5194/acp-9-3777-2009, URL `http://www.atmos-chem-phys.net/9/3777/2009/`, 2009.

# Effects of daily meteorology on the interpretation of space-based remote sensing of $NO_2$

## Response to Anonymous Referee #3

Joshua L. Laughner, Azimeh Zare, and Ronald C. Cohen

October 21, 2016

We thank the reviewer for their helpful comments, especially the points of clarification in the introduction. The reviewer's comments will be shown in red, our response in blue, and changes made to the paper are shown in black block quotes. Unless otherwise indicated, page and line numbers correspond to the original paper. Figures, tables, or equations referenced as "R$n$" are numbered within this response; if these are used in the changes to the paper, they will be replaced with the proper number in the final paper. Figures, tables, and equations numbered normally refer to the numbers in the original discussion paper.

One limitation is the focus on only one area (Atlanta, GA) and one season (Summer). As pointed out by another reviewer, focusing on such a short period leads to a limited dataset, from which it is difficult to obtain estimates of emissions and lifetimes that are significantly different. Since the differences in the estimated emissions are at least a factor of 2, it should be feasible to achieve statistically significant differences by analysing a longer period. This would strengthen the paper considerably.

We are glad to see that the reviewer is interested in the application of daily profiles when constraining emissions and lifetime. It is definitely expected that extending the analysis to a longer time period would allow a more quantitative analysis of emissions and lifetime, but the goal of this paper was primarily to show that there is an important difference in the AMFs and therefore VCDs retrieved using daily vs. monthly profiles, and that these differences do impact the emissions and lifetime inferred from the product. While the uncertainties in the emissions and lifetimes are large, we conclude that the differences due to the a priori are systematic and describe our reasoning why. We hope to extend the time period and geographic area studied to get quantitative estimates of emissions and lifetimes across a number of US cities, and that others will keep these results in mind when considering top-down emissions and lifetime constraints.

The systematic nature of these changes is discussed on P.13 L.20–P.14–L.2. In response to another reviewer's comment, this paragraph has been extended starting from P.13 L.31:

> "In the EMG fit, this manifests as a too short lifetime. As the emissions are inversely proportional to lifetime (Eq. 11), emissions derived using the monthly 12 km a priori profiles will be too great. Therefore, when using a retrieval with a priori profile at fine spatial resolution, daily temporal resolution of the a priori

profiles is necessary to prevent underestimating the lifetime. Further, the spatial resolution of the a priori profiles has a large impact on the magnitude of the derived emissions. To reduce the systematic biases in emissions and lifetime from the choice of a priori profile, it is necessary to simulate these profiles at fine spatial and daily temporal resolution."

We have also added the following sentence on P.4, L.21 to make clear that our goal is not yet to quantitatively constrain emissions and lifetime, but to demonstrate that the systematic error due to the use of monthly average profiles is important and should be addressed:

"...meteorological variables. Our point is not to derive exact answers for the size and frequency of the effects of daily profiles, but rather to illustrate that these effects are large enough that their role should be assessed in any future analysis that does attempt to interpret space-based remote sensing of $NO_x$. We show that the variability..."

Then there is a serious error in the theoretical framework for BEHR AMFs. According to Eq. (2) and the text in section 2.2, the cloudy AMF is calculated only between the cloud pressure level and the tropopause. In principle this can be done, but then the retrieval needs to account for a so-called ghost column [Burrows et al., 1999]. A ghost column correction however, is not being applied here. The better alternative is to calculate both the clear-sky and cloudy-sky AMFs by integrating the NO2 profile from the surface pressure to the tropopause. This formulation ensures that the AMF value returns a tropospheric column that is representative for all NO2 in the troposphere, and not just for the above-cloud fraction (in the limiting case of cloud fraction 1.0). The authors should revisit their integration limits for Eq. (2), probably also for their current BEHR-product.

The reviewer is correct that this formulation of the AMF yields the visible $NO_2$ column, however this is the calculation given in the theoretical basis document for the OMI retrievals (Boersma et al., 2002). P. 20 of the TBD indicates after Eq. 2-15 that "$z$ is the altitude of the lower boundary (ground or **cloud top**)," where $z$ is the lower integration bound in the numerator of the AMF calculation. The publicly available BEHR retrieval includes a multiplicative factor which allows users to add the estimated ghost fraction in, if desired. This allows the user to choose how they want to use the product, e.g. (1) as the observed, visible column, (2) for cloud slicing approaches (e.g. Belmonte Rivas et al. 2015; Choi et al. 2014 for $NO_2$, or Ziemke et al. 2009, 2001 for $O_3$), or (3) with the ghost column included to get a full column.

We acknowledge the various ways of handling below-cloud $NO_2$ on P.2 L.25:

"Finally, the tropospheric slant column density (SCD) must be converted to a vertical column density (VCD) by use of an air mass factor (AMF) and Eq. (1). Depending on the specific algorithm, $NO_2$ obscured by clouds may be ignored (producing a visible-only tropospheric $NO_2$ column, e.g. Boersma et al. 2002), corrected by use of an assumed ghost column (e.g. Burrows et al. 1999; Koelemeijer and Stammes 1999), or corrected via the AMF (e.g. Martin et al. 2002). In all cases, the AMF must account for..."

We also added information about the available ghost column factor in the BEHR product after Eq. (4):

> "Calculating clear and cloudy AMFs and using the weighted average to compute the final AMF is consistent with the OMI algorithm theoretical basis document (Boersma et al., 2002) and yields only the visible $NO_2$ column as the final product; the visible column is the value provided in the BEHRColumnAmountNO2Trop field. A scaling factor is provided in the BEHR product for users who wish to include the ghost column. This factor, $G$, is computed as:
>
> $$G = \frac{V_{\text{surf}}}{(1 - f_{\text{geo}})V_{\text{surf}} + f_{\text{geo}}V_{\text{cld}}} = \frac{\int_{p_{\text{surf}}}^{p_{\text{tp}}} g(p)\, dp}{(1 - f_{\text{geo}}) \int_{p_{\text{surf}}}^{p_{\text{tp}}} g(p)\, dp + f_{\text{geo}} \int_{p_{\text{cld}}}^{p_{\text{tp}}} g(p)\, dp} \quad \text{(R1)}$$
>
> where $V_{\text{surf}}$ and $V_{\text{cld}}$ are the modeled vertical column densities above the ground surface and cloud, respectively, and which are obtained by integrating the a priori profile above the surface or cloud pressure. $f_{\text{geo}}$ is the geometric cloud fraction included in the NASA standard product, which is the OMI $O_2$-$O_2$ cloud product (Acarreta et al., 2004). This factor is stored in the BEHRGhostFraction field of the BEHR product. Multiplying the VCDs stored in BEHRColumnAmountNO2Trop by these values will provide the estimated total (visible + ghost) column.
>
> The results obtained in this work use the visible columns only. The ghost column is not added in for any of the following results."

We have clarified one point in Eq. (2) and (3). In (3), the lower bound of integration is always the surface, but in Eq. (2), the lower bound is the cloud or surface pressure, for cloudy and clear sky AMFs respectively:

> "$p_0$ represents the surface pressure (clear sky AMF) or cloud pressure (cloudy AMF) of the satellite pixel, and $p_{\text{tp}}$ the tropopause pressure...$p_{\text{surf}}$ in Eq. (R3) is the terrain surface pressure.
>
> $$\text{AMF} = \int_{p_0}^{p_{\text{tp}}} w(p)S(p)\, dp \quad \text{(R2)}$$
>
> where
>
> $$S(p) = \frac{1}{\int_{p_{\text{surf}}}^{p_{\text{tp}}} g(p)\, dp} g(p) \quad \text{(R3)}$$
>
> "

This error is also the reason for the incorrect statement on page 7, under point 3: ... a cloudy pixel will have a much greater AMF than a clear one. The statement would be correct only if the word AMF would be replaced by above-cloud AMF. And, in line with the above

criticism, an above-cloud AMF can only return an above-cloud NO2 columns, which cannot be the purpose of a state-of-science retrieval.

As discussed above, the choice to retrieve the visible column only matches the OMI theoretical basis document (Boersma et al., 2002), and both visible only and full column retrievals have uses. Reviewer #2 also pointed out that AMFs for cloudy pixels are not always larger than clear-sky AMFs, which we confirmed by comparing cloudy and clear AMFs from our product and the NASA standard product. Consequently, this sentence now indicates that changing cloud fraction can lead to a very different AMF, and discusses the reasons for that.

> "Setting cloud fractions to 0 ensures that the AMF for every pixel is calculated with the full a priori profile, rather than just the above cloud part. Day-to-day variations in cloud fraction also lead to large changes in AMF because the presence of clouds changes both the scattering weights (due to high assumed reflectivity of clouds and smaller effective surface pressure compared to ground) while also obscuring the $NO_2$ profile below the cloud."

There are difficulties with the interpretation of uncertainties in the tropospheric column retrieval. On page 10, the choice for 1.0x1015 molec. cm-2 as a typical number for the uncertainty in the tropospheric NO2 column is rather arbitrary. Detailed error analyses (e.g. Boersma et al. [2004]) have pointed out that the uncertainty in the tropospheric column is highly variable because of AMF (a multiplicative factor indeed) uncertainties, which depend strongly on variable clouds, surface albedo, and NO2 profile shapes. Moreover, the estimate used by the authors is rather optimistic. More realistic uncer- tainties are on the order of 1.0x1015 molec. cm-2 +25% (of the individual column value).

The value of $1.0 \times 10^{15}$ molec. $cm^{-2}$ was given in Bucsela et al. (2013) as the global average mean clear sky uncertainty based on their error analysis. Since the uncertainty in the AMF is a multiplicative factor, this error may be low for urban signals. We had chosen initially to use this uncertainty, however, because we are introducing new choices for a priori profiles, which may alter the magnitude of each specific element of the uncertainty, and so having a simple, previously determined number to compare to would simplify this for the reader.

To address the reviewer's concern, we have added a new column to what was Table 2 that uses an uncertainty that is the quadrature sum of uncertainty from the slant column fitting, stratospheric subtraction, and AMF, which is $\sqrt{(0.7 \times 10^{15})^2 + (0.2 \times 10^{15})^2 + (20\%)^2}$. The uncertainty in the AMF and stratospheric separation come from Bucsela et al. (2013), which describes the error analysis for the current version of the NASA SP retrieval, and the slant column fitting from Boersma et al. (2011), cited by Bucsela et al. (2013). We add them in quadrature following Boersma et al. (2004) and Bucsela et al. (2013). This leads to the following changes in text:

P.10, L.23–29 changed to:

> "Table 2 describes how frequently significant changes in the retrieved VCD occur for pixels within 50 km of Atlanta, Birmingham, and Montgomery. Changes are considered significant by two different criteria. First, we consider the global mean clear-sky uncertainty from Bucsela et al. (2013). As we are modifying the a priori profiles, and thus potentially the uncertainty associated with the choice

of profiles, this gives us a fixed value to compare against. Second, we use the quadrature sum of uncertainties from spectral fitting ($0.7 \times 10^{15}$ molec. cm$^{-2}$, Boersma et al. 2007, 2011), stratospheric separation ($0.2 \times 10^{15}$ molec. cm$^{-2}$, Bucsela et al. 2013), and AMF calculation (20%, Bucsela et al. 2013), assuming that these are independent and so can be added in quadrature (Boersma et al., 2004). We consider the fraction of days with at least one pixel exhibiting a significant change in VCD (rather than the fraction of pixels) because the main $NO_2$ plume may only fall within a small number of pixels. Up to 54% of days exhibit changes in the VCDs greater than $1 \times 10^{15}$ molec. cm$^{-2}$, and up to 43% exhibit changes greater than the quadrature sum of uncertainties. This indicates that when considering individual daily measurements, a considerable fraction of days with any valid pixels would have biases in the retrieved VCDs above the uncertainty due to the temporal resolution of the a priori $NO_2$ profiles. "

P.11, L.3–5 changed to:

"When considering changes to be significant if they exceed $1 \times 10^{15}$ molec. cm$^{-2}$, Montgomery has the least frequent significant changes because it has the smallest VCDs, so a change to the AMF needs to be rather large to produce a significant change in the VCD by this metric, since the AMF is a multiplicative factor. When considering the quadrature sum of errors as the significance criterion, Montgomery and Atlanta both demonstrate significant changes $\sim$ 20% of the time."

And the update to Table 2:

| | Percent of days with $\Delta$VCD $> 1 \times 10^{15}$ molec. cm$^{-2}$ | Percent of days with $\Delta$VCD $> [\sum_i \sigma_i]^{1/2}$ | Min. change (molec. cm$^{-2}$) | Max. change (molec. cm$^{-2}$) |
|---|---|---|---|---|
| Atlanta | 39% | 23% | $-2.4 \times 10^{15}$ | $+2.5 \times 10^{15}$ |
| Birmingham | 54% | 43% | $-3.8 \times 10^{15}$ | $+3.9 \times 10^{15}$ |
| Montgomery | 27% | 20% | $-2.2 \times 10^{15}$ | $+1.9 \times 10^{15}$ |

Table 1: Statistics on the frequency and magnitude of changes in the retrieved VCDs using a daily vs. monthly average profile for pixels with centers within 50 km of Atlanta, GA, USA (84.39° W, 33.775° N), Birmingham, AL, USA (86.80° W, 33.52° N) and Montgomery, AL, USA (86.30° W, 32.37° N). The "percent of days" values are calculated as the number of days with at least one pixel in that subset with a change greater than the given uncertainty divided by the number of days with at least one pixel unobscured by clouds or the row anomaly. The uncertainty represented by $[\sum_i \sigma_i]^{1/2}$ is the quadrature sum of uncertainties from spectral fitting ($0.7 \times 10^{15}$ molec. cm$^{-2}$, Boersma et al. 2007, 2011), stratospheric separation ($0.2 \times 10^{15}$ molec. cm$^{-2}$, Bucsela et al. 2013), and AMF calculation (20%, Bucsela et al. 2013).

The specific corrections below have all been addressed. We thank the reviewer for their careful reading, and especially for the additional citations for custom retrievals, as we hope

that others will find this list a useful reference for those interested in custom satellite retrievals.

Abstract, line 6: this paper does not address variations of NO2 in power plant plumes, so this should be removed. The paper is about NO2 variations in urban plumes.
Removed.

Introduction, lines 18 and 30: a reference to the work by Vinken et al., ACP, 2014 on ship emissions estimates using improved-resolution a priori profiles would be appropriate here.
Added Vinken et al. (2014), thank you for the suggestion.

P3, lines 7-8: earlier studies by McLinden et al. [2012] showed that the oil sand signals was detectable also for retrievals using coarse-gridded a priori profiles. The statement should be nuanced in that the spatial signatures are more realistically resolved with higher resolution a priori profiles.
This sentence has been changed to:

> "McLinden et al. (2014) showed that using 15 km resolution profiles increased the $NO_2$ signal of the Canadian oil sands by $\sim 100\%$ compared to the DOMINO and NASA SP products, which they state corrects a low bias in the retrieved column amounts."

P3, L13: also include here a reference to the DOMINO retrievals using 0.5 x 0.67 profiles from GEOS-Chem over Europe from Vinken et al. [2014]. These retrievals also use diurnal profiles.
Added:

> "Conversely, the DOMINOv2 (Boersma et al., 2011), POMINO (Lin et al., 2015), and DOMINO2_GC (Vinken et al., 2014) retrievals simulate daily profiles at 3° lon × 2° lat (DOMINO) and 0.667° lon × 0.5° lat (POMINO and DOMINO2_GC), respectively, which is insufficient to capture the full spatial variability of $NO_2$ plumes, but does capture large scale variations in meteorology."

P3, L17: the NASA retrieval is usually indicated as the Standard Product v2 or SP v2. OMNO2 (actually OMNO2A v1) refers to the software for DOAS spectral fitting.
Corrected, for all instances as well as this one.

P4, L30: 13 x 24 km2
Corrected.

P4, L32: 'theoretical daily global coverage is a strange term. Coverage was nearly global every day until the row anomaly, and after that, coverage is more or less global every 2 days.
Rephrased to:

"It has a continuous data record since 1 Oct 2004, with global daily coverage for the first $\sim$ 3 years of operation. Since 25 June 2007..."

P5, L6: please provide the name and appropriate version of the NO2 SCD product used. I think it is OMNO2A v1. This product has recently been evaluated in Marchenko et al. [2015] and van Geffen et al. [2015]. It would be appropriate to cite those papers here.

Thank you for pointing us to the proper identification. This section now reads:

"Briefly, the BEHR retrieval is based on the NASA Standard Product v2 (SP v2) retrieval (Bucsela et al., 2013). The total slant column densities (SCDs) are from OMNO2A v1.2.3 (Boersma et al., 2002; Bucsela et al., 2006, 2013), and have been recently evaluated by van Geffen et al. (2015) and Marchenko et al. (2015). The stratospheric subtraction and destriping used is that of the NASA SP v2 retrieval. The tropospheric AMF is then recalculated..."

P5, L17: apart from albedo, please also provide details on the cloud information (effective cloud fraction, pressure) used in the BEHR-approach.

We have added information about the cloud pressure and cloud radiance fraction used in the retrieval. For cloud pressure, the sentence "The cloud pressure is that provided in the NASA SP v2 product, and is retrieved using the OMI $O_2$-$O_2$ cloud algorithm (Acarreta et al., 2004; Sneep et al., 2008; Bucsela et al., 2013)," was added before Eq. 2. For cloud radiance fraction, the sentence "The cloud radiance fraction is taken from the SP v2 data product (Bucsela et al., 2013)," was added before Eq. 4.

P5, L27: which version of the WRF-Chem model is used?

Version 3.5.1. The first sentence of sect. 2.3 now reads:

"Modeled $NO_2$ a priori profiles are simulated using the WRF-Chem model v3.5.1 (Grell et al., 2005)."

P6, section 2.3: please provide some more details on the WRF-Chem model such as what is the NOx emission total over the US in the period of interest, and on the meteorological and chemical boundary conditions used. It is unclear how realistic WRF-Chem simulations of NO2 profiles are. Have these been validated against surface and aircraft measurements of NO2?

The chemical mechanism used has been validated against surface data from the SOAS campaign. However, the purpose of this paper is to illustrate that using daily profiles at high spatial resolution can and does alter the retrieved $NO_2$ columns. We feel that it is important to demonstrate that the temporal resolution of the profiles is important first, and because the monthly and daily 12 km *a priori* profiles are taken from the same model run (and the 108 km profiles from a run using the same inputs at different resolution), any error in the model is in all three sets of *a priori* profiles. In this way, our goal is to show that daily, high spatial resolution profiles are important in general.

We have added details of the meteorology, boundary conditions, and emissions to the paragraph on P.5 L.26–P.6 L.4. It now reads:

"Modeled $NO_2$ a priori profiles are simulated using the WRF-Chem model v3.5.1 (Grell et al., 2005). The domain is 81 (east-west) by 73 (north-south) grid cells centered on 84.35° W, 34.15° N on a Lambert Conformal map projection (approximate edges of the domain are 89.5° W–79.2° W and 30.3° N–38° N). Meteorological initial and boundary conditions are driven by the North American Regional Reanalysis (NARR) dataset. Anthropogenic emissions are taken from the National Emissions Inventory 2011 (NEI11) and scaled to 88.9% to account for 2011–2013 $NO_x$ reductions (EPA, 2016); total emissions of NO for the domain are approximately $3.1 \times 10^6$ kg NO $day^{-1}$. The MEGAN model (Guenther et al., 2006) is used to determine biogenic emissions. Chemical initial and boundary conditions for the domain are obtained from the MOZART chemical model (Emmons et al., 2010). The RACM2 (Goliff et al., 2013) and MADE-SORGAM schemes are used to simulate gas-phase and aerosol chemistry respectively; the RACM2 scheme is customized to reflect recent advancements in understanding of alkyl nitrate chemistry using Browne et al. (2014) and Schwantes et al. (2015) as a basis. Lightning $NO_x$ emissions were inactive."

P7, L19: please clarify what the vertical range is of the 'first five layers of WRF-Chem.

Five model layers is approximately 500 m high, which is the same height used in Lu et al. (2015). The sentence now reads:

"The surface wind direction and speed are calculated as the average of the first five layers ($\sim$ 500 m) of the 9 WRF 12 km grid cells closest to Atlanta at 1400 local standard time for each day."

P8, L6: is it really necessary or relevant to refer to a Matlab function, when explaining how you do the fit? If it is, please provide some more information on why you chose this particular fit approach over other alternatives. As a non-Matlab user, the sentence does not mean much to me. Later on the same for fmincon.

Other reviewers had similar comments; in the main paper, we've replaced references to Matlab functions with the mathematical algorithm behind it, which is an interior-point algorithm.

P8, 12-17: this part is very technical and should be moved to an appendix or supplement.

Again, other reviewers had similar comments. We have moved Table 1 and P8, L12–29 to the supplement. Section 2.5 now ends with "Technical details of the EMG fitting and uncertainty calculation are given in the supplement."

P10, L13: that lightning is not included in this WRF-Chem set-up should not be mentioned only here, but already in the model description section 2.3.

We have added the following sentence on P. 6, L. 4: "Lightning $NO_x$ emissions were inactive," (see end of change for previous comment on WRF-Chem details).

P12, L18: sigma_x represents the width of the Gaussian plume, but also the spatial smearing of the signal caused by the satellite pixel extent, and the fact that cities are covered by different satellite footprints from day to day.

Originally we had focused on its representation of the plume width because that is the most physically intuitive quantity, but we have extended the first sentence of P12, L18 to read:

> "$\sigma_x$ is the Gaussian smoothing length scale, representing both the width of the upwind Gaussian plume and smoothing of the $NO_2$ signal due to the physical extent of the source, the averaging of $NO_2$ within one OMI pixel, and daily variability in the overpass track (Beirle et al., 2011)."

P13, L14-19: this whole section presumably discusses Table 4, but that is not obvious from the text. I'm confused by the statement that the choice of a priori leads to statistically different emissions for all five cases, whereas Table 4 shows emission values that all overlap within the quoted uncertainty estimates.

When comparing two measured values, $t$-tests designed for either comparing replicate measurements or paired tests must be used (Harris, 2010). This paragraph is discussing results from using $t$-tests for comparing replicate measurements, i.e. two sample $t$-tests (Harris 2010, sect. 4-3, case 2). We chose this method because the emissions and lifetime estimates are the result of averaging VCDs over 3 months, so the fitting parameters are effectively means. Additionally, unlike the paired $t$-tests, this method takes into account the uncertainty in each value. Using these tests, any pair of emissions derived using different a priori for the same city and wind division are statistically different, even though the confidence intervals overlap.

To clarify which $t$-tests were used, we have modified P.13 L.14 to read ("2-sample" added):

> "We also use 2-sample $t$-tests at the 95% confidence level (Harris, 2010) to determine if differences in emissions and lifetimes given in Table 4 are significantly different..."

## References


Acarreta, J. R., De Haan, J. F., and Stammes, P.: Cloud pressure retrieval using the O2-O2 absorption band at 477 nm, J. Geophys. Res. Atmos., 109, doi:10.1029/2003JD003915, URL `http://dx.doi.org/10.1029/2003JD003915`, d05204, 2004.

Beirle, S., Boersma, K., Platt, U., Lawrence, M., and Wagner, T.: "Megacity Emissions and Lifetimes of Nitrogen Oxides Probed from Space", Science, 333, 1737–1739, 2011.

Belmonte Rivas, M., Veefkind, P., Eskes, H., and Levelt, P.: OMI tropospheric $NO_2$ profiles from cloud slicing: constraints on surface emissions, convective transport and lightning $NO_x$, Atmos. Chem. Phys., 15, 13 519–13 553, doi:10.5194/acp-15-13519-2015, URL `http://www.atmos-chem-phys.net/15/13519/2015/`, 2015.

Boersma, K., Bucsela, E., Brinksma, E., and Gleason, J.: $NO_2$, in: OMI Algorithm Theoretical Basis Document, vol 4, OMI Trace Gas Algorithms, ATB-OMI-04, version 2.0, pp. 13–36, URL http://eospso.nasa.gov/sites/default/files/atbd/ATBD-OMI-04.pdf, 2002.

Boersma, K., Eskes, H., and Brinksma, E.: "Error analysis for tropospheric $NO_2$ retrieval from space, J. Geophys. Res. Atmos., 106, D04 311, doi:10.1029/2003JD003962, 2004.

Boersma, K., Eskes, H., Dirksen, R., van der A, R., Veefkind, J., Stammes, P., Huijnen, V., Kleipool, Q., Sneep, M., Claas, J., Leitão, J., Richter, A., Zhou, Y., and Brunner, D.: "An improved tropospheric $NO_2$ column retrieval algorithm for the Ozone Monitoring Instrument, Atmos. Meas. Tech., 4, 1905–1928, doi:10.5194/amt-4-1905-2011, 2011.

Boersma, K. F., Eskes, H. J., Veefkind, J. P., Brinksma, E. J., van der A, R. J., Sneep, M., van den Oord, G. H. J., Levelt, P. F., Stammes, P., Gleason, J. F., and Bucsela, E. J.: Near-real time retrieval of tropospheric NO¡sub¿2¡/sub¿ from OMI, Atmos. Chem. Phys., 7, 2103–2118, doi:10.5194/acp-7-2103-2007, 2007.

Browne, E. C., Wooldridge, P. J., Min, K.-E., and Cohen, R. C.: On the role of monoterpene chemistry in the remote continental boundary layer, Atmos. Chem. Phys., 14, 1225–1238, doi:10.5194/acp-14-1225-2014, 2014.

Bucsela, E., Krotkov, N., Celarier, E., Lamsal, L., Swartz, W., Bhartia, P., Boersma, K., Veefkind, J., Gleason, J., and Pickering, K.: "A new tropospheric and stratospheric $NO_2$ retrieval algorithm for nadir-viewing satellite instruments: applications to OMI, Atmos. Meas. Tech., 6, 2607–2626, doi:10.5194/amt-6-2607-2013, 2013.

Bucsela, E. J., Celarier, E. A., Wenig, M. O., Gleason, J. F., Veefkind, J. P., Boersma, K. F., and Brinksma, E. J.: Algorithm for $NO_2$ vertical column retrieval from the ozone monitoring instrument, IEEE T. Geosci. Remote, 44, 1245–1258, doi:10.1109/TGRS.2005.863715, 2006.

Burrows, J., Weber, M., Buchwitz, M., Rozanov, V., Ladstätter-Weißenmayer, A., Richter, A., DeBeek, R., Hoogan, R., Bramstedt, K., Eichmann, K.-U., Eisinger, M., and Perner, D.: The Global Ozone Monitoring Experiment (GOME): Mission Concept and First Scientific Results, 56, 151–175, doi:10.1175/1520-0469(1999)056⟨0151:TGOMEG⟩2.0.CO;2, 1999.

Choi, S., Joiner, J., Choi, Y., Duncan, B. N., Vasilkov, A., Krotkov, N., and Bucsela, E.: First estimates of global free-tropospheric $NO_2$ abundances derived using a cloud-slicing technique applied to satellite observations from the Aura Ozone Monitoring Instrument (OMI), Atmos. Chem. Phys., 14, 10 565–10 588, doi:10.5194/acp-14-10565-2014, URL http://www.atmos-chem-phys.net/14/10565/2014/, 2014.

Emmons, L. K., Walters, S., Hess, P. G., Lamarque, J.-F., Pfister, G. G., Fillmore, D., Granier, C., Guenther, A., Kinnison, D., Laepple, T., Orlando, J., Tie, X., Tyndall, G., Wiedinmyer, C., Baughcum, S. L., and Kloster, S.: Description and evaluation of the Model for Ozone and Related chemical Tracers, version 4 (MOZART-4), Geosci. Model

Dev., 3, 43–67, doi:10.5194/gmd-3-43-2010, URL http://www.geosci-model-dev.net/3/43/2010/, 2010.

EPA: Air Pollutant Emissions Trends Data, URL https://www.epa.gov/air-emissions-inventories/air-pollutant-emissions-trends-data, 2016.

Goliff, W. S., Stockwell, W. R., and Lawson, C. V.: The regional atmospheric chemistry mechanism, version 2, Atmos. Environ., 68, 174 – 185, doi:10.1016/j.atmosenv.2012.11.038, 2013.

Grell, G. A., Peckham, S. E., Schmitz, R., McKeen, S. A., Frost, G., Skamarock, W. C., and Eder, B.: Fully coupled online chemistry within the {WRF} model, Atmos. Environ., 39, 6957 – 6975, doi:10.1016/j.atmosenv.2005.04.027, 2005.

Guenther, A., Karl, T., Harley, P., Wiedinmyer, C., Palmer, P. I., and Geron, C.: Estimates of global terrestrial isoprene emissions using MEGAN (Model of Emissions of Gases and Aerosols from Nature), Atmos. Chem. Phys., 6, 3181–3210, doi:10.5194/acp-6-3181-2006, URL http://www.atmos-chem-phys.net/6/3181/2006/, 2006.

Harris, D.: Comparison of Means with Student's $t$, chap. 4-3, pp. 76–78, W.H. Freeman, 8th edn., 2010.

Koelemeijer, R. B. A. and Stammes, P.: Effects of clouds on ozone column retrieval from GOME UV measurements, J. Geophys. Res. Atmos., 104, 8281–8294, doi:10.1029/1999JD900012, 1999.

Lin, J.-T., Liu, M.-Y., Xin, J.-Y., Boersma, K. F., Spurr, R., Martin, R., and Zhang, Q.: Influence of aerosols and surface reflectance on satellite $NO_2$ retrieval: seasonal and spatial characteristics and implications for $NO_x$ emission constraints, Atmos. Chem. Phys., 15, 11 217–11 241, doi:10.5194/acp-15-11217-2015, 2015.

Lu, Z., Streets, D., de Foy, B., Lamsal, L., Duncan, B., and Xing, J.: "Emissions of nitrogen oxides from US urban areas: estimation from Ozone Monitoring Instrument retrievals for 2005–2014", Atmos. Chem. Phys., 15, 10 367–10 383, doi:10.5194/acp-15-10367-2015, 2015.

Marchenko, S., Krotkov, N. A., Lamsal, L. N., Celarier, E. A., Swartz, W. H., and Bucsela, E. J.: Revising the slant column density retrieval of nitrogen dioxide observed by the Ozone Monitoring Instrument, J. Geophys. Res. Atmos., 120, 5670–5692, doi:10.1002/2014JD022913, 2014JD022913, 2015.

Martin, R. V., Chance, K., Jacob, D. J., Kurosu, T. P., Spurr, R. J. D., Bucsela, E., Gleason, J. F., Palmer, P. I., Bey, I., Fiore, A. M., Li, Q., Yantosca, R. M., and Koelemeijer, R. B. A.: An improved retrieval of tropospheric nitrogen dioxide from GOME, J. Geophys. Res. Atmos., 107, doi:10.1029/2001JD001027, 4437, 2002.

McLinden, C. A., Fioletov, V., Boersma, K. F., Kharol, S. K., Krotkov, N., Lamsal, L., Makar, P. A., Martin, R. V., Veefkind, J. P., and Yang, K.: Improved satellite retrievals

of $NO_2$ and $SO_2$ over the Canadian oil sands and comparisons with surface measurements, Atmos. Chem. Phys., 14, 3637–3656, doi:10.5194/acp-14-3637-2014, 2014.

Schwantes, R. H., Teng, A. P., Nguyen, T. B., Coggon, M. M., Crounse, J. D., St. Clair, J. M., Zhang, X., Schilling, K. A., Seinfeld, J. H., and Wennberg, P. O.: Isoprene $NO_3$ Oxidation Products from the $RO_2$ + $HO_2$ Pathway, J. Phys. Chem. A, 119, 10 158–10 171, doi:10.1021/acs.jpca.5b06355, 2015.

Sneep, M., de Haan, J. F., Stammes, P., Wang, P., Vanbauce, C., Joiner, J., Vasilkov, A. P., and Levelt, P. F.: Three-way comparison between OMI and PARASOL cloud pressure products, J. Geophys. Res. Atmos., 113, doi:10.1029/2007JD008694, d15S23, 2008.

van Geffen, J. H. G. M., Boersma, K. F., Van Roozendael, M., Hendrick, F., Mahieu, E., De Smedt, I., Sneep, M., and Veefkind, J. P.: Improved spectral fitting of nitrogen dioxide from OMI in the 405465 nm window, Atmos. Meas. Tech., 8, 1685–1699, doi: 10.5194/amt-8-1685-2015, 2015.

Vinken, G. C. M., Boersma, K. F., van Donkelaar, A., and Zhang, L.: Constraints on ship $NO_x$ emissions in Europe using GEOS-Chem and OMI satellite $NO_2$ observations, Atmos. Chem. Phys., 14, 1353–1369, doi:10.5194/acp-14-1353-2014, URL `http://www.atmos-chem-phys.net/14/1353/2014/`, 2014.

Ziemke, J., Chandra, S., and Bhartia, P.: "Cloud slicing: A new technique to derive upper tropospheric ozone from satellite measurements", J. Geophys. Res. Atmos., 106, 9853–9867, 2001.

Ziemke, J. R., Joiner, J., Chandra, S., Bhartia, P. K., Vasilkov, A., Haffner, D. P., Yang, K., Schoeberl, M. R., Froidevaux, L., and Levelt, P. F.: Ozone mixing ratios inside tropical deep convective clouds from OMI satellite measurements, Atmos. Chem. Phys., 9, 573–583, doi:10.5194/acp-9-573-2009, 2009.

# Effects of daily meteorology on the interpretation of space-based remote sensing of $NO_2$

Joshua L. Laughner[1], Azimeh Zare[1], and Ronald C. Cohen[1,2]

[1]Department of Chemistry, University of California, Berkeley, Berkeley, CA, USA
[2]Department of Earth and Planetary Science, University of California, Berkeley, Berkeley, CA, USA

*Correspondence to:* R.C. Cohen (rccohen@berkeley.edu)

**Abstract.** Retrievals of tropospheric $NO_2$ columns from UV/visible observations of reflected sunlight require a priori vertical profiles to account for the variation in sensitivity of the observations to $NO_2$ at different altitudes. These profiles vary in space and time but are usually approximated using models that do not resolve the full details of this variation. Currently, no operational retrieval simulates these a priori profiles at both high spatial and high temporal resolution. Here we examine the additional benefits of daily variations in a priori profiles for retrievals already simulating a priori $NO_2$ profiles at sufficiently high spatial resolution to identify variations of $NO_2$ within urban ~~and power plant~~ plumes. We show the effects of introducing daily variation into a priori profiles can be as large as 40% and $3 \times 10^{15}$ molec. $cm^{-2}$ for an individual day and lead to corrections as large as ~~10~~–13% for a monthly average in a case study of Atlanta, GA~~. Comparing an optimized retrieval to a more standard one, we find~~ , USA. Additionally, we show that $NO_x$ emissions estimated from space-based remote sensing ~~can increase by~~ using daily, high spatial resolution a priori profiles are $\sim 100\%$ ~~when dailyvariations in plume location and shape are accounted for in the retrieval~~ greater compared to a retrieval using spatially coarse a priori profiles, and 20–45% less compared to a retrieval using monthly averaged high spatial resolution profiles.

## 1 Introduction

$NO_x$ (= NO + $NO_2$) is an atmospheric trace gas family that plays an important role in regulating the production of $O_3$ and particulate matter. $NO_x$ is emitted into the atmosphere by natural processes (e.g. lightning, biomass burning) and anthropogenic sources, notably combustion. Understanding the contribution of each source is vital to determining the effectiveness of current and future efforts to improve air quality and to understanding the chemistry of the atmosphere. ~~A substantial number of studies~~ Studies have utilized satellite observations to constrain $NO_x$ emissions from lightning (e.g. Miyazaki et al. 2014; Beirle et al. 2010; Martin et al. 2007; Schumann and Huntrieser 2007), biomass burning (e.g. Castellanos et al. 2014; Mebust and Cohen 2014, 2013; Miyazaki et al. 2012; Mebust et al. 2011), anthropogenic $NO_x$ emissions and trends ~~(Ding et al., 2015; Lamsal et al., 2015; Tong et al., 2015; Huang et al., 2014; Gu et al., 2013; Miyazaki et al., 2012; Russell et al., 2012; L~~ (e.g. Ding et al. 2015; Lamsal et al. 2015; Tong et al. 2015; Huang et al. 2014; Vinken et al. 2014b; Gu et al. 2013; Miyazaki et al. 2012; F soil $NO_x$ emissions, (e.g. Zörner et al. 2016; Vinken et al. 2014a; Hudman et al. 2012 ), and $NO_x$ lifetime ~~(Lu et al., 2015; de Foy et al., 20~~

The process of retrieving a ~~troposphere~~ tropospheric $NO_2$ column ~~from satellite observations~~ with UV/visible spectroscopy from satellites requires three main steps. First, the raw radiances are fit using Differential Optical Absorption Spectroscopy (DOAS) to yield slant column densities (Richter and Wagner, 2011). Then, the stratospheric $NO_2$ signal must be removed (Boersma et al., 2011; Bucsela et al., 2013). Finally, the tropospheric slant column density (SCD) must be converted to a vertical column density (VCD) by use of an air mass factor (AMF) and Eq. (1). ~~The AMF~~ Depending on the specific algorithm, $NO_2$ obscured by clouds may be ignored (producing a visible-only tropospheric $NO_2$ column, e.g. Boersma et al. 2002 ), corrected by use of an assumed ghost column (e.g. Burrows et al. 1999; Koelemeijer and Stammes 1999 ), or corrected via the AMF (e.g. Martin et al. 2002 ). In all cases, the AMF must account for the varying sensitivity of the satellite to $NO_2$ at different altitudes, and therefore a priori knowledge of that sensitivity and the vertical profile of $NO_2$ is required. ~~Because the satellite is less sensitive to~~ Over low-reflectivity surfaces, light scattered in the atmosphere is the primary source of radiance

at the detector. The probability of back-scattered light penetrating to a given altitude is greater for higher altitudes; thus there is greater interaction with, and therefore greater sensitivity to, $NO_2$ ~~near the surface, the AMF should be~~ at higher altitudes (Richter and Wagner, 2011; Hudson et al., 1995) . Because of this, the correct AMF is smaller in locations influenced by surface $NO_x$ sources. The relative contribution of errors in the calculated sensitivity and in the a priori profiles of $NO_2$ to error in the final VCD varies between polluted and clean pixels (Boersma et al., 2004) . Previous work (e.g. Russell et al. 2011 ) has sought to reduce errors in both, and highlighted the importance of accurate a priori profiles in urban areas.

$$\mathrm{VCD} = \frac{\mathrm{SCD}}{\mathrm{AMF}} \tag{1}$$

A priori $NO_2$ profiles are generated using chemical transport models. Previous studies (e.g. Cohan et al. 2006, Wild and Prather 2006, Valin et al. 2011, Vinken et al. 2014b , Schaap et al. 2015) have demonstrated these modeled $NO_2$ profiles are strongly dependent on the spatial resolution of the chemical transport model used. The impact of model spatial resolution on satellite retrievals has been evaluated through case studies (Valin et al., 2011; Heckel et al., 2011; Yamaji et al., 2014) and through what could be termed "regional" retrievals (Russell et al., 2011; McLinden et al., 2014; Kuhlmann et al., 2015; Lin et al., 2015) that trade complete global coverage for improved spatial resolution of the input assumptions. These studies recommend model resolution of $< 20$ km to accurately capture $NO_x$ chemistry on a priori profiles. Russell et al. (2011) showed that increasing the spatial resolution of the input $NO_2$ profiles produces a retrieval that ~~better retrieves~~ more accurately represents contrast in the spatial features of $NO_2$ plumes, reducing systematic bias by as much as 30%. Reducing these biases improves the clarity of the observed urban-rural gradients by providing unique urban and rural profiles, rather than one that averages over both types of locations. McLinden et al. (2014) showed that using 15 km resolution profiles ~~was necessary to distinguish~~ increased the $NO_2$ signal of the Canadian oil sands ~~from the background~~by $\sim 100\%$ compared to the DOMINO and NASA SP products, which they state corrects a low bias in the retrieved column amounts.

Currently, only the Hong Kong-OMI retrieval has made use of daily a priori $NO_2$ profiles at $< 20$ km spatial resolution (Kuhlmann et al., 2015)~~, covering~~ . Their retrieval covered the Pearl River Delta for the period October 2006 to January 2007. No operational retrieval covering the majority of the OMI data record does so. The current generation ~~BEHR~~ Berkeley High Resolution (BEHR) (Russell et al., 2011, 2012) and OMI-EC (McLinden et al., 2014) retrievals simulate monthly average $NO_2$ profiles at 12 and 15 km, respectively. Conversely, the DOMINOv2 (Boersma et al., 2011)~~and POMINO (Lin et al., 2015)~~ , POMINO (Lin et al., 2015) , and DOMINO2 SUBSCRIPTNBGC (Vinken et al., 2014b) retrievals simulate daily profiles at ~~$2^\circ \times 3^\circ$ and $0.5^\circ \times 0.667^\circ$~~$3^\circ$ lon $\times$ $2^\circ$ lat (DOMINO) and $0.667^\circ$ lon $\times$ $0.5^\circ$ lat (POMINO and DOMINO2 SUBSCRIPTNBGC), respectively, which is insufficient to capture the full spatial variability of $NO_2$ plumes, but does capture large scale variations in meteorology. Lamsal et al. (2014) quantitatively compared $NO_2$ average profile shapes measured from the P3-B aircraft for each of six sites in the DISCOVER-AQ Baltimore/DC campaign with the modeled profile shape from the GMI chemical transport model used to compute the $NO_2$ a priori profiles in the NASA ~~OMNO2~~ Standard Product v2 retrieval, which uses monthly average $NO_2$ profiles at $2^\circ \times 2.5^\circ$ spatial resolution. They found up to 30% differences between the mea-

sured and modeled profile shape factors (i.e. $S(p)$ in Eq. 3) at any single pressure throughout the troposphere. Several sites (Edgewood, Essex, and Beltsville) had less $NO_2$ than the model throughout the free troposphere, and Edgewood also exhibited an elevated $NO_2$ layer at 970 hPa not captured in the model.

Lamsal et al. (2014) also noted that there was significant day-to-day variability in the measured profiles that cannot be captured by a monthly average model; however, they do not quantify those differences. These day-to-day differences can be significant in a priori $NO_2$ profiles. Valin et al. (2013) showed that the concentration of $NO_2$ downwind of a city increases significantly with wind speed, observing that $NO_2$ 100–200 km downwind from Riyadh, Saudi Arabia was approximately 130–250% greater for wind speeds between 6.4–8.3 m $s^{-1}$ than wind speeds $< 1.9$ m $s^{-1}$. When monthly average a priori profiles are used, this is not accounted for in the retrieval. The effect on the AMF is illustrated in Fig. 1c. Compared to the monthly average a priori profiles, daily profiles from a day with fast winds would contain greater near-surface $NO_2$ further from the city. As discussed before Eq. (1), UV/visible satellite observations of $NO_2$ are less sensitive to $NO_2$ at low altitudes, so this requires smaller AMFs at a greater distance from the city on days with fast winds to compensate through Eq. (1).

These day-to-day variations may be particularly important for methods such as Beirle et al. (2011), Valin et al. (2013), Lu et al. (2015), and Liu et al. (2016) that use observations sorted by wind speed to derive detailed information about $NO_x$ chemistry and emissions from space-borne observations. This is a very valuable tool because of the wealth of data available from OMI (Levelt et al., 2006) and expected from upcoming instruments such as TROPOMI (Veefkind et al., 2012), TEMPO (Chance et al., 2013), Sentinel-4 (Ingmann et al., 2012), and GEMS (Bak et al., 2013; Choi and Ho, 2015). However, the act of sorting data by wind speed transforms errors in the profile shape resulting from day-to-day variability in wind speed from random to systematic. For example, Beirle et al. (2011), Valin et al. (2013), and Lu et al. (2015) derive an effective $NO_x$ lifetime using data with fast wind speed, and Liu et al. (2016) does so by fitting a function with a component derived at slow wind speeds to data derived from days with fast wind speeds. On a day when the wind speed is faster than average, a priori $NO_2$ profiles taken from a monthly average model would have less near-surface $NO_2$ further from the city than is actually present for that day (i.e. Fig. 1c vs. 1a). The resulting incorrect AMFs would lead to an underestimation of the spatial extent of the plume, and could lead to an underestimate of the $NO_x$ lifetime as a consequence.

In this paper we explore how day-to-day changes in the a priori $NO_2$ profiles ~~will~~ affect satellite retrievals of urban $NO_2$. ~~In~~ Several scenarios are illustrated in Fig. 1. In each case the change in the AMF results because, over low albedo surfaces, a UV/visible satellite spectrometer is less sensitive to near surface trace gases, necessitating a smaller AMF to account for the reduced sensitivity. In Fig. 1a, the monthly average $NO_2$ plume is shown as the grayscale gradient, to emphasize that it is static from day to day. Most of the plume follows the prevailing wind direction (here, to the right), but because days with different wind directions are averaged together, there is some influence of the plume upwind of the city. Figure 1b shows a case where the daily winds are similar to the monthly average. This leads to a similar $NO_2$ plume as in the monthly average, but because we are not averaging different wind directions, the upwind plume influence is removed (increasing the AMF, reflecting the reduction in near-surface $NO_2$) and conversely the downwind AMFs are slightly smaller, due to a slight increase in near-surface $NO_2$ from not averaging in days when the wind direction is different. Figure 1c shows a case where the daily winds are faster than the average. Here the AMFs within the city need to be larger, as near-surface $NO_2$ is being removed more efficiently

and transported downwind, where the AMFs must therefore be smaller. Finally, Fig. 1d has the wind change direction from the monthly average. Left of the city must have smaller AMFs to account for the presence of the plume not seen in the monthly average, and the opposite change occurs to the right.

~~To do so, we~~ We combine the high spatial resolution a priori previously developed as part of the BErkeley High Resolution (BEHR) algorithm (Russell et al., 2011) with high temporal resolution to demonstrate the impact of day-to-day variations in the modeled $NO_2$ profiles on the calculated AMFs surrounding a major urban area such as Atlanta, GA, USA. Atlanta provides an example of a strong $NO_x$ area source relatively isolated from other sources, with straightforward response of the day-to-day a priori profiles to meteorological variables. Our point is not to derive exact answers for the size and frequency of the effects of daily profiles, but rather to illustrate that these effects are large enough that their role should be assessed in any future analysis that does attempt to interpret space-based remote sensing of $NO_x$. We show that ~~this variability~~ the variability in the a priori profiles is largely due to changes in wind speed and direction. We first ~~isolate~~ consider the effects of day-to-day variations in ~~boundary layer alone (retaining a monthly average a priori profile in the free troposphere)~~ a priori profile on AMFs for the region surrounding Atlanta ~~,~~ for a fixed grid of OMI pixels, simplifying day-to-day comparisons. We then fully implement 91 days of retrieval to examine the effect on both day-to-day and monthly average $NO_2$ columns. Finally, we apply the ~~EMG~~ exponentially-modified Gaussian (EMG) fitting method of Lu et al. (2015) to the new retrieval and show that the spatial and temporal resolution of the a priori profiles can significantly alter the derived emission rate and lifetime.

## 2 Methods

### 2.1 The Ozone Monitoring Instrument

The Ozone Monitoring Instrument (OMI), onboard the Aura satellite, is a polar-orbiting, nadir-viewing, ~~UV-visible~~ UV/visible spectrometer with a swath width of 2600 km and a pixel size at nadir of $13 \times 24$ km$^2$. It observes backscattered solar radiation in the range of 270–500 nm with an average spectral resolution of 0.5 nm. (Levelt et al., 2006). It has a continuous data record since 1 Oct 2004, with ~~theoretical~~ global daily coverage for the first $\sim$3 years of operation. Since 25 June 2007, anomalous radiances have been observed in several of the pixel rows. These have been classified as the "row anomaly" ~~and as~~ (http://projects.knmi.nl/omi/research/product/rowanomaly-background.php). As of 5 July 2011~~affect~~, one-third of ~~the pixels~~ ~~(), reducing coverage from global daily to global every two days~~ OMI pixels are flagged as affected by the row anomaly, indicating that data from these pixels should not be used. Using only the pixels unaffected by the row anomaly, it takes two days to observe the entire globe. There are two publicly available global $NO_2$ products, the KNMI DOMINO product (Boersma et al., 2011) and the NASA Standard Product (Bucsela et al., 2013).

### 2.2 BErkeley High Resolution (BEHR) Retrieval

The ~~BErkeley High Resolution (BEHR )~~ BEHR retrieval is described in detail in Russell et al. (2011), and updates are described on the BEHR website (http://behr.cchem.berkeley.edu/Portals/2/Changelog.txt). The product is openly available for

download at http://behr.cchem.berkeley.edu/. Briefly, the BEHR retrieval ~~uses the tropospheric SCD from the NASA OMNO2 retrieval (Bucsela et al., 2013) as a starting point. The radiance fitting, stratospheric subtration, and destriping is thus the same as the NASA OMNO2~~ is based on the NASA Standard Product v2 (SP v2) retrieval (Bucsela et al., 2013) . The total slant column densities (SCDs) are from OMNO2A v1.2.3 (Boersma et al., 2002; Bucsela et al., 2006, 2013) , and have been recently evaluated by van Geffen et al. (2015) and Marchenko et al. (2015) . The stratospheric subtraction and destriping used is that of the NASA SP v2 retrieval. The tropospheric AMF is then recalculated similarly to the AMF formalism described in Palmer et al. (2001). Clear and cloudy AMFs are calculated as shown in Eq. (2). ~~$w_s(p)$ represents~~ $p$ represents the vertical coordinate as pressure. $w(p)$ represents scattering weights derived from the NASA ~~OMNO2~~ SP v2 look up table. $g(p)$ represents the mixing ratio $NO_2$ a priori profile taken from WRF-Chem, simulated at 12 km resolution in the published BEHR product. $p_0$ represents the surface pressure (clear sky AMF) or cloud pressure (cloudy AMF) of the satellite pixel, and $p_{\mathrm{tp}}$ the tropopause pressure. The cloud pressure is that provided in the NASA SP v2 product, and is retrieved using the OMI $O_2$-$O_2$ cloud algorithm (Acarreta et al., 2004; Sneep et al., 2008; Bucsela et al., 2013) . A static tropopause pressure of 200 hPa is used. $p_{\mathrm{surf}}$ in Eq. (3) is the terrain surface pressure. The integration is carried out using the scheme described in Ziemke et al. (2001) which allows integration of mixing ratio over pressure.

$$\mathrm{AMF} = \int_{p_0}^{p_{\mathrm{tp}}} w(p) S(p)\, dp \tag{2}$$

where

$$S(p) = \frac{1}{\int_{p_0}^{p_{\mathrm{tp}}} g(p)\, dp} \frac{1}{\int_{p_{\mathrm{surf}}}^{p_{\mathrm{tp}}} g(p)\, dp} g(p) \tag{3}$$

The scattering weights, $w(p)$, depend on the viewing geometry, surface albedo, and terrain pressure altitude. The BEHR algorithm uses the $0.05^\circ \times 0.05^\circ$ combined MODIS MCD43C3 black-sky albedo product and a surface pressure derived from the Global Land One-km Base Elevation project database (http://www.ngdc.noaa.gov/mgg/topo/globe.html; Hastings and Dunbar 1999) with a 7.4 km scale height as inputs to the clear sky scattering weights. Cloudy scattering weights treat the cloud pressure as the surface pressure and use an assumed cloud albedo of 0.8 (Stammes et al., 2008; Bucsela et al., 2013) . The final AMF is computed as the cloud radiance fraction (~~$f$~~ $f_{\mathrm{rad}}$) weighted average of the clear and cloudy AMFs (Eq. 4). The cloud radiance fraction is taken from the SP v2 data product (Bucsela et al., 2013) .

$$\mathrm{AMF}_{\mathrm{total}} = f_{\mathrm{rad}} \mathrm{AMF}_{\mathrm{cloudy}} + (1 - f_{\mathrm{rad}}) \mathrm{AMF}_{\mathrm{clear}} \tag{4}$$

~~The BEHR retrieval is available at for the continental US and southern Canada. Updates to the product since Russell et al. (2012) are detailed in the changelog at .~~ Calculating clear and cloudy AMFs and using the weighted average to compute the final AMF is consistent with the OMI algorithm theoretical basis document (Boersma et al., 2002) and yields only the visible $NO_2$ column

as the final product; the visible column is the value provided in the BEHRColumnAmountNO2Trop field. A scaling factor is provided in the BEHR product for users who wish to include the ghost column. This factor, $G$, is computed as:

$$G = \frac{V_{\text{surf}}}{(1 - f_{\text{geo}})V_{\text{surf}} + f_{\text{geo}}V_{\text{cld}}} = \frac{\int_{p_{\text{surf}}}^{p_{\text{tp}}} g(p)\,dp}{(1 - f_{\text{geo}})\int_{p_{\text{surf}}}^{p_{\text{tp}}} g(p)\,dp + f_{\text{geo}}\int_{p_{\text{cld}}}^{p_{\text{tp}}} g(p)\,dp} \tag{5}$$

where $V_{\text{surf}}$ and $V_{\text{cld}}$ are the modeled vertical column densities above the ground surface and cloud, respectively, and which are obtained by integrating the a priori profile above the surface or cloud pressure. $f_{\text{geo}}$ is the geometric cloud fraction included in the NASA standard product, which is the OMI $O_2$-$O_2$ cloud product (Acarreta et al., 2004) . This factor is stored in the BEHRGhostFraction field of the BEHR product. Multiplying the VCDs stored in BEHRColumnAmountNO2Trop by these values will provide the estimated total (visible + ghost) column.

The results obtained in this work use the visible columns only. The ghost column is not added in for any of the following results.

### 2.3 WRF-Chem

Modeled $NO_2$ a priori profiles are simulated using the WRF-Chem model ~~(Grell et al., 2005) . Meteorology is initialized with the~~ v3.5.1 (Grell et al., 2005) . The domain is 81 (east-west) by 73 (north-south) grid cells centered on 84.35° W, 34.15° N on a Lambert Conformal map projection (approximate edges of the domain are 89.5° W–79.2° W and 30.3° N–38° N). Meteorological initial and boundary conditions are driven by the North American Regional Reanalysis (NARR) dataset. Anthropogenic emissions are taken from the National Emissions Inventory 2011 (NEI11) and scaled to 88.9% to account for 2011–2013 $NO_x$ reductions (EPA, 2016)~~, and the MEGAN model~~ ; total emissions of NO for the domain are approximately $3.1 \times 10^6$ kg NO $day^{-1}$. The MEGAN model (Guenther et al., 2006) is used to determine biogenic emissions. ~~Boundary~~ Chemical initial and boundary conditions for the domain are obtained from the MOZART chemical model (Emmons et al., 2010) . The RACM2 (Goliff et al., 2013) and MADE-SORGAM schemes are used to simulate gas-phase and aerosol chemistry respectively; the RACM2 scheme is customized to reflect recent advancements in understanding of alkyl nitrate chemistry ~~(Browne et al., 2014; ?) .~~ using Browne et al. (2014) and Schwantes et al. (2015) as a basis. Lightning $NO_x$ emissions were inactive.

The model is run from 27 May to 30 August, 2013. Similar to Browne et al. (2014) , the five day period 27–31 May ~~are~~ is treated as a spin up period, thus we use 1 June to 30 August as our study time period. ~~Hourly~~ Model output is sampled every half hour; the two output files from the same hour (e.g. UTC 1900 and 1930) are averaged to give a single hourly set of profiles. These hourly $NO_2$ profiles ~~from WRF-Chem~~ are used as the a priori $NO_2$ profiles in the BEHR retrieval (Section 2.2). To produce monthly average profiles, each hourly profile is weighted according to Eq. (7), where $l$ is the longitude of the profile and $h$ is the hour (in UTC) that WRF calculated the profile for. The weights are clamped to the range $[0, 1]$. These are used as the weights in a temporal average over the month in question. This weighting scheme gives higher weights to profiles closest to the OMI overpass time around 1330 local standard time.

$$w_l = 1 - |13.5 - (l/15) - h| \quad (6)$$

$$w_l \in [0, 1]$$

The weighting scheme in Eq. (7) was chosen over simply using the model output for 1400 local standard time ~~(to the nearest hour).~~ for each longitude to create smooth transitions between adjoining time zones. This attempts to account for the day-to-day variability in OMI overpass tracks as well as the fact that pixels on the edge of a swath can be observed in two consecutive overpasses at different local times. More detail is given in the supplement.

$$w_l = 1 - |14 - (l/15) - h|$$

$$w_l \in [0, 1]$$

A spatial resolution of 12 km is used as the high spatial resolution a priori. To determine the effect of coarser spatial resolution, the model is also run at 108 km resolution. At 12 km resolution, profiles are spatially matched to OMI pixels by averaging all profiles that fall within the pixel bounds. At 108 km resolution, the profile closest to the pixel is used. When using daily profiles, they are temporally matched by identifying those closest to the scan time defined in the Time field of the ~~OMNO2~~ NASA SP v2 data product.

### 2.4 Implementation of daily profiles

Two retrievals are used to study the effects of incorporating daily a priori profiles in the BEHR algorithm. The first is what we term a "pseudo-retrieval~~" that is much simplified compared to a full operational retrieval.This allows us to focus on the effects of daily a priori profiles, with fewer confounding variables.~~." To create this retrieval, an $11 \times 19$ (across $\times$ along track) subset of pixels from OMI orbit 47335 centered on the pixel at $84.2513^\circ$ W and $33.7720^\circ$ N is used to provide the pixel corners, solar and viewing zenith and azimuth angles, terrain pressure, and terrain reflectivity. This swath places Atlanta near the nadir view of the OMI instrument (therefore providing pixels with good spatial resolution) while also remaining outside the row anomaly. This same subset of pixels is used for all days in the pseudo-retrieval. Cloud fractions are set to 0 for all pixels to consider clear-sky AMFs and simplify the pseudo-retrieval. AMFs are calculated for this subset of pixels with WRF-Chem $NO_2$ profiles from 1 June to 30 Aug 2013 in Eq. (2). This pseudo-retrieval will allow a simplified discussion of the effects of daily a priori profiles by:

1. Using a fixed set of OMI pixels. Because OMI pixels do not align day-to-day, using each day's true pixels makes a day-to-day comparison more difficult to see. In this pseudo-retrieval, that is alleviated.

2. Using a fixed set of OMI pixels also keeps the scattering weights ($w(p)$ in Eq. 2) constant as the parameters that the scattering weights depend on (solar and viewing zenith angles, relative azimuth angles, terrain albedo, and terrain height) are fixed.

3. Setting cloud fractions to 0 ensures that the AMF for every pixel is calculated with the full a priori profile, rather than just the above cloud part. Day-to-day variations in cloud fraction also lead to large changes in AMF because ~~a cloudy pixel will have a much greater AMF than a clear one, as it is more heavily weighted towards above cloud, higher altitude scattering weights which are greater than near-surface scattering weights~~the presence of clouds changes both the scattering weights (due to high assumed reflectivity of clouds and smaller effective surface pressure compared to ground) while also obscuring the $NO_2$ profile below the cloud.

Essentially, the pseudo-retrieval is a idealized experiment in which we hold all other variables except the a priori profile constant to compute the theoretical magnitude of the effect of using daily a priori profiles on the AMF. It will be used in Sect. 3.1 to demonstrate the effect of incorporating daily a priori profiles. The daily a priori profiles are also implemented in the full BEHR retrieval (no longer using a fixed set of pixels or forcing cloud fractions to 0) to determine the impact of including daily a priori profiles on the VCDs in a realistic case. ~~To allow comparison between days with different OMI overpass tracks~~When averaging in time, all pixels are oversampled to a $0.05^\circ \times 0.05^\circ$ grid. ~~When averaging over time, the~~ The contribution of each pixel is weighted by the inverse of its area.

### 2.5 Evaluation of exponentially-modified Gaussian (EMG) fits

Lu et al. (2015) and Valin et al. (2013) used $NO_2$ data from the ~~NASA OMNO2~~ DOMINO retrieval to study $NO_x$ emissions and lifetime from space, accounting for the effects of wind speed variation. To evaluate the impact of the a priori resolution on methods such as these, a similar procedure to fit an exponentially modified Gaussian function to $NO_2$ line densities is used. The surface wind direction and speed are calculated as the average of the first five layers ($\sim$ 500 m) of the 9 WRF 12 km grid cells closest to Atlanta at 1400 local standard time for each day~~after~~, WRF wind fields are given relative to the model grid; however, the $x$ and $y$ coordinates of the grid do not correspond directly to longitude and latitude. Therefore, the wind fields must be transformed from grid-relative to earth-relative (http://www2.mmm.ucar.edu/wrf/users/FAQ_files/Miscellaneous.html) as:

$$U_{\text{earth}} = U_{\text{model}} \times \cos(\alpha) - V_{\text{model}} \times \sin(\alpha) \tag{7}$$

$$V_{\text{earth}} = V_{\text{model}} \times \cos(\alpha) + U_{\text{model}} \times \sin(\alpha) \tag{8}$$

where $U$ and $V$ are the longitudinal and latitudinal wind fields, and $\cos(\alpha)$ and $\sin(\alpha)$ are outputs from WRF as the variables COSALPHA and SINALPHA.

As in Valin et al. (2013), the satellite pixels are rotated so that wind direction (and therefore $NO_2$ plumes) for each day lie along the $x$-axis. Pixels affected by the row anomaly or with a cloud fraction $> 20\%$ are removed. Pixels within $1^\circ$ upwind and $2^\circ$ downwind are gridded to $0.05^\circ \times 0.05^\circ$ and integrated across $1^\circ$ perpendicular to the $x$-axis. This produces line densities, which are a one-dimensional representation of the $NO_2$ concentration at various distances downwind of the city. Three a priori sets are used to create the retrievals used in this section: coarse (108 km) monthly average, fine (12 km) monthly average, and fine (12 km) daily profiles.

We use the form of the EMG function described in Lu et al. (2015) to fit the calculated $NO_2$ line densities, after expanding the definition of the cumulative distribution function:

$$F(x|a,x_0,\mu_x,\sigma_x,B) = \frac{a}{2x_0}\exp\left(\frac{\mu_x}{x_0}+\frac{\sigma_x^2}{2x_0^2}-\frac{x}{x_0}\right)\mathrm{erfc}\left(-\frac{1}{\sqrt{2}}\left[\frac{x-\mu_x}{\sigma_x}-\frac{\sigma_x}{x_0}\right]\right)+B \quad (9)$$

~~and~~ where erfc is the error function complement, i.e. $\mathrm{erfc}(x) = 1-\mathrm{erf}(x)$. $F(x|a,x_0,\mu_x,\sigma_x,B)$ serves as an analytical function that can be fitted to the observed line densities. We find the values of $a$, $x_0$, $\mu_x$, $\sigma_x$, and $B$ that minimize the sum of squared residuals between $F(x|a,x_0,\mu_x,\sigma_x,B)$ and the line densities, $NO_2(x)$:

$$Resid(a,x_0,\mu_x,\sigma_x,B) = \sum_x \left(F(x|a,x_0,\mu_x,\sigma_x,B) - \mathrm{NO_2}(x)\right)^2 \quad (10)$$

~~The Matlab function fmincon is used to minimize~~ Eq. (10) is minimized using an interior-point algorithm, finding the values of $a$, $x_0$, $\mu_x$, $\sigma_x$, and $B$ that best fit the line densities. The values of $a$, $x_0$, $\mu_x$, $\sigma_x$, and $B$ have physical significance ~~(enumerated in Table ??)~~ and so their optimum values yield information about the $NO_x$ emission and chemistry occurring within the plume ~~. In practice, several additional refinements to the algorithm are necessary to properly fit the line densities:~~ (Beirle et al., 2011; de Foy et al., 2014; Lu et al., 2015) . Specifically:

- ~~The constraints listed in Table ?? must be imposed to ensure physically realistic values of $a$ , $x_0$, $\mu_x$, $\sigma_x$, and $B$ are obtained.~~

  $a$ describes the total amount of $NO_2$ in the plume (referred to as the burden)

- ~~Any not-a-number (NaN) values in the EMG function (Eq. 9) are replaced with infinity, thus making the fitting function (Eq. 10) report that the current values of $a$, $x_0$, $\mu_x$, $\sigma_x$, and $B$ are unacceptable. NaNs occur in the EMG function when the exponential goes to infinity and the error function to zero, typically when the fitting parameters are unrealistically large or small and the fit is incorrectly a flat line. By doing this replacement and using the Matlab function nansum (which ignores NaNs during the summation but will return 0 if all values are NaN) to do the summation in Eq. , we allow NaNs to occur in the line densities (representing missing data, which is thus ignored) but not the fit.~~

  $x_0$ is the distance the plume travels in one lifetime, $\tau$. It relates to $\tau$ by $x_0 = \tau \times w$, where $w$ is wind speed.

- ~~fmincon requires an initial value for $a$, $x_0$, $\mu_x$,~~ $u_x$ describes the effective center of the emission source. In the supplement to Beirle et al. (2011) , it is represented by $X$ which is the point at which exponential decay of the $NO_2$ plume begins.

- $\sigma_x$ ~~, and $B$. For the first minimization, best-guess values for these are computed as specified in Table ?? (see supplement for rationale for each). However, fmincon uses an interior-point minimization algorithm by default. Such algorithms use a line search strategy which minimizes a function by following the derivative at the current point "downhill" (??) . If the algorithm begins in a region from which~~ is the standard deviation of the Gaussian component of the ~~downhill path leads to~~

~~a local, rather than global, minimum, the global minimum may never be found by this algorithm. This can be alleviated by carrying out multiple minimizations, starting from a different point each time, and choosing the result with the smallest residual. The randomization draws from the range of values defined by the upper and lower limits for each parameter with a uniform probability distribution. For $a$ and $x_0$,upper bounds of $5 \times 10^6$ mol and 1000 km, respectively, are used during the randomization process, as a finite upper bound is necessary for the randomization algorithm. This randomization and reoptimization was carried out nine times per fit. Additional randomization of~~ EMG function. Lu et al. (2015) terms this a "smoothing length scale," which describes smoothing of the ~~initial point does not improve the fit. Each time the optimum value of~~ data due to the spatial resolution and overlap of OMI pixels (Boersma et al., 2011) . It can also be thought of as capturing effects of both the spatial extent of emissions and the turbulent wind field.

– $B$ is the ~~fitting function is compared to the previous minimum; if it is less, the new fit is accepted~~background line density.

For each parameter, uncertainty from the fitting process itself is computed as the 95% confidence interval calculated using the standard deviation obtained from the fitting process. This is combined in quadrature with 10% uncertainty due to across wind integration distance, 10% uncertainty due to the choice of wind fields, and ~~$25\%/\sqrt{n}$~~ 25% uncertainty from the VCDs, similar to Beirle et al. (2011) and Lu et al. (2015). ~~A full description of this calculation is provided~~ Technical details of the EMG fitting and uncertainty calculation are given in the supplement.

## 3 Results

### 3.1 Daily variations

Fig. 2 shows the average wind and modeled $NO_2$ columns for June 2013, and the AMF values for the psuedo-retrieval around Atlanta, GA, USA. Atlanta was chosen as the focus of this study because it represents a strong $NO_x$ source relatively isolated from other equally large sources. This ensures that changes to the a priori profiles on a daily basis can be attributed to a local cause. The prevailing wind pattern advects $NO_2$ to the northeast of Atlanta (the location of Atlanta is marked by the star), as can be seen in the wind field shown in Fig. 2b and the WRF-Chem $NO_2$ columns in Fig. 2c. The average surface wind speed over Atlanta for June is ~~3.9~~ 5.0 m/s. This distribution of $NO_2$ leads directly to the lower AMFs seen to the northeast of Atlanta in Fig. 2d through Eq. (2).

To illustrate the effect of incorporating daily a priori profiles into the retrieval, we consider two days: 18 and 22 June 2013. These provide an illustration of the effect of changes in both wind speed and direction. Figure 3a–c shows the result from implementing the daily profiles for 22 June. On this day, the winds over Atlanta blow out of Atlanta to the northwest, with a speed at the surface of ~~3.6~~ 4.5 m/s. This is similar to the monthly average speed (~~3.9~~ 5.0 m $s^{-1}$) but are rotated 90° counterclockwise compared with the monthly average. The change in direction results in much greater near-surface $NO_2$ to the northwest compared to the monthly average (Fig. 3b) as the wind direction advects $NO_2$ into an area with low $NO_2$ in the monthly average.

Figure 3c shows that the greater near-surface $NO_2$ to the northwest results in lower AMFs than average (red), while the opposite is true to the east (blue). The greater near-surface $NO_2$ in profiles to the northwest weights $S(p)$ in Eq. (2) more heavily towards lower altitudes, where $w(p)$ is less, thus decreasing the overall AMF by $\sim$15%. The increase in AMFs to the east reflects the inflow of cleaner air from the shift in winds. This reduces near-surface $NO_2$ and increases the weight of higher altitudes of $S(p)$, increasing the AMFs by ~~26–37~~~10–35% (the colorbar saturates at $\pm$25% to make the decrease to the northwest easier to see).

Wind speed also plays an important role in determining the a priori profile shape through transport and chemistry. Fig. 3d–f shows results from 18 June, where the wind speed over Atlanta averaged ~~6.8~~ 9.1 m/s. This results in faster advection away from emission sources, with 10–15% increases in modeled $NO_2$ columns to the west as the plume is driven east more strongly. The greatest decreases in AMF (and thus increases in VCD) are as much as ~~−11%~~ −13% and occur between 84° and 83° W where the increased wind speed has advected the $NO_2$ plume farther than the average. There is also a ~~2–10~~2–13% increase along the east edge of Atlanta, resulting from the shift of the plume center east.

When the change in AMF from using the hybrid daily a priori profiles is averaged over the full time period studied (1 June–30 Aug), the percent change in AMF is on average +3.6% throughout the domain with a maximum of +9.8%. All pixels show a positive change. This occurs because 77% of the daily profiles have less $NO_2$ than the corresponding monthly average profile, as most pixels will be upwind from the city on any given day and will see a decrease in $NO_2$ when upwind and downwind days are no longer averaged together. This reduces the denominator in Eq. (3) and increases the contribution of upper tropospheric scattering weights to the AMF. Scattering weights increase with altitude; therefore, this results in a systematic increase of the AMF throughout the domain for the pseudo-retrieval.

We also consider the relative importance of day-to-day changes in the boundary layer of the a priori profiles versus day-to-day changes in the free troposphere of the a priori profiles by running the pseudo-retrieval with a set of hybrid daily profiles that only include day-to-day variability below 750 hPa and use a monthly average profile above that. The changes in AMFs using these hybrid profiles versus monthly average profiles are very similar to those observed when using the full daily profiles. In general, the hybrid profiles has a slightly greater average increase in AMFs (~~+4.2% vs. +3.6%~~+3.2% vs. +2.7%) and slightly less extreme changes, but the overall distribution of changes in AMFs is very similar. From this, we can conclude that changes in the boundary layer of the a priori profiles are the dominant reason for changes to the AMFs. However, the WRF-Chem simulations used to produce the a priori profiles did not include lightning $NO_x$, so this should be considered a lower bound for the effect of day-to-day changes in the free troposphere. The detailed comparison is described in the supplement.

### 3.2 Effects on retrieved ~~VCDs~~ vertical column densities in full retrieval

To determine the effect the inclusion of daily a priori profiles has on the final retrieved ~~VCDs~~vertical column densities (VCDs), the daily profiles were implemented in the full BEHR retrieval. Effects on individual days and multi-month average VCDs are presented here. The cities of Birmingham, AL, USA and Montgomery, AL, USA are included to demonstrate that this effect is significant for cities of various sizes. Atlanta, GA, USA is the largest with approximately 5.7 million people, followed by Birmingham, AL, USA with 1.1 million, and Montgomery, AL, USA with 374,000 (United States Census Bureau). ~~For~~

~~simplicity, we will consider changes significant if they are greater than the global mean uncertainty of $1 \times 10^{15}$ molec. cm$^{-2}$ in tropospheric vertical column densities computed by Bucsela et al. (2013) for the NASA OMNO2 OMI product version 2.1.~~

Table 1 describes how frequently significant ~~($> 1 \times 10^{15}$ molec. cm$^{-2}$)~~ changes in the retrieved VCD occur for pixels within 50 km of Atlanta, Birmingham, and Montgomery. Changes are considered significant by two different criteria. First, we consider the global mean clear-sky uncertainty from Bucsela et al. (2013) . As we are modifying the a priori profiles, and thus potentially the uncertainty associated with the choice of profiles, this gives us a fixed value to compare against. Second, we use the quadrature sum of uncertainties from spectral fitting ($0.7 \times 10^{15}$ molec. cm$^{-2}$, Boersma et al. 2007, 2011 ), stratospheric separation ($0.2 \times 10^{15}$ molec. cm$^{-2}$, Bucsela et al. 2013 ), and AMF calculation (20%, Bucsela et al. 2013 ), assuming that these are independent and so can be added in quadrature (Boersma et al., 2004) . We consider the fraction of days with at least one pixel exhibiting a significant change in VCD (rather than the fraction of pixels) because the main $NO_2$ plume may only fall within a small number of pixels. ~~Approximately one-third to two-thirds of days will~~ Up to 54% of days exhibit changes in the VCDs greater than $1 \times 10^{15}$ molec. cm$^{-2}$, and up to 43% exhibit changes greater than the quadrature sum of uncertainties. This indicates that when considering individual daily measurements, a considerable fraction of days with any valid pixels would have biases in the retrieved VCDs above the ~~global mean~~ uncertainty due to the temporal resolution of the a priori $NO_2$ profiles.

For both significance criteria, Table 1 also indicates that Birmingham and its surrounding area exhibits the largest and most frequent changes when using a daily a priori profile. Figure 4a shows the NO emissions throughout this domain. Birmingham has the second largest $NO_x$ emission rate, after Atlanta, while Montgomery has the smallest of the three cities considered. We note that the largest changes are not associated with the city with the greatest $NO_x$ emissions. Both Atlanta and Birmingham fall entirely within the $NO_x$ suppressed regime in the model, so the larger changes in Birmingham are not because $NO_x$ chemistry transitions between the $NO_x$ suppressed and $NO_x$ limited regimes. Instead, the magnitude of these changes is due to Birmingham's intermediate size, where significant $NO_2$ is present, but emission occurs over a small enough area that changes in wind direction can significantly affect $NO_2$ concentration at a short distance from the source. When considering changes to be significant if they exceed $1 \times 10^{15}$ molec. cm$^{-2}$, Montgomery has the least frequent significant changes because it has the smallest VCDs, so a change to the AMF needs to be rather large to produce a significant change in the VCD by this metric, since the AMF is a multiplicative factor. When considering the quadrature sum of errors as the significance criterion, Montgomery and Atlanta both demonstrate significant changes $\sim 20\%$ of the time.

Implementing the daily profiles also changes the average VCDs, in addition to the day-to-day changes in VCDs discussed above. Figure 4b shows the changes in VCDs averaged over the period studied. The ~~main~~ largest decrease around Atlanta is to the northeast, along the direction that the monthly average model results placed the $NO_2$ plume~~. A~~, but clear decreases can also be seen to the northwest and southwest. In these directions, a systematic decrease of ~~5–10to the northeast of Atlanta is observed; this is the plume direction inthe monthly average profiles. The absolute change is small~~ (up to 8% ($4 \times 10^{14}$ molec. cm$^{-2}$) is observed. Although this change is small, it is expected to be systematic. Statistically, a pixel's a priori profile is more likely to have less surface $NO_2$ when different wind directions are no longer averaged in, thus decreases in the VCD when using a daily a priori profile are more common.

Greater relative changes are observed around the smaller cities of Birmingham (down to $-12.9\%$, $5 \times 10^{-14}$ molec. cm$^{-2}$) ~~but this is above the~~ and Montgomery (down to $-13\%$, $4 \times 10^{-14}$ molec. cm$^{-2}$). This appears to be due primarily because the areas of emissions are smaller which makes shifts in wind direction have a greater average relative effect on the plume shape.

We also compare this average change to the measurement uncertainty. The uncertainty due to random errors in the retrieval should reduce as the square root of the number of observations, but delineating random and systematic errors in the retrieval is challenging (Boersma et al., 2004) . The most optimistic approach assumes that the global average uncertainty ~~, as the nominal uncertainty~~ of $1 \times 10^{15}$ molec. cm$^{-2}$ ~~can be~~ (Bucsela et al., 2013) can be treated entirely as random error, and can be reduced by $\sqrt{40}$ for the number of observations (not impacted by clouds or the row anomaly), to a lower bound of $\sim 1.6 \times 10^{14}$ molec. cm$^{-2}$. ~~The greatest changes are observed around the smaller cities of Birmingham (down to $-13.8\%$) and Montgomery (down to $-14.8\%$). This appears to be due primarily because the areas of emissions are smaller which makes shifts in wind direction have a greater average effecton the plume shape.~~ Most of the changes near the three cities exceed this lower limit. More realistically, the spectral fitting and stratospheric uncertainty may be considered largely random, but only part of the error in the AMF calculation is random, due to spatial or temporal autocorrelation in the models or ancillary products (Boersma et al., 2004) . For simplicity, we assume that the spectral fitting and stratospheric subtraction errors are entirely random, while only half of the error in the AMF is random. This reduces the error from $\sqrt{(0.7 \times 10^{15})^2 + (0.2 \times 10^{15})^2 + (20\%)^2}$ to $\sqrt{(0.11 \times 10^{15})^2 + (0.03 \times 10^{15})^2 + (11.6\%)^2}$. Only the largest changes near Birmingham and Montgomery exceed this threshold. This more conservative estimate suggests that the changes in averages are primarily important for smaller or very geographically concentrated cities, where wind direction can have a large effect. Nevertheless, larger cities may exhibit important changes as well.

Unlike the pseudo-retrieval, where we only allowed the a priori profiles to vary day-to-day and clouds were set to zero, there is a some spatial structure to these average changes. This is primarily a statistical phenomenon. We use only pixels with cloud fraction $< 20\%$, which reduces the number of pixels in the average. Within this subset, the wind blows to the southeast out of Atlanta more frequently than other directions; so the increases due to properly accounting for the presence of surface $NO_2$ average with the more typical decreases to give a small average change. The other directions exhibit the expected average decrease in VCDs due to the average increase in AMFs discussed in section 3.1. We expect that over longer periods of time all directions would see a 2–6% decrease in the average VCDs.

## 4 Discussion

### 4.1 Importance of model uncertainty

WRF-Chem has generally been found to reproduce wind fields, especially above 2 m s$^{-1}$ (Tie et al., 2007; Zhang et al., 2009) , and spatial variability of trace gases (Follette-Cook et al., 2015) well. Nevertheless, a natural concern when modeling daily $NO_2$ profiles for satellite retrievals is the accuracy of the plume location. We, however, note that the transition from monthly average to daily profiles does not necessarily result in increased model uncertainty, but rather a change in the type of uncertainty.

When using monthly average profiles, the uncertainty in the modeled $NO_2$ concentrations compared to the true mean will be reduced (assuming at least some component of the error is random in nature), but the true day-to-day variability not captured by the monthly average effectively becomes a new error term. In contrast, when using daily profiles, the random model error is not reduced, but the day-to-day variability is also not averaged out. Ideally, the error in a set of daily profiles will manifest as deviation from the true set of profiles for that day, rather than the monthly profiles' smaller deviation from a mean set of profiles that itself may not represent any single day. An important step in managing the uncertainty in the daily profiles is to constrain the modeled meteorology with observations or reanalysis datasets. By default, meteorology in WRF is constrained via initial and boundary conditions only. With larger domains and longer runs, further constraints using four-dimensional data assimilation (FDDA, Liu et al. 2006 ) and/or objective analysis (Follette-Cook et al., 2015; Wang et al., 2014; Yegorova et al., 2011) , possibly combined with periodic model reinitialization (Otte, 2008) are strongly recommended.

### 4.2 Effects on space-based lifetime and emissions constraints

Recently several authors have used wind-sorted satellite $NO_2$ observations to probe $NO_x$ chemistry and emissions from space (Beirle et al., 2011; Valin et al., 2013; de Foy et al., 2014; Lu et al., 2015; Liu et al., 2016). We apply the EMG fitting method of Lu et al. (2015) to $NO_2$ line densities derived from $NO_2$ columns retrieved using the daily and monthly average a priori profiles, as well as a monthly average profile simulated at 108 km resolution for both Atlanta and Birmingham. To match the method of Lu et al. (2015) as closely as possible, we use 3 m $s^{-1}$ as the division between slow and fast winds.

We acknowledge that a 91 day averaging period is significantly shorter than those used in Beirle et al. (2011), Valin et al. (2013), or Lu et al. (2015) (5 years, summer half-year for 7 years, and summer half-year for 3 year periods, respectively). However, since the goal of this section is to compare the results obtained using three different sets of a priori profiles with all other variables equal, we believe that 91 days is sufficient for this purpose.

Additionally, we do not include days around Atlanta in which the wind blows towards the southeast (specifically 0° to -112.5°, 0° is defined as east, negative values are clockwise from east). Significant suburban $NO_2$ columns near 83.5° W, 33° N add a secondary maximum to the line densities which can erroneously lengthen the decay time of the fit. All wind directions are used for Birmingham.

Accounting for the spatial and temporal variability of $NO_2$ in the a priori profiles leads to several notable changes in the line densities and the resulting EMG fits. Figure 5 shows the line densities and the corresponding EMG fits around Atlanta for the average over the 91 day study period. Table 2 enumerates the values obtained for the fitting parameters in Eq. (9) for the fits of the Atlanta $NO_2$ plume in Fig. 5 and fits for the Birmingham $NO_2$ plume (not shown).

The spatial scale of the a priori makes the greatest difference to the maximum value of the line density, causing a significant increase in $a$ when the spatial resolution of the a priori profiles increases from 108 km to 12 km. This reflects the impact of the blurring of urban and rural profiles described in Russell et al. (2011).

Both the spatial and temporal resolution impact the determination of $x_0$, the distance traveled in one lifetime. This parameter is determined at fast wind speeds (Lu et al., 2015; Valin et al., 2013), so we consider only the results for wind speed $\geq 3.0$ m $s^{-1}$. For Atlanta, using a daily a priori results in an $x_0$ value 30% greater than that obtained using a monthly average profile

at the same spatial resolution (12 km). The same comparison for Birmingham ~~, AL~~ shows a 66% increase in $x_0$ between the monthly and daily 12 km a priori.

$\mu_x$ represents the apparent center of the $NO_2$ plume relative to the geographic center of the city. This moves downwind (positive) when changing from the monthly average 12 km or 108 km a priori to the daily 12 km a priori. This reflects the ability of the daily a priori to capture how the wind distorts the plume shape.

$\sigma_x$ is the Gaussian smoothing length scale, representing both the width of the upwind Gaussian plume and smoothing of the $NO_2$ signal due to the physical extent of the source, the averaging of $NO_2$ within one OMI pixel, and daily variability in the overpass track (Beirle et al., 2011) . There is a slight decrease when going from a monthly average to daily profiles, which reflects the general increase in upwind AMFs (i.e. compare Fig. 1a and 1b), but because this is outside of the main $NO_2$ plume, the effect is small.

Finally, $B$ is the background line density. Ideally, it is derived sufficiently far from any $NO_x$ sources that spatial and temporal variability should be minimal. Indeed, in ~~three of the four cases any change in derived background is less than the uncertainty~~both fast wind cases no change is observed. When considering slow winds ~~around Birmingham~~ there is a $\sim 25\%$ increase when improving the spatial resolution of the a priori profiles. This is likely attributable to the general increase in urban signal discussed several times so far pulling the edges of the line density upward. However, a greater selection of cities is necessary to demonstrate this more conclusively.

Ultimately, the goal of this method is to extract information about chemically relevant quantities such as emission rate and lifetime. Since de Foy et al. (2014) and Valin et al. (2013) showed that choice of wind speed bins affects the values obtained, we also consider if the effect of implementing the daily a priori profile changes if the observations are binned by different wind speed criteria. Table 3 compares the values of the $NO_x$ emission rate, $E$, and effective lifetime, $\tau_{\text{eff}}$, derived from different wind speed bins for Atlanta and Birmingham. Restricting the analysis to days with wind speed greater than 5 m s$^{-1}$ results in too few days for a meaningful analysis around Atlanta (due to the need to remove days with winds to the southeast), so results for Atlanta are restricted to $\geq 3$ m s$^{-1}$ and $\geq 4$ m s$^{-1}$ only.

$\tau_{\text{eff}}$ and $E$ are each computed from several of the EMG fitting parameters. $\tau_{\text{eff}}$ depends on $x_0$ and $w$ (the mean wind speed) through Eq. (11):

$$\tau_{\text{eff}} = \frac{x_0}{w} \tag{11}$$

$E$ depends on $a$, $x_0$, and $w$ ~~(the mean wind speed)~~ through Eq. (12):

$$E = 1.32 \times \frac{a \times w}{x_0} = 1.32 \times \frac{a}{\tau_{\text{eff}}} \tag{12}$$

where the factor of 1.32 accounts for the $NO_x$:$NO_2$ ratio throughout the tropospheric column (Beirle et al., 2011).

Both Valin et al. (2013) and de Foy et al. (2014) show that lifetime should decrease at faster wind speeds. We see this trend for Birmingham but not Atlanta. de Foy et al. (2014) also saw that, for a chemical lifetime of 1 h, greater derived emissions were

found at faster wind speeds. This is also better seen in our results for Birmingham than Atlanta. Previous measurements of $NO_x$ lifetime in urban plumes ~~which~~ average 3.8 h and range from 2-6 h (Beirle et al., 2011; Ialongo et al., 2014; Nunnermacker et al., 1998; Spicer, 1982), and, using the EMG method, Lu et al. (2015) saw effective lifetimes between 1.2 and 6.8 h. The lifetimes we calculate are at the low end of the previously observed ranges. However, this is similar to the instantaneous lifetime of $1.2 \pm 0.5$ h and $0.8 \pm 0.4$ h calculated from the WRF-Chem model for days in June 2013 with wind speed $\geq 3$ m s$^{-1}$ and grid cells within 50 km of Atlanta and Birmingham, respectively (see the supplement for the calculation details).

~~We use $t$-tests at the 95confidence level (Harris, 2010) to determine if differences in emissions and lifetimes are significantly different among the results derived from using the three different a priori profile sets for a given city and wind speed bin (i.e. we compare the three values of~~ The differences in the lifetimes and emissions derived using ~~different a priori profiles for Atlanta and wind speeds $\geq 3$ m s$^{-1}$). For emissions, the choice of a priori leads to statistically different emissions for all five cases. For the derived lifetimes, in all cases the monthly 108 km and daily 12 km a priori are statistically indistinguishable, but the monthly 12 km a priori is statistically different.~~

~~We note that there is a systematic difference in the lifetimes derived using the daily~~ the daily and monthly 12 km a priori profiles are systematic. In all cases, the lifetime derived using the daily profiles is 30–50% longer. When using monthly average a priori profiles, profiles resulting from different wind directions are averaged together. The AMFs calculated from these profiles thus reflect the ~~the~~ average distance from the city the plume reaches in a given direction, e.g. east of the city, with smaller AMFs near the city and greater AMFs more distant (Fig. 1). In this hypothetical example, when the wind blows to the east, the spatial extent of the plume is underestimated because the average AMFs towards the end of the plume will be too large, so the VCDs will be too small by Eq. (1). On days when the wind does not blow east, the reverse is true: the plume extent is overestimated because the AMFs nearer to the city are too small (Fig. 1d). If one considers a simple average change in the VCDs, these two errors will partially cancel and we will see the average change from Sect. 3.2. However, in the EMG fitting approach, these errors do not cancel at all because the EMG method both rotates the $NO_2$ plumes so that the wind directions align before calculating the line densities and systematically selects fast winds to determine $\tau_{\text{eff}}$, so we are always dealing with the first case and the plume extent is always underestimated. In the EMG fit, this manifests as a too short lifetime. As the emissions are inversely proportional to lifetime (Eq. 12), emissions derived using the monthly 12 km a priori profiles will be too great. Therefore, when using a retrieval with a priori profile at fine spatial resolution, daily temporal resolution of the a priori profiles is necessary to prevent underestimating the lifetime. Further, the spatial resolution of the a priori profiles has a large impact on the magnitude of the derived emissions. To reduce the systematic biases in emissions and lifetime from the choice of a priori profile, it is necessary to simulate these profiles at fine spatial and daily temporal resolution.

We also ~~compare the derived emissions~~ use 2-sample $t$-tests at the 95% confidence level (Harris, 2010) to determine if differences in emissions and lifetimes given in Table 3 are significantly different among the results derived from using the three different a priori profile sets for a given city and wind speed bin (i.e. we compare the three values of emissions derived using different a priori profiles for Atlanta and wind speeds $\geq 3$ m s$^{-1}$). This found that, for emissions, the choice of a priori leads to statistically different emissions for all five cases. For the derived lifetimes, in all cases the monthly 108 km and daily 12 km a priori are statistically indistinguishable, but the monthly 12 km a priori is statistically different. We note that a Durbin-Watson

test indicates some spatial autocorrelation remains, and so the uncertainty may be underestimated and the $t$-tests may be incorrectly identifying the differences as significant in this case (Chatterjee and Hadi, 2012) . Even if this is true, with a longer averaging period such as those in Beirle et al. (2011) , Valin et al. (2013) , and Lu et al. (2015) , we would expect the random uncertainties to reduce while the systematic difference from the choice of a priori profile remains. Therefore, the choice of a priori profiles does have an important effect on derived emissions and lifetimes.

We also compare the derived emissions rates to the emissions in a 12 km WRF-Chem model driven by the NEI 11 emission inventory with $NO_x$ emissions scaled to 88.9% of the 2011 values to account for the decrease between 2011 and 2013 (EPA, 2016). WRF-Chem emissions are calculated as the sum of all grid cells within a 50 km radius of the city. 50 km was chosen as the line densities were integrated for $\sim 50$ km to either side perpendicular to the wind direction. The coarse monthly a priori are ~~43–62~~43–61% lower than the NEI-driven emissions, while emissions derived using daily 12 km a priori are within 5–24% (both greater and less than the NEI emissions). Recent work (e.g. Travis et al. 2016 and references within) suggests that the NEI inventory is overestimated by $\sim 50\%$ using both satellite and in situ observations. Emissions derived using daily 12 km show the best agreement to the current NEI inventory, and emissions derived using monthly 108 km a priori profile agree with the NEI inventory reduced by 50%. Therefore, we cannot say which a priori profiles provide the best measurement of emissions by comparing to NEI. It is likely that emissions derived using the monthly 12 km a priori profiles are an overestimate, ~~possibly~~ because the systematically low lifetimes discussed above increase $E$ through Eq. (12); that these emissions are consistently higher than the NEI emission reinforces this likelihood. Conversely, we expect that emissions derived using the coarse monthly a priori profiles are biased low due to the known underestimate of urban $NO_x$ signals using coarse a priori (Russell et al., 2011) . ~~Emissions derived using daily 12 km and monthly 108 km a priori profile agree with the current and 50% reduced NEI emissions, respectively.~~ From this, it is clear the choice of a priori profiles has a substantial impact on emissions derived from satellite observations, and that both spatial and temporal resolution of the a priori profiles contribute to that difference~~, and further work is needed to fully evaluate this impact in light of work such as Travis et al. (2016)~~ . This explains why the OMI derived emissions from Lu et al. (2015) are lower that the bottom up NEI inventory, but needs to be reconciled with work by Travis et al. (2016) which indicates that NEI is overestimated.

In summary, the two most important parameters ($a$ and $x_0$) and values derived from them ($E$, $\tau_{\text{eff}}$) are significantly affected by the spatial and temporal resolution of the a priori. $a$ ~~and~~ is most affected by increasing the spatial resolution of the a priori, while using daily profiles corrects a systematic bias in $x_0$ when the profiles are simulated at high spatial resolution. $E$ is affected by both the spatial and temporal resolution of the a priori profiles, increasing by $\sim 100\%$ between the retrievals using coarse monthly and fine daily a priori profiles. Therefore the use of daily a priori $NO_2$ profiles at high spatial resolution significantly alters the results obtained from fitting wind aligned retrieved $NO_2$ columns with an analytical function. ~~This will be most important when considering absolute measurements rather than trends, as the systematic biases should cancel out in a trend analysis.~~

## 5 Conclusions

We have demonstrated that incorporating daily $NO_2$ a priori profiles simulated at sufficiently fine spatial scales to capture the spatial variation of an $NO_2$ plume leads to significant changes in the final VCDs when compared to monthly average profiles at the same spatial resolution. Changes to VCDs on a single day are up to ~~40~~50% (relative) and ~~$3 \times 10^{15}$~~ $4 \times 10^{15}$ molec. cm$^{-2}$ (absolute). This is attributable to changes in the direction of the $NO_2$ plume. Up to 59% of days with valid observations exhibit changes in VCDs $> 1 \times 10^{15}$ molec. cm$^{-2}$ in at least one pixel. Additionally, the inclusion of daily profiles affects a systematic change in time-averaged VCDs around Atlanta, GA, USA. Pixels downwind in the average exhibited VCD decreases up to ~~10~~8% (~~$0.4 \times 10^{15}$~~ $4 \times 10^{14}$ molec. cm$^{-2}$). Larger relative changes of as much as $-13\%$ were found around the nearby cities of Birmingham, AL and Montgomery, AL. Day-to-day variations in the free troposphere have a smaller impact on the value of the AMF, and average out to no net change over the period studied. These results were obtained using WRF-Chem without lightning $NO_x$ emissions; it is likely that the inclusion of lightning $NO_x$ would increase the magnitude of positive changes to the AMF due to the presence of $NO_2$ at altitude to which OMI is highly sensitive.

When the methods of Lu et al. (2015) are applied to these prototype retrievals, significant changes in derived $NO_x$ emissions are found, increasing by as much as 100% for Atlanta compared to emissions derived from a retrieval using coarse a priori profiles. Using high spatial resolution, monthly average a priori profiles results in the highest derived emissions rates, followed by high spatial resolution, daily a priori, with spatially coarse a priori leading to the lowest derived emissions. ~~Further work is needed to understand the impact of this change on top down constraints of emissions, given the recent work showing that bottom up estimates are high by $\sim$ 50%.~~ Emissions derived using the fine daily a priori are within 25% of the bottom up number from the NEI inventory, a smaller reduction than that suggested by Travis et al. (2016) . Future work will aim to resolve this difference. Lifetimes derived from satellite observations using a spatially fine but monthly averaged a priori are systematically biased low due to the spatial pattern of AMF imposed by such a priori; ~~the~~ consequently, emissions derived using these a priori profiles are likely biased high. The use of daily profiles at fine spatial resolution corrects this systematic bias.

Having shown that the use of daily a priori $NO_2$ profiles in the retrieval algorithm significantly alters emissions and lifetimes derived from this retrieval, we plan to implement such profiles for several years at the beginning and current end of the OMI data record to investigate how $NO_x$ lifetimes have changed in urban plumes over the past decade. Such work can provide a greater understanding of the most effective means of improving air quality in years to come, as it will allow us to determine whether reductions in $NO_x$ or VOC emissions will provide the most benefit in ozone reduction.

*Acknowledgements.* The authors gratefully acknowledge support from the NASA ESS Fellowship NNX14AK89H, NASA grants NNX15AE37G and NNX14AH04G, and the TEMPO project grant SV3-83019. The MODIS Aqua L2 Clouds 5-Min Swath 1km and 5 km (MYD06_L2) and MODIS Terra+Aqua Albedo 16-Day L3 Global 0.05Deg CMG V005 were acquired from the Level-1 and Atmospheric Archive and Distribution System (LAADS) Distributed Active Archive Center (DAAC), located in the Goddard Space Flight Center in Greenbelt, Maryland (https://ladsweb.nascom.nasa.gov/). We acknowledge use of the WRF-Chem preprocessor tool mozbc, fire SUBSCRIPTNBemiss, etc. provided by the Atmospheric Chemistry Observations and Modeling Lab (ACOM) of NCAR. This research used

the Savio computational cluster resource provided by the Berkeley Research Computing program at the University of California, Berkeley (supported by the UC Berkeley Chancellor, Vice Chancellor of Research, and Office of the CIO).

## References


Acarreta, J. R., De Haan, J. F., and Stammes, P.: Cloud pressure retrieval using the O2-O2 absorption band at 477 nm, J. Geophys. Res. Atmos., 109, doi:10.1029/2003JD003915, http://dx.doi.org/10.1029/2003JD003915, d05204, 2004.

Bak, J., Kim, J. H., Liu, X., Chance, K., and Kim, J.: Evaluation of ozone profile and tropospheric ozone retrievals from GEMS and OMI spectra, Atmos. Meas. Tech., 6, 239–249, doi:10.5194/amt-6-239-2013, 2013.

Beirle, S., Huntrieser, H., and Wagner, T.: Direct satellite observations of lightning-produced $NO_x$, Atmos. Chem. Phys., 10, 10 965–10 986, doi:10.5194/acp-10-10965-2010, 2010.

Beirle, S., Boersma, K., Platt, U., Lawrence, M., and Wagner, T.: "Megacity Emissions and Lifetimes of Nitrogen Oxides Probed from Space", Science, 333, 1737–1739, 2011.

Boersma, K., Bucsela, E., Brinksma, E., and Gleason, J.: $NO_2$, in: OMI Algorithm Theoretical Basis Document, vol 4, OMI Trace Gas Algorithms, ATB-OMI-04, version 2.0, pp. 13–36, http://eospso.nasa.gov/sites/default/files/atbd/ATBD-OMI-04.pdf, 2002.

Boersma, K., Eskes, H., and Brinksma, E.: "Error analysis for tropospheric $NO_2$ retrieval from space, J. Geophys. Res. Atmos., 106, D04 311, doi:10.1029/2003JD003962, 2004.

Boersma, K., Eskes, H., Dirksen, R., van der A, R., Veefkind, J., Stammes, P., Huijnen, V., Kleipool, Q., Sneep, M., Claas, J., Leitão, J., Richter, A., Zhou, Y., and Brunner, D.: "An improved tropospheric $NO_2$ column retrieval algorithm for the Ozone Monitoring Instrument, Atmos. Meas. Tech., 4, 1905–1928, doi:10.5194/amt-4-1905-2011, 2011.

Boersma, K. F., Eskes, H. J., Veefkind, J. P., Brinksma, E. J., van der A, R. J., Sneep, M., van den Oord, G. H. J., Levelt, P. F., Stammes, P., Gleason, J. F., and Bucsela, E. J.: Near-real time retrieval of tropospheric NO<sub>2</sub> from OMI, Atmos. Chem. Phys., 7, 2103–2118, doi:10.5194/acp-7-2103-2007, 2007.

Browne, E. C., Wooldridge, P. J., Min, K.-E., and Cohen, R. C.: On the role of monoterpene chemistry in the remote continental boundary layer, Atmos. Chem. Phys., 14, 1225–1238, doi:10.5194/acp-14-1225-2014, 2014.

Bucsela, E., Krotkov, N., Celarier, E., Lamsal, L., Swartz, W., Bhartia, P., Boersma, K., Veefkind, J., Gleason, J., and Pickering, K.: "A new tropospheric and stratospheric $NO_2$ retrieval algorithm for nadir-viewing satellite instruments: applications to OMI, Atmos. Meas. Tech., 6, 2607–2626, doi:10.5194/amt-6-2607-2013, 2013.

Bucsela, E. J., Celarier, E. A., Wenig, M. O., Gleason, J. F., Veefkind, J. P., Boersma, K. F., and Brinksma, E. J.: Algorithm for $NO_2$ vertical column retrieval from the ozone monitoring instrument, IEEE T. Geosci. Remote, 44, 1245–1258, doi:10.1109/TGRS.2005.863715, 2006.

Burrows, J., Weber, M., Buchwitz, M., Rozanov, V., Ladstätter-Weißenmayer, A., Richter, A., DeBeek, R., Hoogan, R., Bramstedt, K., Eichmann, K.-U., Eisinger, M., and Perner, D.: The Global Ozone Monitoring Experiment (GOME): Mission Concept and First Scientific Results, 56, 151–175, doi:10.1175/1520-0469(1999)056<0151:TGOMEG>2.0.CO;2, 1999.

Castellanos, P., Boersma, K. F., and van der Werf, G. R.: Satellite observations indicate substantial spatiotemporal variability in biomass burning $NO_x$ emission factors for South America, Atmos. Chem. Phys., 14, 3929–3943, doi:10.5194/acp-14-3929-2014, 2014.

Chance, K., Liu, X., Suleiman, R. M., Flittner, D. E., Al-Saadi, J., and Janz, S. J.: Tropospheric emissions: monitoring of pollution (TEMPO), doi:10.1117/12.2024479, 2013.

Chatterjee, S. and Hadi, A.: Regression Analysis by Example, Ch 8: The Problem of Correlated Errors, John Wiley & Sons Inc., 2012.

Choi, Y.-S. and Ho, C.-H.: Earth and environmental remote sensing community in South Korea: A review, Remote Sensing Applications: Society and Environment, 2, 66–76, doi:10.1016/j.rsase.2015.11.003, 2015.

Cohan, D. S., Hu, Y., and Russell, A. G.: Dependence of ozone sensitivity analysis on grid resolution, Atmos. Environ., 40, 126–135, doi:10.1016/j.atmosenv.2005.09.031, 2006.

de Foy, B., Wilkins, J., Lu, Z., Streets, D., and Duncan, B.: Model evaluation of methods for estimating surface emissions and chemical lifetimes from satellite data, Atmos. Environ., 98, 66–77, doi:10.1016/j.atmosenv.2014.08.051, 2014.

Ding, J., van der A, R. J., Mijling, B., Levelt, P. F., and Hao, N.: $NO_x$ emission estimates during the 2014 Youth Olympic Games in Nanjing, Atmos. Chem. Phys., 15, 9399–9412, doi:10.5194/acp-15-9399-2015, 2015.

Emmons, L. K., Walters, S., Hess, P. G., Lamarque, J.-F., Pfister, G. G., Fillmore, D., Granier, C., Guenther, A., Kinnison, D., Laepple, T., Orlando, J., Tie, X., Tyndall, G., Wiedinmyer, C., Baughcum, S. L., and Kloster, S.: Description and evaluation of the Model for Ozone and Related chemical Tracers, version 4 (MOZART-4), Geosci. Model Dev., 3, 43–67, doi:10.5194/gmd-3-43-2010, http://www.geosci-model-dev.net/3/43/2010/, 2010.

EPA: Air Pollutant Emissions Trends Data, https://www.epa.gov/air-emissions-inventories/air-pollutant-emissions-trends-data, 2016.

Follette-Cook, M., Pickering, K., Crawford, J., Duncan, B., Loughner, C., Diskin, G., Fried, A., and Weinheimer, A.: Spatial and temporal variability of trace gas columns derived from WRF/Chem regional model output: Planning for geostationary observations of atmospheric composition, Atmos. Environ., 118, 28–44, doi:10.1016/j.atmosenv.2015.07.024, 2015.

Goliff, W. S., Stockwell, W. R., and Lawson, C. V.: The regional atmospheric chemistry mechanism, version 2, Atmos. Environ., 68, 174 – 185, doi:10.1016/j.atmosenv.2012.11.038, 2013.

Grell, G. A., Peckham, S. E., Schmitz, R., McKeen, S. A., Frost, G., Skamarock, W. C., and Eder, B.: Fully coupled "online" chemistry within the {WRF} model, Atmos. Environ., 39, 6957 – 6975, doi:10.1016/j.atmosenv.2005.04.027, 2005.

Gu, D., Wang, Y., Smeltzer, C., and Liu, Z.: Reduction in NOx Emission Trends over China: Regional and Seasonal Variations, Environ. Sci. Technol., 47, 12 912–12 919, doi:10.1021/es401727e, 2013.

Guenther, A., Karl, T., Harley, P., Wiedinmyer, C., Palmer, P. I., and Geron, C.: Estimates of global terrestrial isoprene emissions using MEGAN (Model of Emissions of Gases and Aerosols from Nature), Atmos. Chem. Phys., 6, 3181–3210, doi:10.5194/acp-6-3181-2006, http://www.atmos-chem-phys.net/6/3181/2006/, 2006.

Harris, D.: Comparison of Means with Student's $t$, chap. 4-3, pp. 76–78, W.H. Freeman, 8th edn., 2010.

Hastings, D. and Dunbar, P.: Global Land One-kilometer Base Elevation (GLOBE) Digital Elevation Model, Documentation, Volume 1.0. National Oceanic and Atmospheric Administration, National Geophysical Data Center, 325 Broadway, Boulder, Colorado 80303, U.S.A., 1999.

Heckel, A., Kim, S.-W., Frost, G. J., Richter, A., Trainer, M., and Burrows, J. P.: Influence of low spatial resolution a priori data on tropospheric $NO_2$ satellite retrievals, Atmos. Meas. Tech., 4, 1805–1820, doi:10.5194/amt-4-1805-2011, 2011.

Huang, M., Bowman, K. W., Carmichael, G. R., Chai, T., Pierce, R. B., Worden, J. R., Luo, M., Pollack, I. B., Ryerson, T. B., Nowak, J. B., Neuman, J. A., Roberts, J. M., Atlas, E. L., and Blake, D. R.: Changes in nitrogen oxides emissions in California during 2005–2010 indicated from top-down and bottom-up emission estimates, J. Geophys. Res. Atmos., 119, 12,928–12,952, doi:10.1002/2014JD022268, 2014.

Hudman, R. C., Moore, N. E., Mebust, A. K., Martin, R. V., Russell, A. R., Valin, L. C., and Cohen, R. C.: Steps towards a mechanistic model of global soil nitric oxide emissions: implementation and space based-constraints, Atmos. Chem. Phys., 12, 7779–7795, doi:10.5194/acp-12-7779-2012, http://www.atmos-chem-phys.net/12/7779/2012/, 2012.

Hudson, R., Kim, J.-H., and Anne M., T.: On the derivation of tropospheric column ozone from radiances measured by the total ozone mapping spectrometer, J. Geophys. Res. Atmos., 100, 11,134–11,145, 1995.

Ialongo, I., Hakkarainen, J., Hyttinen, N., Jalkanen, J.-P., Johansson, L., Boersma, K. F., Krotkov, N., and Tamminen, J.: Characterization of OMI tropospheric $NO_2$ over the Baltic Sea region, Atmos. Chem. Phys., 14, 7795–7805, doi:10.5194/acp-14-7795-2014, 2014.

Ingmann, P., Veihelmann, B., Langen, J., Lamarre, D., Stark, H., and Courrèges-Lacoste, G. B.: Requirements for the {GMES} Atmosphere Service and ESA's implementation concept: Sentinels-4/-5 and -5p, Remote Sens. of Environ., 120, 58–69, doi:10.1016/j.rse.2012.01.023, 2012.

Kim, S.-W., Heckel, A., Frost, G. J., Richter, A., Gleason, J., Burrows, J. P., McKeen, S., Hsie, E.-Y., Granier, C., and Trainer, M.: NO2 columns in the western United States observed from space and simulated by a regional chemistry model and their implications for NOx emissions, J. Geophys. Res. Atmos., 114, doi:10.1029/2008JD011343, 2009.

Koelemeijer, R. B. A. and Stammes, P.: Effects of clouds on ozone column retrieval from GOME UV measurements, J. Geophys. Res. Atmos., 104, 8281–8294, doi:10.1029/1999JD900012, 1999.

Krotkov, N. and Veefkind, P.: OMI/Aura Nitrogen Dioxide (NO2) Total and Tropospheric Column 1-orbit L2 Swath 13x24 km V003, version 003, Greenbelt, MD, USA, Goddard Earth Sciences Data and Information Services Center (GES DISC), accessed 19 May 2014, doi:10.5067/Aura/OMI/DATA2017.

Kuhlmann, G., Lam, Y. F., Cheung, H. M., Hartl, A., Fung, J. C. H., Chan, P. W., and Wenig, M. O.: Development of a custom OMI $NO_2$ data product for evaluating biases in a regional chemistry transport model, Atmos. Chem. Phys., 15, 5627–5644, doi:10.5194/acp-15-5627-2015, 2015.

Lamsal, L. N., Krotkov, N. A., Celarier, E. A., Swartz, W. H., Pickering, K. E., Bucsela, E. J., Gleason, J. F., Martin, R. V., Philip, S., Irie, H., Cede, A., Herman, J., Weinheimer, A., Szykman, J. J., and Knepp, T. N.: Evaluation of OMI operational standard $NO_2$ column retrievals using in situ and surface-based $NO_2$ observations, Atmos. Chem. Phys., 14, 11 587–11 609, doi:10.5194/acp-14-11587-2014, 2014.

Lamsal, L. N., Duncan, B. N., Yoshida, Y., Krotkov, N. A., Pickering, K. E., Streets, D. G., and Lu, Z.: U.S. $NO_2$ trends (2005–2013): EPA Air Quality System (AQS) data versus improved observations from the Ozone Monitoring Instrument (OMI), Atmos. Environ., 110, 130–143, doi:10.1016/j.atmosenv.2015.03.055, 2015.

Levelt, P., van der Oord, G., Dobber, M., Mälkki, A., Visser, H., de Vries, J., Stammes, P., Lundell, J., and Saari, H.: The Ozone Monitoring Instrument, IEEE Trans. Geosci. Remote Sense., 44, 1093–1101, doi:10.1109/TGRS.2006.872333, 2006.

Lin, J.-T., McElroy, M. B., and Boersma, K. F.: Constraint of anthropogenic $NO_x$ emissions in China from different sectors: a new methodology using multiple satellite retrievals, Atmos. Chem. Phys., 10, 63–78, doi:10.5194/acp-10-63-2010, 2010.

Lin, J.-T., Liu, M.-Y., Xin, J.-Y., Boersma, K. F., Spurr, R., Martin, R., and Zhang, Q.: Influence of aerosols and surface reflectance on satellite $NO_2$ retrieval: seasonal and spatial characteristics and implications for $NO_x$ emission constraints, Atmos. Chem. Phys., 15, 11 217–11 241, doi:10.5194/acp-15-11217-2015, 2015.

Liu, F., Beirle, S., Zhang, Q., Dörner, S., He, K., and Wagner, T.: NOx lifetimes and emissions of cities and power plants in polluted background estimated by satellite observations, Atmos. Chem. Phys., 16, 5283–5298, doi:10.5194/acp-16-5283-2016, 2016.

Liu, Y., Bourgeois, A., Warner, T., Swerdlin, S., and Hacker, J.: Implementation of the observation-nudging based on FDDA into WRF for supporting AFEC test operations. 6th WRF Conference, NCAR, Boulder, CO, USA, 2006.

Lu, Z., Streets, D., de Foy, B., Lamsal, L., Duncan, B., and Xing, J.: "Emissions of nitrogen oxides from US urban areas: estimation from Ozone Monitoring Instrument retrievals for 2005–2014", Atmos. Chem. Phys., 15, 10 367–10 383, doi:10.5194/acp-15-10367-2015, 2015.

Marchenko, S., Krotkov, N. A., Lamsal, L. N., Celarier, E. A., Swartz, W. H., and Bucsela, E. J.: Revising the slant column density retrieval of nitrogen dioxide observed by the Ozone Monitoring Instrument, J. Geophys. Res. Atmos., 120, 5670–5692, doi:10.1002/2014JD022913, 2014JD022913, 2015.

Martin, R., Sauvage, B., Folkins, I., Sioris, C., Boone, C., Bernath, P., and Ziemke, J.: Space-based constraints on the production of nitric oxide by lightning, J. Geophys. Res. Atmos., 112, doi:10.1029/2006JD007831, 2007.

Martin, R. V., Chance, K., Jacob, D. J., Kurosu, T. P., Spurr, R. J. D., Bucsela, E., Gleason, J. F., Palmer, P. I., Bey, I., Fiore, A. M., Li, Q., Yantosca, R. M., and Koelemeijer, R. B. A.: An improved retrieval of tropospheric nitrogen dioxide from GOME, J. Geophys. Res. Atmos., 107, doi:10.1029/2001JD001027, 4437, 2002.

McLinden, C. A., Fioletov, V., Boersma, K. F., Kharol, S. K., Krotkov, N., Lamsal, L., Makar, P. A., Martin, R. V., Veefkind, J. P., and Yang, K.: Improved satellite retrievals of $NO_2$ and $SO_2$ over the Canadian oil sands and comparisons with surface measurements, Atmos. Chem. Phys., 14, 3637–3656, doi:10.5194/acp-14-3637-2014, 2014.

Mebust, A. and Cohen, R.: Observations of a seasonal cycle in $NO_x$ emissions from fires in African woody savannas, Geophys. Res. Lett., 40, 1451–1455, doi:10.1002/grl.50343, 2013.

Mebust, A. and Cohen, R.: Space-based observations of fire $NO_x$ emissions coefficients: a global biome-scale comparison, Atmos. Chem. Phys., 14, 2509–2524, doi:10.5194/acp-14-2509-2014, 2014.

Mebust, A. K., Russell, A. R., Hudman, R. C., Valin, L. C., and Cohen, R. C.: Characterization of wildfire $NO_x$ emissions using MODIS fire radiative power and OMI tropospheric $NO_2$ columns, Atmos. Chem. Phys., 11, 5839–5851, doi:10.5194/acp-11-5839-2011, 2011.

Miyazaki, K., Eskes, H., and Sudo, K.: Global $NO_x$ emissions estimates derived from an assimilation of OMI tropospheric $NO_2$ columns, Atmos. Chem. Phys., 12, 2263–2288, doi:10.5194/acp-12-2263-2012, 2012.

Miyazaki, K., Eskes, H., Sudo, K., and Zhang, C.: Global lightning $NO_x$ production estimated by an assimilation of multiple satellite data sets, Atmos. Chem. Phys., 14, 3277–3305, doi:10.5194/acp-14-3277-2014, 2014.

Nunnermacker, L. J., Imre, D., Daum, P. H., Kleinman, L., Lee, Y.-N., Lee, J. H., Springston, S. R., Newman, L., Weinstein-Lloyd, J., Luke, W. T., Banta, R., Alvarez, R., Senff, C., Sillman, S., Holdren, M., Keigley, G. W., and Zhou, X.: Characterization of the Nashville urban plume on July 3 and July 18, 1995, J. Geophys. Res. Atmos., 103, 28 129–28 148, doi:10.1029/98JD01961, 1998.

Otte, T.: The Impact of Nudging in the Meteorological Model for Retrospective Air Quality Simulations. Part I: Evaluation against National Observation Networks., J. Appl. Meteorol. Clim., 47, 1853–1867, doi:10.1175/2007JAMC1790.1, 2008.

Palmer, P., Jacob, D., Chance, K., Martin, R., Spurr, R., Kurosu, T., Bey, I., Yantosca, R., Fiore, A., and Li, Q.: "Air mass factor formulation for spectroscopic measurements from satellites: Applications to formaldehyde retrievals from the Global Ozone Monitoring Experiment", J. Geophys. Res. Atmos., 106, 14 539–14 550, 2001.

Richter, A. and Wagner, T.: The Use of UV, Visible and Near IR Solar Back Scattered Radiation to Determine Trace Gases, in: The Remote Sensing of Tropospheric Composition from Space, edited by Burrows, J., Platt, U., and Borrell, P., Springer, New York, 2011.

Russell, A., Perring, A., Valin, L., Bucsela, E., Browne, E., Min, K., Wooldridge, P., and Cohen, R.: "A high spatial resolution retrieval of $NO_2$ column densities from OMI: method and evalutation", Atmos. Chem. Phys., 11, 8543–8554, doi:10.5194/acp-11-8543-2011, 2011.

Russell, A. R., Valin, L. C., and Cohen, R. C.: Trends in OMI $NO_2$ observations over the United States: effects of emission control technology and the economic recession, Atmos. Chem. Phys., 12, 12 197–12 209, doi:10.5194/acp-12-12197-2012, 2012.

Schaap, M., Cuvelier, C., Hendriks, C., Bessagnet, B., Baldasano, J., Colette, A., Thunis, P., Karam, D., Fagerli, H., Graff, A., Kranenburg, R., Nyiri, A., Pay, M., Rouïl, L., Schulz, M., Simpson, D., Stern, R., Terrenoire, E., and Wind, P.: Performance of European chemistry transport models as function of horizontal resolution, Atmos. Environ., 112, 90–105, doi:10.1016/j.atmosenv.2015.04.003, 2015.

Schumann, U. and Huntrieser, H.: The global lightning-induced nitrogen oxides source, Atmos. Chem. Phys., 7, 3823–3907, 2007.

Schwantes, R. H., Teng, A. P., Nguyen, T. B., Coggon, M. M., Crounse, J. D., St. Clair, J. M., Zhang, X., Schilling, K. A., Seinfeld, J. H., and Wennberg, P. O.: Isoprene $NO_3$ Oxidation Products from the $RO_2$ + $HO_2$ Pathway, J. Phys. Chem. A, 119, 10 158–10 171, doi:10.1021/acs.jpca.5b06355, 2015.

Sneep, M., de Haan, J. F., Stammes, P., Wang, P., Vanbauce, C., Joiner, J., Vasilkov, A. P., and Levelt, P. F.: Three-way comparison between OMI and PARASOL cloud pressure products, J. Geophys. Res. Atmos., 113, doi:10.1029/2007JD008694, d15S23, 2008.

Spicer, C.: Nitrogen Oxide Reactions in the Urban Plume of Boston, Science, 215, 1095–1097, doi:10.1126/science.215.4536.1095, 1982.

Stammes, P., Sneep, M., de Haan, J. F., Veefkind, J. P., Wang, P., and Levelt, P. F.: Effective cloud fractions from the Ozone Monitoring Instrument: Theoretical framework and validation, J. Geophys. Res. Atmos., 113, n/a–n/a, doi:10.1029/2007JD008820, 10.1029/2007JD008820, d16S38, 2008.

Tie, X., Madronich, S., Li, G., Ying, Z., Zhang, R., Garcia, A., Lee-Taylor, J., and Liu, Y.: Characterizations of chemical oxidants in Mexico City: A regional chemical dynamical model (WRF-Chem) study, Atmos. Environ., 41, 1989 – 2008, doi:10.1016/j.atmosenv.2006.10.053, 2007.

Tong, D. Q., Lamsal, L., Pan, L., Ding, C., Kim, H., Lee, P., Chai, T., Pickering, K. E., and Stajner, I.: Long-term {NOx} trends over large cities in the United States during the great recession: Comparison of satellite retrievals, ground observations, and emission inventories, Atmos. Environ., 107, 70–84, doi:10.1016/j.atmosenv.2015.01.035, 2015.

Travis, K. R., Jacob, D. J., Fisher, J. A., Kim, P. S., Marais, E. A., Zhu, L., Yu, K., Miller, C. C., Yantosca, R. M., Sulprizio, M. P., Thompson, A. M., Wennberg, P. O., Crounse, J. D., St. Clair, J. M., Cohen, R. C., Laugher, J. L., Dibb, J. E., Hall, S. R., Ullmann, K., Wolfe, G. M., Pollack, I. B., Peischl, J., Neuman, J. A., and Zhou, X.: NOx emissions, isoprene oxidation pathways, vertical mixing, and implications for surface ozone in the Southeast United States, Atmos. Chem. Phys. Discuss., 2016, 1–32, doi:10.5194/acp-2016-110, 2016.

United States Census Bureau: Annual Estimates of the Resident Population: April 1, 2010 to July 1, 2015. Metropolitan and Micropolitan Statistical Area; and for Puerto Rico., http://www.census.gov/popest/data/metro/totals/2015/index.html.

Valin, L., Russell, A., Hudman, R., and Cohen, R.: Effects of model resolution on the interpretation of satellite $NO_2$ observations, Atmos. Chem. Phys., 11, 11 647–11 655, doi:10.5194/acp-11-11647-2011, 2011.

Valin, L., Russell, A., and Cohen, R.: "Variations of OH radical in an urban plume inferred from $NO_2$ column measurements", Geophys. Res. Lett., 40, 1856–1860, doi:10.1002/grl.50267, 2013.

van Geffen, J. H. G. M., Boersma, K. F., Van Roozendael, M., Hendrick, F., Mahieu, E., De Smedt, I., Sneep, M., and Veefkind, J. P.: Improved spectral fitting of nitrogen dioxide from OMI in the 405â€“465 nm window, Atmos. Meas. Tech., 8, 1685–1699, doi:10.5194/amt-8-1685-2015, 2015.

Veefkind, J., Aben, I., McMullan, K., Förster, H., de Vries, J., Otter, G., Claas, J., Eskes, H., de Haan, J., Kleipool, Q., van Weele, M., Hasekamp, O., Hoogeveen, R., Landgraf, J., Snel, R., Tol, P., Ingmann, P., Voors, R., Kruizinga, B., Vink, R., Visser, H., and Levelt, P.: TROPOMI on the ESA Sentinel-5 Precursor: A GMES mission for global observations of the atmospheric composition for climate, air quality and ozone layer applications, Remote Sens. Environ., 120, 70–83, doi:10.1016/j.rse.2011.09.027, 2012.

Vinken, G. C. M., Boersma, K. F., Maasakkers, J. D., Adon, M., and Martin, R. V.: Worldwide biogenic soil $NO_x$ emissions inferred from OMI $NO_2$ observations, Atmos. Chem. Phys., 14, 10 363–10 381, doi:10.5194/acp-14-10363-2014, 2014a.

Vinken, G. C. M., Boersma, K. F., van Donkelaar, A., and Zhang, L.: Constraints on ship $NO_x$ emissions in Europe using GEOS-Chem and OMI satellite $NO_2$ observations, Atmos. Chem. Phys., 14, 1353–1369, doi:10.5194/acp-14-1353-2014, http://www.atmos-chem-phys.net/14/1353/2014/, 2014b.

Wang, W., Bruyère, C., Duda, M., Dudhia, J., Gill, D., Kavulich, M., Keene, K., Lin, H.-C., Michalakes, J., Rizvi, S., and Zhang, X.: WRF-ARW Version 3.5 User's Guide: Chapter 7: Objective Analysis (OBSGRID), 2014.

Wild, O. and Prather, M. J.: Global tropospheric ozone modeling: Quantifying errors due to grid resolution, J. Geophys. Res. Atmos., 111, D11 305, doi:10.1029/2005JD006605, 2006.

Yamaji, K., Ikeda, K., Irie, H., Kurokawa, J.-i., and Ohara, T.: Influence of model-grid resolution on $NO_2$ vertical column densities over East Asia, J. Air. Waste. Manage., 64, 436–444, doi:10.1080/10962247.2013.827603, 2014.

Yegorova, E. A., Allen, D. J., Loughner, C. P., Pickering, K. E., and Dickerson, R. R.: Characterization of an eastern U.S. severe air pollution episode using WRF/Chem, J. Geophys. Res. Atmos., 116, doi:10.1029/2010JD015054, d17306, 2011.

Zhang, Y., Dubey, M. K., Olsen, S. C., Zheng, J., and Zhang, R.: Comparisons of WRF/Chem simulations in Mexico City with ground-based RAMA measurements during the 2006-MILAGRO, Atmos. Chem. Phys., 9, 3777–3798, doi:10.5194/acp-9-3777-2009, http://www.atmos-chem-phys.net/9/3777/2009/, 2009.

Ziemke, J., Chandra, S., and Bhartia, P.: "Cloud slicing: A new technique to derive upper tropospheric ozone from satellite measurements", J. Geophys. Res. Atmos., 106, 9853–9867, 2001.

Zörner, J., Penning de Vries, M., Beirle, S., Sihler, H., Veres, P. R., Williams, J., and Wagner, T.: Multi-satellite sensor study on precipitation-induced emission pulses of $NO_x$ from soils in semi-arid ecosystems, Atmos. Chem. Phys., 16, 9457–9487, doi:10.5194/acp-16-9457-2016, 2016.

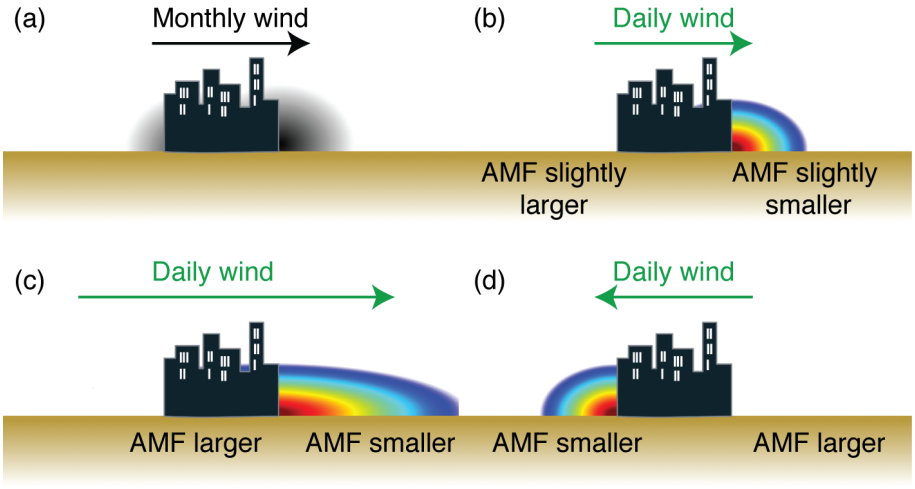


**Figure 1.** An illustration of the central issues that will be discussed in this paper. (a) The monthly average a priori profiles, shown as the grayscale plumes. (b) A case when the daily wind is similar to the monthly average wind. (c) A case where the daily wind is significantly faster than average, but blows in the same direction. (d) A case where the daily wind direction is different than average. The text below each panel describes how the AMF derived from the daily profile would compare with those derived from the monthly a priori.

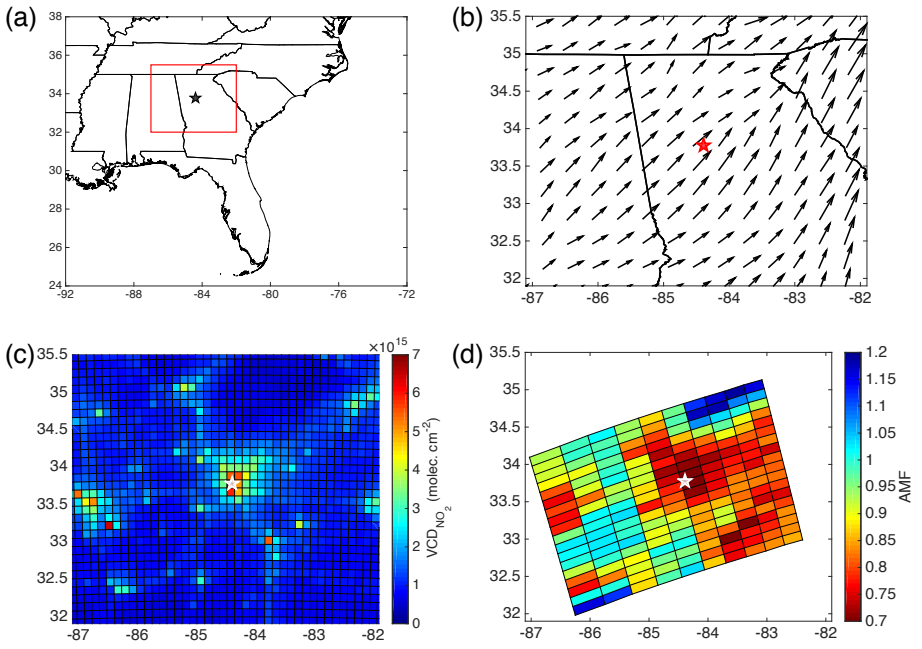


**Figure 2.** Average conditions for ~~1 June–30 Aug,~~ June 2013. (a) The red box indicates the part of the SE US being considered. (b) Surface wind directions from the WRF model; average wind speed is 5.0 m $s^{-1}$ (min 1.7 m $s^{-1}$, max 12.7 m $s^{-1}$). (c) WRF-Chem tropospheric $NO_2$ columns. (d) AMFs for the pseudo-retrieval calculated using the average monthly $NO_2$ a priori. The direction of the colorbar is reversed in (d), as small AMFs correspond to high modeled VCDs. In all panels, the star (★) indicates the position of Atlanta. Longitude and latitude are marked on the $x$- and $y$- axes, respectively.

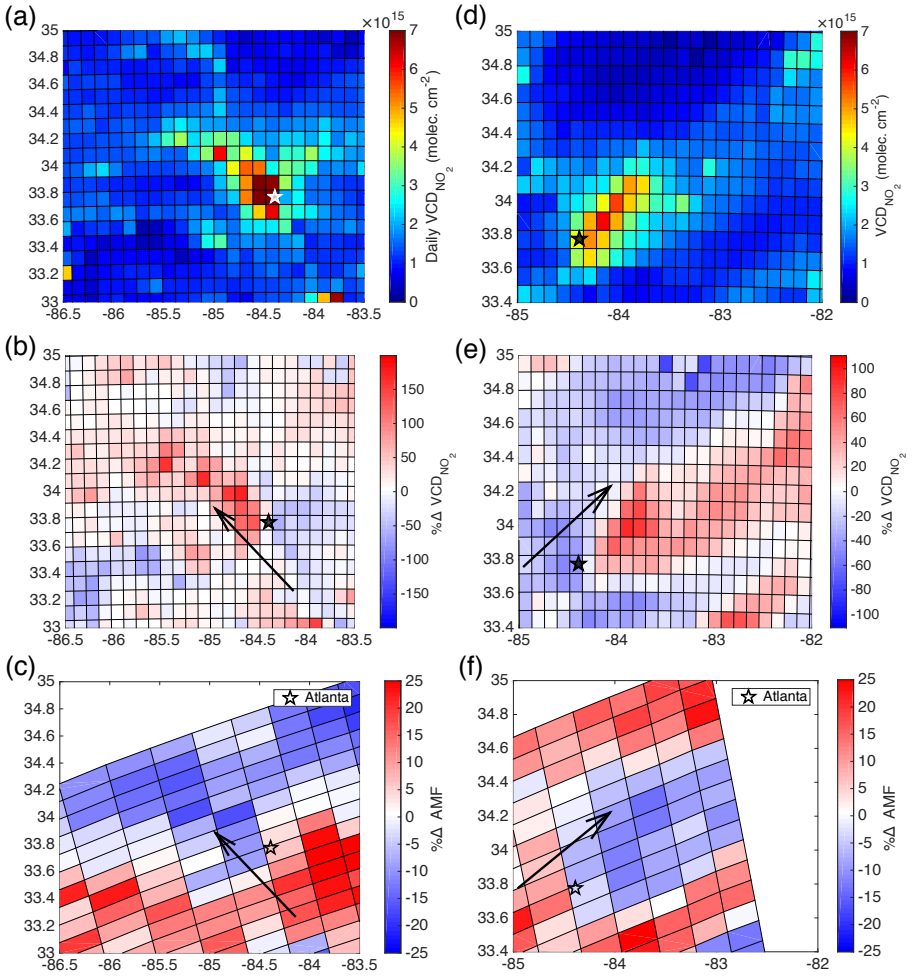


**Figure 3.** Results from 22 June (a–c) and 18 June (d–f). (a,d) WRF-Chem tropospheric $NO_2$ columns for 1900 UTC. (b,e) The percent difference in WRF-Chem tropospheric $NO_2$ columns at 1900 UTC for that day vs. the monthly average. (c,f) Percent difference in AMFs using hybrid daily profiles vs. the monthly average profiles in the pseudo-retrieval. In all panels, the star (★) indicates the position of Atlanta, and the wind direction around Atlanta is shown by the arrow in the lower four panels. Longitude and latitude are marked on the $x$- and $y$-axes, respectively.

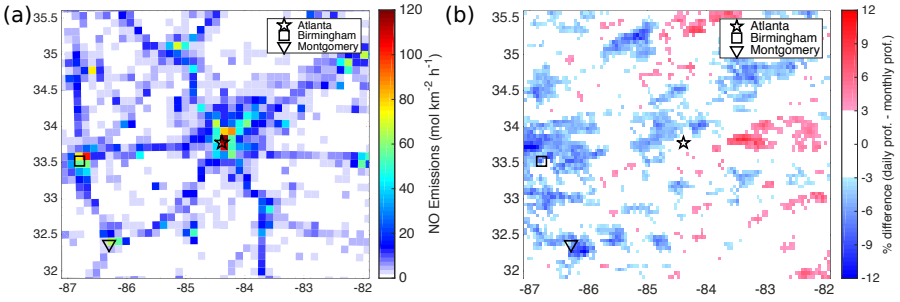


**Figure 4.** (a) 24 h average NO emissions from WRF-Chem at 12 km resolution. (b) The change in retrieved VCDs averaged over 1 June to 30 Aug. Pixels with a cloud fraction $> 20\%$ or that are affected by the row anomaly are excluded from the average. The color scale is reversed from Fig. 3c,f to reflect the inverse relationship between VCD and AMF. Longitude and latitude are marked on the $x$- and $y$- axes, respectively, for both panels.

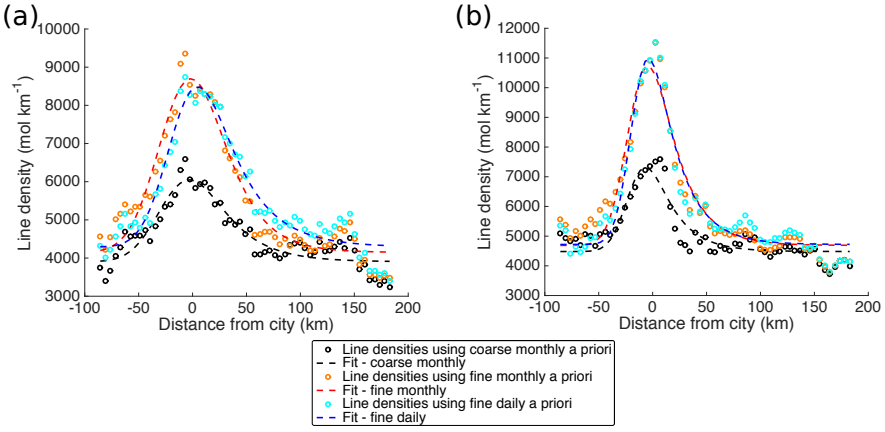


**Figure 5.** Line densities around Atlanta, GA, USA averaged over the study period when using monthly average and daily a priori (open circles), and the corresponding fits of exponentially-modified Gaussian functions (dashed lines). Black series are derived from a retrieval using a monthly average a priori at 108 km resolution; red series from a monthly average a priori at 12 km resolution, and blue from the daily profiles at 12 km resolution. (a) Average of days with wind speed $\geq 3.0$ m/s. (b) Average of days with wind speed $< 3.0$ m/s.

| | Percent of days with $\Delta$VCD $> 1\times10^{15}$ $\Delta$VCD $> 1\times10^{15}$ molec. cm$^{-2}$ | Percent of days with $\Delta$VCD $> \left[\sum_i \sigma_i\right]^{1/2}$ | Min. change (molec. cm$^{-2}$) | Max. change (molec. cm$^{-2}$) |
|---|---|---|---|---|
| Atlanta | 43 39% | $-2.0\times10^{15}$ 23% | $+2.0\times10^{15}$ $-2.4\times10^{15}$ | $+2.5\times10^{15}$ |
| Birmingham | 59 54% | $-3.9\times10^{15}$ 43% | $+3.7\times10^{15}$ $-3.8\times10^{15}$ | $+3.9\times10^{15}$ |
| Montgomery | 27% | $-2.1\times10^{15}$ 20% | $+2.3\times10^{15}$ $-2.2\times10^{15}$ | $+1.9\times10^{15}$ |

**Table 1.** Statistics on the frequency and magnitude of changes in the retrieved VCDs using a daily vs. monthly average profile for pixels with centers within 50 km of Atlanta, GA, USA (84.39° W, 33.775° N), Birmingham, AL, USA (86.80° W, 33.52° N) and Montgomery, AL, USA (86.30° W, 32.37° N). The "percent of days" values are calculated as the number of days with at least one pixel in that subset with a change $> 1\times10^{15}$ molec. cm$^{-2}$ greater than the given uncertainty divided by the number of days with at least one pixel unobscured by clouds or the row anomaly. The uncertainty represented by $\left[\sum_i \sigma_i\right]^{1/2}$ is the quadrature sum of uncertainties from spectral fitting ($0.7\times10^{15}$ molec. cm$^{-2}$, Boersma et al. 2007, 2011 ), stratospheric separation ($0.2\times10^{15}$ molec. cm$^{-2}$, Bucsela et al. 2013 ), and AMF calculation (20%, Bucsela et al. 2013 ).

Parameter Physical significance Lower Bound Upper Bound Best guess initial value$a$ (mol) burden 0 $\infty$ $\int_{x_{\min}}^{x_{\max}} \mathrm{NO}_2(x)\,dx x_0$ (km) Distance traveled in 1 lifetime 1.6 $\infty$ 54 $\mu_x$ (km) Emission center $\min(x)$ $\max(x)$ $x_{\max(\mathrm{NO2})}$ $\sigma_x$ (km) Gaussian smoothing 2.5 $x_{\max(\mathrm{NO2})} - \min(x)$ FWHM / 2.355 $B$ (mol) Background 0 max() $\min(\mathrm{NO}_2)$ Constraints imposed on the solutions permitted to fmincon, in the form of upper and lower bounds, with additional linear and nonlinear constraints. $x$ refers to the $x$-coordinates associated with the data, i.e. distance from the city center. $x_{\max(\mathrm{NO2})}$ indicates the $x$ coordinate where the greatest line density is present. refers to the values of the line density. FWHM is the full width at half maximum of the Gaussian. For additional discussion of the reasoning for the selection of these values, see the supplement.

| | | Wind $\geq$ 3.0 m/s | | | Wind $<$ 3.0 m/s | | |
|---|---|---|---|---|---|---|---|
| | | Monthly | Monthly | Daily | Monthly | Monthly | Daily |
| | | 108 km | 12 km | 12 km | 108 km | 12 km | 12 km |
| Atlanta | $a$ (mol $NO_2$) | $1.8 \pm 0.7 \times 10^5$ | $4. \pm 2 \times 10^5$ | $3. \pm 1 \times 10^5$ | $1.5 \pm 0.6 \times 10^5$ | $4. \pm 1 \times 10^5$ | $3. \pm 1$ |
| | $x_0$ (km) | $32 \pm 13$ | $26 \pm 11$ | ~~$34 \pm 14$~~ $33 \pm 14$ | $23 \pm 10$ | $24 \pm 10$ | $24 \pm$ |
| | $\mu_x$ (km) | ~~$-23. \pm 9$~~ $-22. \pm 9$ | $-20. \pm 8$ | $-15. \pm 6$ | $-20. \pm 8$ | $-18. \pm 7$ | $-17$ |
| | $\sigma_x$ (km) | $23. \pm 9$ | $30 \pm 10$ | $22. \pm 9$ | $14. \pm 6$ | $15. \pm 6$ | $13.$ |
| | $B$ (mol $NO_2$ $km^{-1}$) | $4. \pm 2 \times 10^3$ | $4. \pm 2 \times 10^3$ | $4. \pm 2 \times 10^3$ | ~~$5. \pm 2 \times 10^3$~~ $4. \pm 2 \times 10^3$ | $5. \pm 2 \times 10^3$ | $5. \pm 2$ |
| Birmingham | $a$ (mol $NO_2$) | $1.6 \pm 0.5 \times 10^5$ | $3. \pm 1 \times 10^5$ | $4. \pm 1 \times 10^5$ | $4. \pm 1 \times 10^5$ | $3. \pm 1 \times 10^5$ | $4. \pm 1$ |
| | $x_0$ (km) | $50 \pm 20$ | $30 \pm 10$ | $50 \pm 20$ | $220 \pm 80$ | $40 \pm 10$ | $70 \pm$ |
| | $\mu_x$ (km) | $-21. \pm 7$ | ~~$-25. \pm 8$~~ $-24. \pm 8$ | ~~$-15. \pm 5$~~ $-14. \pm 5$ | $-50 \pm 20$ | $-27. \pm 9$ | $-26$ |
| | $\sigma_x$ (km) | $24. \pm 8$ | $27. \pm 9$ | $23. \pm 8$ | $21. \pm 7$ | $25. \pm 8$ | $22.$ |
| | $B$ (mol $NO_2$ $km^{-1}$) | $4. \pm 1 \times 10^3$ | $4. \pm 1 \times 10^3$ | $4. \pm 1 \times 10^3$ | $4. \pm 1 \times 10^3$ | $5. \pm 2 \times 10^3$ | $5. \pm 2$ |

**Table 2.** Values of the five fitting parameters for the EMG functions (Eq. 9) used to fit the distributions of line densities around Atlanta and Birmingham. $a$ represents the total $NO_x$ burden, $x_0$ is the distance the plume travels in one lifetime, $\mu_x$ is the center of emissions relative to the city center, $\sigma_x$ describes the Gaussian smoothing, and $B$ the background line density.

| | | | Atlanta | | | Birmingham | |
|---|---|---|---|---|---|---|---|
| | Wind speed bin | Monthly 108 km | Monthly 12 km | Daily 12 km | Monthly 108 km | Monthly 12 km | |
| E (Mg $NO_x$ $h^{-1}$) | WRF-Chem NEI | | **13.74** | | | **10.49** | |
| | $\geq 3.0$ | $6. \pm 4$ | $16. \pm 9$ | $11. \pm 7$ | $4. \pm 2$ | ~~$10. \pm 5$~~ $10. \pm 6$ | |
| | $\geq 4.0$ | $6. \pm 3$ | ~~$20 \pm 10$~~ $17 \pm 11$ | $11. \pm 6$ | $4. \pm 2$ | ~~$13. \pm 6$~~ $13. \pm 7$ | |
| | $\geq 5.0$ | - | - | - | $6. \pm 3$ | $15. \pm 9$ | |
| $\tau$ (h) | $\geq 3.0$ | $1.6 \pm 0.7$ | $1.3 \pm 0.5$ | $1.7 \pm 0.7$ | ~~$2.5 \pm 0.9$~~ $2.5 \pm 1.0$ | ~~$1.8 \pm 0.6$~~ $1.8 \pm 0.7$ | |
| | $\geq 4.0$ | $1.8 \pm 0.7$ | $1.2 \pm 0.5$ | ~~$1.8 \pm 0.8$~~ $1.8 \pm 0.7$ | ~~$2.2 \pm 0.8$~~ $2.1 \pm 0.9$ | ~~$1.5 \pm 0.5$~~ $1.5 \pm 0.6$ | |
| | $\geq 5.0$ | - | - | - | $1.8 \pm 0.7$ | $1.3 \pm 0.5$ | |

**Table 3.** Values of the emission rates ($E$) and effective lifetime ($\tau$) obtained when the separation between slow and fast winds is set at 3, 4, and 5 m $s^{-1}$. For comparison, the total $NO_x$ emission for all 12 km WRF-Chem grid cells within 50 km of each city is given. These emissions are derived from NEI 11 and scaled to 88.9% to account for 2011–2013 reductions. Uncertainties calculated as described in the supplement.

## S1 Choice of weights for the monthly average profiles

When computing the monthly average profiles, it is necessary to use profiles that represent OMI's overpass time, typically quoted as 13:30 to 13:45 local standard time (e.g. McLinden et al. 2014; Levelt et al. 2006 ). To average the profiles output from WRF-Chem, weights were calculated that fulfilled two requirements:

1. The weights should be 1 at OMI overpass time and 0 when more than 1 hour away from overpass time.
2. The transition between profiles from different hours should be smooth.

For #1, we assume that the average overpass time is 1330 local standard time. We compute local standard time as:

$$t_{\text{apriori, local}} = \frac{l}{15} + t_{\text{apriori, utc}} \tag{S1}$$

where $t_{\text{apriori, local}}$ is the local standard time in hours past midnight, $t_{\text{apriori, utc}}$ the UTC time in hours past midnight, and $l$ the longitude (west is negative). To meet the second requirement, this is a continuous function, rather than a step function (where each 15° longitudinal segment/time zone has a single local time). Areas further west in a time zone are more likely to be observed on the east edge of a later OMI swath, and vice versa for areas further east. This weighting includes some influence from later profiles to account for this.

The weights from Eq. (6) are derived from:

$$w = 1 - |t_{\text{overpass}} - t_{\text{apriori, local}}| = 1 - \left|13.5 - \frac{l}{15} - h\right| \tag{S2}$$

where $t_{\text{overpass}}$ is the assumed overpass time for OMI and $h \equiv t_{\text{apriori, utc}}$. If $w < 0$, $w$ is set to 0. This gives us the desired form where the weights smoothly vary in time.

## S2 Influence of boundary layer vs. free troposphere

Figure S2 illustrates the possible effects on the AMF of day-to-day changes in the a priori upper troposphere $NO_2$ profile. From Sect. 2.2, Eq. (2) and Eq. (3) show that it is the relative contribution of each altitude to the a priori profile that determines the AMF. Therefore, if an increase in near-surface $NO_2$ is balanced by an increase in upper tropospheric $NO_2$, there may be no or very little net change to the AMF. This is the case to the left of the city in Fig. S2. However, the reverse can also occur,

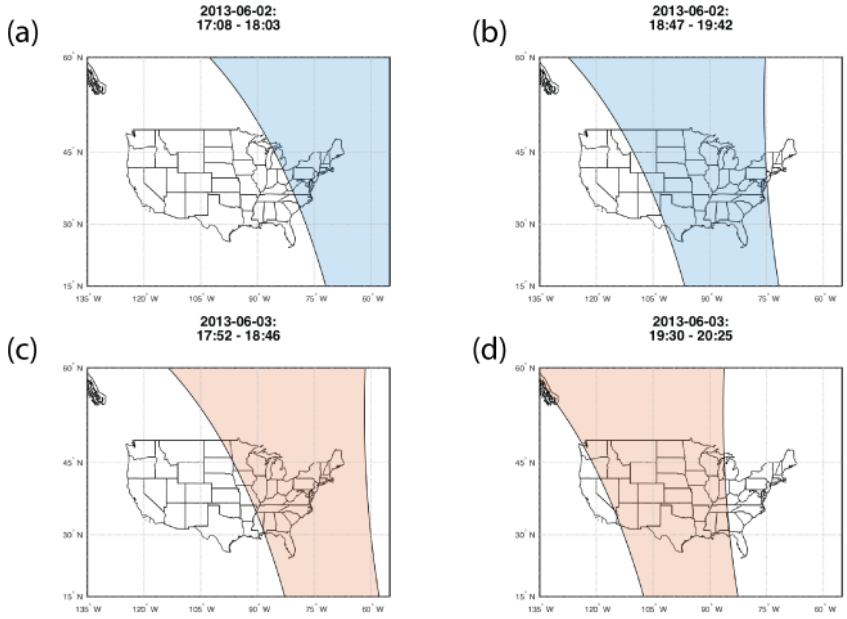


**Figure S1.** Swaths covering the east coast of the US for 2 June 2013 (a,b) and 3 June 2013 (c,d). The times given are the start and end times of the daytime half of the orbit in UTC. As shown, on different days, the time of the OMI swath that covers Atlanta can vary by up to an hour.

where changes in the upper tropospheric a priori profile accentuate the effect of changes near the surface. This occurs to the right of the city in Fig. S2.

Here we consider the magnitude of the effect day-to-day changes in the free tropospheric $NO_2$ profile have on the retrieval. Figure S3 compares the difference in pseudo-retrieval AMFs among the three a priori types used: the daily profiles over the full extent of the troposphere, "hybrid" daily profiles which include day-to-day variation in boundary layer but use a monthly average above 750 hPa, and the monthly average profiles. These statistics are derived over the entire pseudo-retrieval domain for the entire time period. Comparing either the full or hybrid daily profile to the monthly average profile yields very similar statistics. Both exhibit a ~~median change near $+2.5\%$ ($+2.8\%$ hybrid, $+2.5\%$ full~~positive median change ($+1.7\%$ full, $+2.0\%$ hybrid) and show similar upper and lower quartiles. When using the full daily profile, the range of the most extreme values is slightly greater, occurring when the changes in the boundary layer and free troposphere act in the same direction on the AMF.

The third column shows the difference between the hybrid and full daily profile AMFs. ~~As expected, the~~ The mean and median differences are nearly 0 ($-0.4\%$ and $-0.2\%$ respectively), with upper and lower quartile values of $+2.20\%$ and $-2.88\%$. This is $\sim 35\%$ of the interquartile range of the difference between AMFs resulting from either the full or hybrid daily profiles and the monthly average profile. Day-to-day changes in the free tropospheric a priori profile are smaller in magnitude than those in the boundary layer, but usually occur over a much greater vertical extent. ~~This, combined with the greater scattering~~

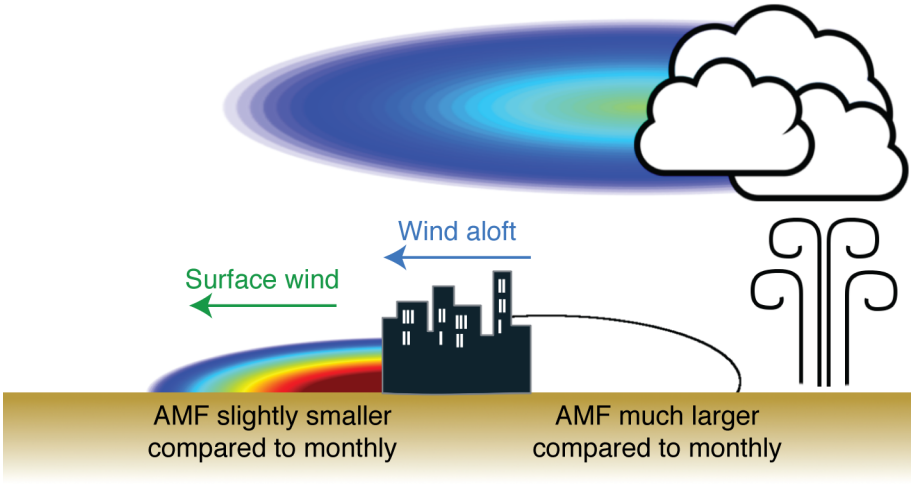


**Figure S2.** An illustration of how day-to-day variations in the upper troposphere impact the calculation of the AMF. The colored gradients represent the day-to-day $NO_2$ plumes, the black outline represents the monthly average plume. To the left of the city, the increase in near-surface $NO_2$ compared to the monthly average would result in a much smaller AMF; however the addition of $NO_2$ in the upper troposphere balances this, keeping the difference in AMF smaller. To the right, both the lack of near-surface $NO_2$ and the introduction of $NO_2$ in the upper troposphere result in a much greater AMF than the monthly average.

~~weights~~ Further, the scattering weights are greater at these altitudes ~~,~~ (~2–8 times those near the surface), amplifying the effect of small changes in the profile shape at these altitudes. This explains why the effect on the AMF is as large as it is, although day-to-day changes in the boundary layer still dominate the effect using daily profiles has on the AMFs~~,~~. It should be noted that these a priori are derived from a model without lightning NO emission; therefore this should be considered a lower bound for the effect of the free tropospheric profile. The presence of lightning $NO_x$ would likely lead to larger increases in AMF due to the higher upper tropospheric sensitivity.

The implications of this response are varied. For applications (such as data assimilation) where reducing the uncertainty in a single day's observations is critical, this result indicates that accurate modeling of upper tropospheric $NO_2$ is important. However, over the 91 days of this study, the effect of including a daily free tropospheric a priori profile averages out to nearly 0. Winds in the free troposphere are not correlated with surface winds (Endlick et al., 1969). In methods sorting observations by wind speed or direction (Valin et al., 2013; Lu et al., 2015), day-to-day variations in the AMF due to changes in the free troposphere will therefore be random in character. Over long periods of averaging, the impact due to these variations will have no net impact. Only changes associated with the surface winds will lead to systematic changes in the results obtained by these methods.

## S3 ~~Expansion on number of days with change in VCD greater than uncertainty~~EMG fitting algorithm details

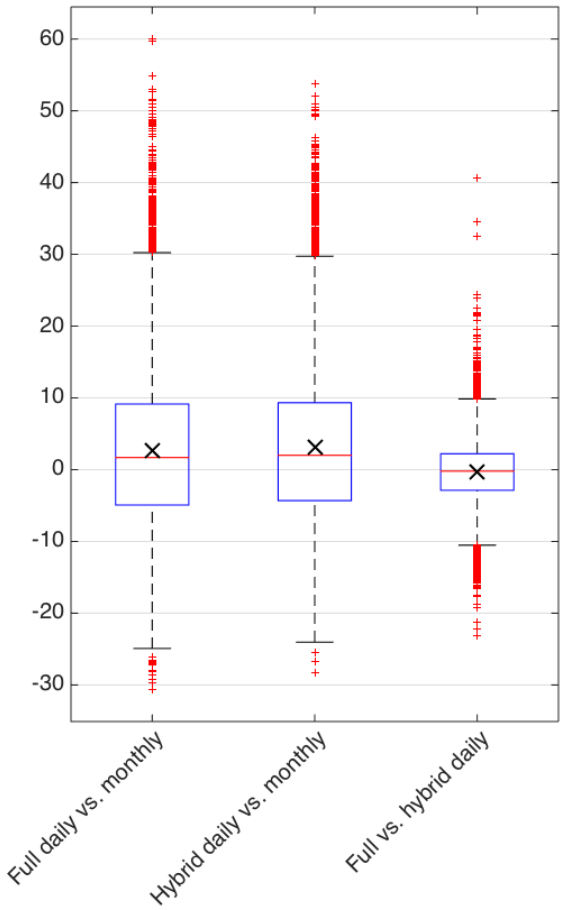


**Figure S3.** Percent changes in the AMF for the pseudo-retrieval over the full time period (1 June to 30 Aug) among the three a priori used in the pseudo-retrieval. For "new vs. base," the percent change is calculated as $(\text{new} - \text{base})/\text{base} \times 100\%$. The red line is the median, the box edges are the 25th and 75th percentiles, the whiskers cover the remainder of the data not considered outliers, and the red pluses are outliers. A point is considered an outlier if it is more than 1.5 times the interquartile range from the closer quartile. The black X marks the average.

~~In the main paper, we used $1 \times 10^{15}$ molec. cm$^{-2}$ as the uncertainty of a single pixel VCD based on the global mean uncertainty reported in ? . Here we will consider two other criteria.~~ The EMG fitting was carried out by minimizing the residuals between the EMG function and the line densities using the Matlab function `fmincon`, which allows constrained non-linear fitting using an interior-point algorithm. Additionally, the following three refinements were necessary.

- The constraints listed in Table S1 must be imposed to ensure physically realistic values of $a$, $x_0$, $\mu_x$, $\sigma_x$, and $B$ are obtained.

- Any not-a-number (NaN) values in the EMG function (Eq. 9) are replaced with infinity, thus making the fitting function (Eq. 10) report that the current values of $a$, $x_0$, $\mu_x$, $\sigma_x$, and $B$ are unacceptable. NaNs occur in the EMG function when the exponential goes to infinity and the error function to zero, typically when the fitting parameters are unrealistically large or small and the fit is incorrectly a flat line. By doing this replacement and treating NaNs as 0 in the summation in Eq. (10), we allow NaNs to occur in the line densities (representing missing data, which is thus ignored) but not the fit.

- The minimization algorithm requires an initial value for $a$, $x_0$, $\mu_x$, $\sigma_x$, and $B$. For the first minimization, best-guess values for these are computed as specified in Table S1 (see supplement for rationale for each). However, an interior-point minimization algorithm uses a line search strategy which minimizes a function by following the derivative at the current point "downhill" (Robere, 2012; Wright, 2005) . If the algorithm begins in a region from which the downhill path leads to a local, rather than global, minimum, the global minimum may never be found by this algorithm. This can be alleviated by carrying out multiple minimizations, starting from a different point each time, and choosing the result with the smallest residual. The randomization draws from the range of values defined by the upper and lower limits for each parameter with a uniform probability distribution. For $a$ and $x_0$, upper bounds of $5 \times 10^6$ mol and 1000 km, respectively, are used during the randomization process, as a finite upper bound is necessary for the randomization algorithm. This randomization and reoptimization was carried out nine times per fit. Additional randomization of the initial point does not improve the fit. Each time the optimum value of the fitting function is compared to the previous minimum; if it is less, the new fit is accepted.

The ~~other new criterion requires the difference be greater than the quadrature sum of 20uncertainty in the AMF estimated by (?) and the minimum threshold uncertainty imposed by the stratospheric separation and DOAS fitting of $0.6 \times 10^{15}$ molec. cm$^{-3}$. The percent of days with changes above this threshold decreases the most for Atlanta, Nevertheless, still up to half of days with any valid observations will exhibit significant changes in the retrieved VCD when using daily profiles.~~

~~We retain $\geq 1 \times 10^{15}$ molec. cm$^{-2}$ for the main discussion as it is simplest reasonable criterion.~~

## S4 ~~Selection of constraints on and initial values of EMG fitting~~

~~The~~ constraints listed in Table S1 were found to be necessary to ensure that a physically realistic fit was obtained. The following upper and lower limits for each of the parameters were imposed:

| Parameter | Percent of days with $\Delta$ VCD $\geq 1.0 \times 10^{15}$ molec. cm$^{-2}$ | Physical significance | Percent of days with $\Delta$ VCD $\geq 0.6 \times 10^{15}$ molec. cm$^{-2}$ | Lower Bound | Pe 0.6 |
|---|---|---|---|---|---|
| Atlanta $a$ (mol) | 43 | $NO_2$ burden | 750 | | 25 |
| Birmingham $x_0$ (km) | 59 | Distance traveled in 1 lifetime | 831.6 | | 48 |
| Montgomery $\mu_x$ (km) | 27 | Emission center | 66 | min($x$) | 25 |
| $\sigma_x$ (km) | | Gaussian smoothing | 2.5 | | $x_n$ |
| $B$ (mol) | | Background | 0 | | ma |

| Additional constraints |
|---|
| $\mu_x + x_0 \leq \max(x)$ |
| $\exp\left(\frac{\mu_x}{x_0} + \frac{\sigma_x^2}{2x_0^2} - \frac{x}{x_0}\right) \leq 20$ |

Expansion of Table 1 with different values for the single measurement uncertainty; percent of days with at least one clear pixel that have a change in retrieved tropospheric VCDs above the specified uncertainty.

Table **??** introduces two additional values for the uncertainty. The lowest value of $0.6 \times 10^{15}$ molec. cm$^{-2}$ is the quadrature sum of estimated uncertainty due to DOAS fitting ($0.4 \times 10^{15}$ molec. cm$^{-2}$) and stratospheric subtraction ($0.45 \times 10^{15}$ molec. cm$^{-2}$) in Boersma et al. (2004) . We compare against this because it is the sum of errors outside the calculation of the AMF, which we are revising here. Naturally, this significantly increases the number of days for which the inclusion of a daily profile changes the retrieved VCD by an amount greater than this uncertainty. This is an overly generous assumption of uncertainty because errors in the AMF are not solely due to the a priori profile.

**Table S1.** Constraints imposed on the solutions permitted to the interior point algorithm, in the form of upper and lower bounds, with additional linear and nonlinear constraints. $x$ refers to the $x$-coordinates associated with the data, i.e. distance from the city center. $x_{\max(NO2)}$ indicates the $x$ coordinate where the greatest $NO_2$ line density is present. $NO_2$ refers to the values of the line density. FWHM is the full width at half maximum of the Gaussian. For additional discussion of the reasoning for the selection of these values, see the supplement.

- $a \in [0, \infty)$: $a$ corresponds to the total $NO_2$ burden and therefore must be a positive value.
- $x_0 \in [1.6, \infty)$: $x_0$ is the distance traveled by the plume in one lifetime. Therefore it must be positive; however, if it becomes too small, the fit fails (returning a flat line). At very slow wind speeds of 1 m s$^{-1}$, a short lifetime of 1 h would translate to an $x_0$ of 3.6 km, we choose a minimum value for $x_0$ shorter than this to allow for the possibility of very short lifetimes. 1.6 km was specifically chosen as one-third the distance between adjacent data points in the line densities on the oversampled $0.05^\circ \times 0.05^\circ$ ($\approx 5 \times 5$ km) grid. This means that three lifetimes would pass and $> 95\%$ of the $NO_x$ enhancement due to a source would be removed; shorter lifetimes than this are unlikely to be resolved at this grid resolution.
- $\mu_x \in [\min(x), \max(x)]$: $\mu_x$ is the apparent position of the emission center relative to the geographic city center. It must be within the domain of distances chosen, otherwise the domain was chosen poorly.

- $\sigma_x \in [2.5, x_{\mathrm{maxNO_2}} - \min(x)]$: $\sigma_x$ is the Gaussian smoothing parameter, serving the same role as the $\sigma$ parameter in any Gaussian function. 2.5 km was chosen as the lower bound under the assumption that the smallest observable Gaussian requires at least 3 data points (the base on either side and the maximum). As $\sigma = 4 \times$ (full width at base) this implies that the smallest observable signal is $\frac{1}{2}$ the oversampled grid resolution: if only 3 points defined the Gaussian, one-half the full width at the base ($= 2\sigma$) would fit within one grid cell. The upper limit simply specifies that $\sigma_x$ cannot be larger than the distance from the upwind edge of the domain to the $x$-coordinate of maximum line density, i.e. that the Gaussian build-up on the upwind side is fully captured in the domain.

- $B \in [0, \max(\mathrm{NO_2})]$: $B$ is the background line density. It must be positive, and should not be larger than the maximum observed line density.

Two additional constraints were imposed using the ability of `fmincon` to accept linear and nonlinear relationships between the fitting parameters:

- $x_0 + \mu_x \leq \max(x)$: Simply, one lifetime must pass between the apparent emissions center and the downwind edge of the domain. If not, the domain was chosen poorly.

- $\exp\left(\frac{\mu_x}{x_0} + \frac{\sigma_x^2}{2x_0^2} - \frac{x}{x_0}\right) \leq 20$: This is a second numerical constraint to prevent the case where the exponential goes to infinity and the error function complement goes to 0, thus creating a return value of NaN from the fitting function. (The first numerical constraint is the replacement of NaNs with infinity discussed in the main text.)

For the best-guess initial values:

- $a = \int_{x_{\min}}^{x_{\max}} \mathrm{NO_2}(x)\, dx$: Since $a$ corresponds to the total burden of $\mathrm{NO_2}$ present, we use the integral over the domain as the initial guess.

- $x_0 = 54$: A best guess of 54 km follows from an average summer lifetime of 3 h (Lu et al., 2015) and a wind speed of 5 m $\mathrm{s}^{-1}$.

- $\mu_x = x_{\mathrm{max(NO2)}}$: Logically, one would expect the apparent emission source to be somewhat near the maximum concentration, the fitting procedure can then identify if it is slightly displaced.

- $\sigma_x = \mathrm{FWHM}/2.355$: This uses the relationship between the full width at half max and the standard deviation of a Gaussian. The half maximum line density is computed as:

$$\mathrm{HM} = \frac{\max(\mathrm{NO_2}) - \mathrm{NO_2}(x_{\min})}{2} \tag{S3}$$

The FWHM is then:

$$\mathrm{FWHM} = |x_{\mathrm{HM}} - x_{\mathrm{max(NO2)}}| \tag{S4}$$

where $x_{\mathrm{HM}}$ is the $x$-coordinate where the half-max exists, found by interpolating to the half maximum line density.

- $B = \min(\mathrm{NO_2})$: It is a natural guess that the background is simply the lowest observed line density.

| Source | Uncertainty | Citation |
|---|---|---|
| VCD | ~~25%/$\sqrt{n}$*~~ 25% | Lu et al. (2015) |
| Across wind integration dist. | 10% | Beirle et al. (2011) |
| Choice of wind fields | 10% | Beirle et al. (2011) |
| Fitting uncertainty | Computed | §S5 |
| $NO_x$:$NO_2$ ratio | 10% | Beirle et al. (2011) |

**Table S2.** Values of uncertainty for the various steps of the EMG fitting process.~~*Note: Lu et al. (2015) do not indicate that the uncertainty in VCDs is reduced by $\sqrt{n}$, i.e. the number of observations; we are doing so here.~~

## S4 Computation of uncertainty in EMG parameters ($a$, $x_0$, $\mu_x$, $\sigma_x$, $B$, $E$, and $\tau$)

To compute the uncertainty in both the fitting parameters and the values of $E$ and $\tau$ derived from them, we base our calculation off those in Beirle et al. (2011) and Lu et al. (2015). Lu et al. (2015) use the values in Table S2. The value of 25% for the uncertainty in the VCDs used in Lu et al. (2015) is below the lower bound of uncertainty given in Boersma et al. (2004), likely reflecting improvements such as the temperature correction of the $NO_2$ cross section used in determining the scattering weights. ~~Lu et al. (2015) do not reduce the uncertainty by $\sqrt{n}$, where $n$ is the number of observations. We do reduce this uncertainty by $\sqrt{n}$, as the errors contributing to it should be random in nature. We determine $n$ for a given fit as the smallest number of observations used in a single grid cell of the rotated column densities (§2.5). This is a conservative estimate, as the number of observations used in computing a single line density will be several times that because multiple pixels span the across wind distance. Since we oversample these pixels, each grid cell is not necessarily an independent measurement, and so we choose to treat this value conservatively.~~

Our computation of uncertainty ~~also~~ differs from Lu et al. (2015) in that we include the uncertainty for the VCDs in the calculation of uncertainty for $\tau$. As shown in this paper, the choice of a priori profiles can introduce a spatial bias into the exponential decay related to effective lifetime, therefore the inclusion of the VCD uncertainty in the lifetime uncertainty is logical.

To compute the uncertainty due to the fitting process itself, we first need the standard deviations of the fitting parameters. We begin by computing the variance-covariance matrix as (Bard, 1974; Dovì et al., 1991):

$$Cov([a, x_0, \mu_x, \sigma_x, B]) \approx \mathrm{diag}(s^2\, \mathbf{H}^{-1});\ \text{where} \tag{S5}$$

$$s^2 = \frac{1}{n_{\mathrm{fit}} - 5} \sum_x \left[\mathrm{NO_2}(x) - F(x|a, x_0, \mu_x, \sigma_x, B)\right]^2 \tag{S6}$$

that is, the variance-covariance matrix of the fitting parameters is approximately equal to the inverse Hessian matrix for the fitting function (Eq. 10) evaluated at the optimum values of the fitting parameters and scaled by $s^2$, the sum of squared residuals for the optimum fit divided by the number of degrees of freedom. The variance for each parameter is, as usual, the corresponding element on the diagonal of the variance-covariance matrix.

In Eq. S5, we use the Hessian matrix returned by the unconstrained Matlab minimization function `fminunc`. The documentation for `fmincon` states that the Hessian matrix returned can be inaccurate; therefore we pass the fitting function (Eq. 10) to `fminunc` and initialize it at the optimum values of the fitting parameters. `fminunc` is set to only evaluate the fitting function once; this returns the unconstrained Hessian at the constrained optimum found by `fmincon`.

As in Beirle et al. (2011), we represent the uncertainty in the fitting parameters due to the fitting process as 95% confidence intervals. We compute these for each individual parameter with:

$$c_{95} = \frac{t\sigma}{\sqrt{n_{\mathrm{fit}}}} \tag{S7}$$

where $t$ is Student's $t$-value and is computed in Matlab as `tinv(0.975, n_fit - 5)`. (0.975 is used as the $p$ value because `tinv` returns one-tailed $t$ values, so 0.975 returns the 0.95 two-tailed value.) $n_{\mathrm{fit}}$ is the number of points used to obtain the fit, and $n_{\mathrm{fit}} - 5$ degrees of freedom are used for determinine the value of $t$ because 5 degrees of freedom have been fixed in the fitting process, one each for the five parameters fit. The standard deviation, $\sigma$, is taken as the square root of the corresponding diagonal element of the variance-covariance matrix from Eq. (S5). This treatment assumes that each of the fitting parameters is independent. Both the covariance matrix and an analysis of the change in optimum values for four of the parameters if one is fixed shows that the parameters are not fully independent, but using individual confidence intervals for each parameter lends itself to a more intuitive understanding of the uncertainty than would attempting to derive a five-dimensional confidence region for the five fitting parameters.

To combine this uncertainty with the other sources identified in Beirle et al. (2011) (VCD, across wind distance, and wind field), the uncertainties are then simply added in quadrature:

$$u_p = p \cdot \sqrt{\left(\frac{c_{95,p}}{p}\right)^2 + (\%u_{\mathrm{VCD}})^2 + (\%u_b)^2 + (\%u_{\mathrm{wf}})^2} \tag{S8}$$

where $p$ is the value of the fitting parameter, $u_p$ the total uncertainty for the parameter, $c_{95,p}$ the confidence interval for that parameter, and $\%u_{\mathrm{VCD}}$, $\%u_b$, and $\%u_{\mathrm{wf}}$ are the percent uncertainties in VCDs, across wind integration direction, and choice of wind fields given in Table S2 as decimal values (i.e. $\%u_b = 0.1$).

The uncertainty for lifetime ($\tau$) and emissions ($E$) are then propagated from the fitting parameter uncertainties. For lifetime:

$$\tau = \frac{x_0}{w} \tag{S9}$$

$$\begin{aligned} u_\tau^2 &= \left(\frac{\partial \tau}{\partial x_0} u_{x_0}\right)^2 + \left(\frac{\partial \tau}{\partial w} u_w\right)^2 \\ &= \left(\frac{1}{w} u_{x_0}\right)^2 + \left(\frac{-x_0}{w^2} u_w\right)^2 \end{aligned} \tag{S10}$$

where $w$ is the average wind speed. We compute $u_w$ as the 95% confidence interval of the distribution of winds that fall within the bin used; that is, if we consider all days with wind speed $> 3$ m s$^{-1}$, then this is the 95% confidence interval of the

distribution of wind speeds $> 3$ m s$^{-1}$. This helps account for the uncertainty in lifetime introduced because different wind speeds lead to different $\mathrm{NO_x}$ lifetimes (Valin et al., 2013).

For emissions:

$$E = \frac{raw}{x_0} = \frac{ra}{\tau} \tag{S11}$$

$$\begin{aligned} u_E^2 &= \left(\frac{\partial E}{\partial r}u_r\right)^2 + \left(\frac{\partial E}{\partial a}u_a\right)^2 + \left(\frac{\partial E}{\partial \tau}u_\tau\right)^2 \\ &= \left(\frac{a}{\tau}u_r\right)^2 + \left(\frac{r}{\tau}u_a\right)^2 + \left(\frac{-ra}{\tau^2}u_\tau\right)^2 \end{aligned} \tag{S12}$$

where $r$ is the $\mathrm{NO_x}$:$\mathrm{NO_2}$ ratio of 1.32 from (Beirle et al., 2011).

## S5 Validation of EMG fitting

To determine if the EMG fitting process is returning good fits to the data, we consider several criteria. First, we examine each fit to the data; all the best fits reproduce the shape of the data very well. Second, we consider the $R$ value of the fits. Beirle et al. (2011) required an $R > 0.9$ for a fit to be considered acceptable. Out of 30 fits with an across-wind distance of $1^\circ$ (2 wind bins for Atlanta and 3 for Birmingham times 3 a priori), only 2 had $R < 0.9$, and even then were $> 0.89$. The algorithm is finding good fits in nearly every case.

We also consider whether the `fmincon` algorithm is finding the global minimum of the fitting function or becoming trapped in a local minimum. As described in Sect. 2.5, we carry out 9 optimizations from random starting points, in addition to that from the best guess initial values, to sample different parts of the parameter space. We tested increasing the number of random starting points to 99 and found no change in the optimal fitting parameter values. In a separate experiment, we found only one case in which a local minimum, rather than the global minimum, was returned, but repeated fitting with 9 random start point optimizations returned the global minimum. Therefore we find that optimizing from 9 random starting points plus one best guess is a good balance between accuracy and computational efficiency.

## S6 Model lifetime calculation

To compare the EMG derived $\mathrm{NO_x}$ lifetime against that from the WRF-Chem model, two loss processes were considered:

$$\mathrm{NO_2 + OH} \quad \rightarrow \mathrm{HNO_3} \tag{R1}$$

$$\mathrm{NO + RO_2} \quad \rightarrow \alpha\mathrm{RONO_2} \tag{R2}$$

where $\alpha$ is the $\mathrm{RONO_2}$ branching ratio. This leads to a total lifetime:

$$\tau_{\mathrm{total}} = \left(\frac{1}{\tau_{\mathrm{HNO_3}}} + \frac{1}{\tau_{\mathrm{RONO_2}}}\right)^{-1} \tag{S13}$$

The lifetime with respect to $HNO_3$ is simply:

$$\tau_{\mathrm{HNO_3}} = \frac{1}{k_{R1}[\mathrm{OH}]} \tag{S14}$$

while the lifetime with respect to $RONO_2$ is:

$$\tau_{\mathrm{RONO_2}} = \left( \sum_i \alpha_i k_{R2,i} [\mathrm{RO_2}]_i \right)^{-1} \tag{S15}$$

The concentrations of the $RO_2$ species are not stored in the model output, so we assume steady state (Murphy et al., 2006):

$$\frac{d[\mathrm{RO_2}]}{dt} = 0 = -k_{R2}[\mathrm{RO_2}][\mathrm{NO}] + \sum_i k_{\mathrm{RH_i+OH}}[\mathrm{RH}]_i[\mathrm{OH}] \tag{S16}$$

$$\Rightarrow [\mathrm{RO_2}]_{SS,i} = \left( \sum_i k_{\mathrm{RH_i+OH}}[\mathrm{RH}]_i[\mathrm{OH}] \right) / \left( k_{R2}[\mathrm{NO}] \right) \tag{S17}$$

The overall lifetime is then:

$$\tau_{\mathrm{total}} = \left( k_{R1}[\mathrm{OH}] + \sum_i \alpha_i k_{R2,i} [\mathrm{RO_2}]_{SS,i} \right)^{-1} \tag{S18}$$

## References


Bard, Y.: Interpretation of the Estimates, chap. VII, Academic Press Inc., 1974.

Beirle, S., Boersma, K., Platt, U., Lawrence, M., and Wagner, T.: "Megacity Emissions and Lifetimes of Nitrogen Oxides Probed from Space", Science, 333, 1737–1739, 2011.

Boersma, K., Eskes, H., and Brinksma, E.: "Error analysis for tropospheric $NO_2$ retrieval from space, J. Geophys. Res. Atmos., 106, D04 311, doi:10.1029/2003JD003962, 2004.

Dovì, V., Paladino, O., and Reverberi, A.: Some remarks on the Use of the Inverse Hessian Matrix of the Likelihood Function in the Estimation of Statistical Properties of Parameters, Appl. Math. Lett., 4, 87–90, 1991.

Endlick, R., Singleton, R., and Kaufman, J.: Spectral Analysis of Detailed Vertical Wind Speed Profiles, J. Atmos. Sci., 26, 1030–1041, 1969.

Levelt, P., van der Oord, G., Dobber, M., Mälkki, A., Visser, H., de Vries, J., Stammes, P., Lundell, J., and Saari, H.: The Ozone Monitoring Instrument, IEEE Trans. Geosci. Remote Sense., 44, 1093–1101, doi:10.1109/TGRS.2006.872333, 2006.

Lu, Z., Streets, D., de Foy, B., Lamsal, L., Duncan, B., and Xing, J.: "Emissions of nitrogen oxides from US urban areas: estimation from Ozone Monitoring Instrument retrievals for 2005–2014", Atmos. Chem. Phys., 15, 10 367–10 383, doi:10.5194/acp-15-10367-2015, 2015.

McLinden, C. A., Fioletov, V., Boersma, K. F., Kharol, S. K., Krotkov, N., Lamsal, L., Makar, P. A., Martin, R. V., Veefkind, J. P., and Yang, K.: Improved satellite retrievals of $NO_2$ and $SO_2$ over the Canadian oil sands and comparisons with surface measurements, Atmos. Chem. Phys., 14, 3637–3656, doi:10.5194/acp-14-3637-2014, 2014.

Murphy, J. G., Day, D. A., Cleary, P. A., Wooldridge, P. J., Millet, D. B., Goldstein, A. H., and Cohen, R. C.: The weekend effect within and downwind of Sacramento: Part 2. Observational evidence for chemical and dynamical contributions, Atmos. Chem. Phys. Discuss., 6, 11 971–12 019, doi:10.5194/acpd-6-11971-2006, 2006.

Robere, R.: Interior Point Methods and Linear Programming, http://www.cs.toronto.edu/~robere/paper/interiorpoint.pdf, 2012.

Valin, L., Russell, A., and Cohen, R.: "Variations of OH radical in an urban plume inferred from $NO_2$ column measurements", Geophys. Res. Lett., 40, 1856–1860, doi:10.1002/grl.50267, 2013.

Wright, M.: The interior-point revolution in optimization: History, recent developments, and lasting consequences, Bull. Amer. Math. Soc., 42, 39–56, http://www.ams.org/journals/bull/2005-42-01/S0273-0979-04-01040-7/, 2005.